The role of inhibitory G proteins in the central nervous mechanisms of autonomic control of the heart

Richard Ang

A thesis submitted to University College London, in part fulfilment for the degree of Doctor of Philosophy

Centre for Clinical Pharmacology, Division of Medicine
University College London

Primary supervisor: Professor Andrew Tinker
Secondary supervisor: Professor Alexander Gourine

September 2015

Signed Declaration

I, Richard Ang, confirm that the work presented in this thesis is my own. Where information has been derived from other sources, I confirm that this has been indicated in the thesis.

Richard Ang

Date: 18 September 2015

Abstract

The heart is controlled by the sympathetic and parasympathetic limbs of the autonomic nervous system with inhibitory signalling mechanisms recruited in both limbs. This study aimed to determine the role of inhibitory G proteins in the mechanisms underlying autonomic control of the heart. Mice with conditional deletion of G protein $G\alpha_O$ in the cardiac conduction tissue and the central nervous system (CNS) were generated to determine the effect of specific $G\alpha_O$ deletions on autonomic control and electrophysiological properties of the heart.

Mice with conditional deletion of $G\alpha_O$ in the cardiac conduction tissue demonstrated normal diurnal heart rate (HR) profile and heart rate variability (HRV). Mice with conditional deletion of $G\alpha_{i2}$ displayed higher daytime HR and selective loss of the high frequency component of HRV, suggesting that signalling mediated by $G\alpha_{i2}$ (but not by $G\alpha_O$) is important for the parasympathetic control of the sinoatrial node.

$G\alpha_O$ deletion in the presympathetic area of the rostral ventral lateral medulla (RVLM) was not associated with changes in HR or the arterial blood pressure (BP) at rest (home cage, normal behaviour). However, exposure to stressful conditions (novel environment, hypoxia or hypercapnia) in these mice was associated with profoundly exaggerated heart rate responses and an increased baroreflex gain when studied under urethane anaesthesia. This was associated with a reduced ventricular effective refractory period and lower ventricular tachycardia threshold. This phenotype was reversed by systemic administration of a beta-adrenoceptor blocker atenolol, suggesting that $G\alpha_O$ loss in the RVLM increases central sympathetic drive.

The data obtained suggest that $G\alpha_O$-mediated signalling within the presympathetic circuits of the RVLM but not at the level of the cardiac conduction system contributes to the autonomic control of the heart. $G\alpha_O$ deficiency in the RVLM is associated with exaggerated cardiovascular responses to stress, altered cardiovascular reflexes and electrical properties of the heart.

Table of Contents

List of Figures

List of Tables

Commonly used abbreviations

AC	Adenylyl Cyclase
Ach	Acetylcholine
AVV	Adenoviral vector
BP	Blood pressure
BRS	Baroreflex sensitivity
cAMP	Cyclic adenosine monophosphate
CCPA	2-Chloro-N6-cyclopentyladenosine
CMV	Cytomegalovirus
CVLM	Caudal ventrolateral medulla
DVMN	Dorsal vagal motorneurone
GABA	Gamma-amino butyric acid
GIRK	G protein coupled inwardly rectifying K^+ channel
GFP	Green fluorescent protein
GPCR	G protein coupled receptor
HR	Heart rate
HRV	Heart rate variability
HF	High frequency
IML	Intermediolateral cell column
IPSP	Inhibitory post synaptic potential
KO	Knock out
LF	Low frequency
NA	Nucleus ambiguous
NTS	Nucleus tractus solitarius
PKA	Protein kinase A
PLC	Phospholipase C
PTX	Pertussis toxin

PVN	Paraventricular hypothalamic nucleus
RGS	Regulator of G protein signalling
RR	Respiratory rate
RVLM	Rostral ventrolateral medulla
SAN	Sinoatrial node
SR	Sarcoplasmic reticulum
TH	Tyrosine hydroxylase
VERP	Ventricular effective refractory period
VLF	Very low frequency
VT	Ventricular tachycardia

Acknowledgements

The work described in this thesis was generously supported by the Medical Research Council through the award of a Clinical Research Training Fellowship.

This work would not have been possible without the excellent supervision and support of my supervisors Professors Andy Tinker and Alex Gourine. Thank you both for putting up with me over these years and Alex, for making me appreciate Pink Floyd.

I would also like to extend my heartfelt gratitude to all my colleagues and friends during my time in the Tinker and Gourine labs. In the Tinker lab: Sonia Sebastian, who showed me the ropes initially and whom I collaborated with for some of the work described in Chapter 3, the ‘wise heads’ of Qadeer Aziz, Steve Harmer, Alison Thomas and Muriel Nobles, and of course my clinical colleagues and friends Aaisha Opel and Malcolm Finlay. In the Gourine lab: Nephtali Marina who kept me going, my ‘partners in crime’ Asif Machhada and Isabel Christie, and to Alla Korsak, Vitaly Kasimov, Marina Basalay, Svetlana Mastitskaya, Stefan Trapp and Anastassios Karagiannis. Special thanks also to Professor Andrew Rammage for taking the time out to help me with my experiments.

Finally, and most importantly, to my long-suffering wife Jane. Thank you for holding the fort.

And to my Mum and my late Father. This is for you.

Publications and abstracts derived from work described in this thesis

Publications

Ang, R., Opel, A. & Tinker, A., 2012. The Role of Inhibitory G Proteins and Regulators of G Protein Signaling in the in vivo Control of Heart Rate and Predisposition to Cardiac Arrhythmias. *Frontiers in physiology*, 3, p.96.

Sebastian, S. Ang R. et al., 2013. The in-vivo regulation of heart rate in the murine sinoatrial node by stimulatory and inhibitory heterotrimeric G-proteins. *AJP: Regulatory, Integrative and Comparative Physiology*, 305(4), pp. R435-42

Abstracts

Ang, R., Birnbaumer L., et al 2013. Tachycardia and increased baroreflex sensitivity in mice with conditional deletion of GalphaO in the pre-sympathetic area of the brain stem. 37th Congress of IUPS (Birmingham, UK) Proc 37th IUPS, PCC063

Ang, R., Birnbaumer L., et al 2013. The role of Galpha-O mediated signaling in the central nervous mechanisms controlling sympathetic outflow to the heart. European Society of Cardiology. *European Heart Journal*, 34 (Abstract Supplement), pp. 928

Ang, R., Birnbaumer L., et al 2013. Loss of inhibitory G protein GαO in the pre-sympathetic area of the brainstem leads to increased sympathetic tone to the heart and predisposes to ventricular arrhythmia. Heart Rhythm Congress. *Europace*, 15 (Suppl_4), pp. iv 31

Chapter 1

General Introduction

In vertebrates, the autonomic nervous system is essential to support a broad range of bodily functions and maintain homeostasis. Autonomic regulation of the cardiovascular activities ensures adequate perfusion and oxygenation of the end organs in health. Autonomic dysfunction is associated with a wide range of cardiovascular diseases, including hypertension, heart failure and cardiac arrhythmias.

Hypertension is one of the major risk factors associated with the development of many cardiovascular diseases. The pathophysiology of essential hypertension is complex and multifactorial. There is significant evidence from animal studies and hypertensive patients that autonomic dysfunction, specifically activation of the sympathetic nervous system, is linked to the development and maintenance of this condition (Malpas 2010).

Heart failure, irrespective of underlying aetiology, result in reduced end-organ perfusion. Complex changes in autonomic function occur to compensate for this and result in overall increase in sympathetic outflow to the heart and peripheral vasculature with reduction in vagal outflow (Grassi et al. 1995; Floras 2009). In the short-term these changes have an adaptive effect. However, in the longer term they are maladaptive, resulting in increased myocardial oxygen consumption, promote adverse cardiac re-modeling and increases the likelihood of ventricular arrhythmias (Milner et al. 1999; Frenneaux 2004). Reduced heart variability (HRV) and baroreflex sensitivity (BRS), both markers of reduced vagal tone and resulting sympathovagal imbalance, have been shown to be independently associated with increased cardiac mortality in a large cohorts of patients followed up following myocardial infarction (La Rovere et al. 1998) and with chronic heart failure (Nolan et al. 1998). Reduced BRS has also been independently associated with an increase in lethal arrhythmic events following myocardial infarction (Farrell et al. 1992).

Autonomic precipitants are also well recognized to trigger arrhythmias outside of the context of heart failure. Increased vagal tone has been shown to precipitate atrial fibrillation (Bettoni & Zimmermann 2002) and sympatho-

vagal imbalance can trigger ventricular arrhythmia in patients with inherited ‘channelopathies’ such as the long QT syndrome, Brugada syndrome and catecholaminergic polymorphic ventricular tachycardia (Verrier & Antzelevitch 2004).

Although progress has been made in the diagnosis and management of these conditions, there remains a significant morbidity and mortality burden. For example, only approximately half of patients show satisfactory response to current available treatment for hypertension (Go et al. 2013). Despite contemporary pharmacological and device treatment for heart failure, 5-year survival remains poor at about 50% (Cleland et al. 2014). The limited efficacy of current management strategies may be due to the fact that only downstream peripheral mechanisms are targeted and not the underlying primary factors responsible for the development and maintenance of the condition.

It is increasingly recognised that autonomic dysfunction is not just a marker of disease progression but also a modifier of the underlying pathology and therefore a target for therapeutic interventions. Renal denervation (Myat et al. 2013), vagal nerve stimulation (De Ferrari et al. 2011) and baroreceptor stimulation (Heusser et al. 2010) are among interventions currently undergoing clinical evaluation for the treatment of cardiovascular diseases.

However, the initial results reported from renal denervation for hypertension and vagal nerve stimulation for heart failure trials have not delivered on the initial promise from preliminary studies (Bhatt et al. 2014; Zannad et al. 2014). It would appear that much remains to be learned regarding the autonomic regulation of the heart to allow for more precise targeting of future therapeutic interventions.

1.1 Autonomic regulation of the heart

The autonomic nervous system maintains homeostasis and coordinates physiological responses in the body via its two functional limbs: the sympathetic and parasympathetic nervous systems. The heart is regulated in this manner within the cardio-respiratory system. Afferent nerves convey baroreceptor and chemoreceptor inputs to the cardio-respiratory centres within the brainstem and integrated reflex responses are mediated by the sympathetic and parasympathetic efferents to the heart, blood vessels and other effector organs such as the adrenal glands. Sympathetic efferents cause an increase in heart rate (HR), blood pressure (BP), and diversion of visceral blood flow to skeletal muscles and metabolic changes that mobilises energy stores, with generally opposite effects mediated by the parasympathetic fibres.

Although the sympathetic and parasympathetic effects are largely opposing in nature, the balance between sympathetic and parasympathetic activity is not a simple see–saw effect as co-activation also occurs (Koizumi & Kollai 1981; Koizumi et al. 1982). It appears that 'protective' responses such as diving, peripheral chemoreflex, startle, noxious, ocular and defense reflexes activate both autonomic limbs simultaneously to the heart (Paton et al. 2005). For example in the diving reflex, activation of the parasympathetic limb results in slowing of the heart via its action on the sinoatrial node whilst activation of the sympathetic nervous system results in increased contractility of the heart. Co-activation of both limbs of the autonomic nervous system would also allow for precise control of dynamic range and gain of the response, with the direction of the response determined by the dominating limb. Since the dynamic range and the gain of the response are restricted, this leads towards stabilization of the functional state of the target organ. This is important in protective reflexes where the operating range needs to be confined but precisely controlled. In contrast, reciprocal control may be better suited for homeostatic regulatory responses such as the baroreflex response where the range and gain can oscillate in either direction due to the synergism of both limbs of the system (Berntson et al. 1991).

Both sympathetic and parasympathetic systems are made up of central and peripheral components. The central component consists of cell groups in the brain and spinal cord, and myelinated preganglionic neurons. It is responsible for maintenance of autonomic tone, and integration of afferent inputs to generate appropriate autonomic activites. Much of the basic structure involved in the reflex control of the cardiovascular system is contained within the medulla oblongata. Integrated and behaviorally appropriate responses also require reciprocal connections between the medulla oblongata, pons, midbrain and the hypothalamus (Spyer 1994). The peripheral components consist of ganglia and unmyelinated postganglionic afferent and efferent fibres innervating the heart and associated effector organs (eg: blood vessels).

In this thesis, I shall concentrate on the central autonomic control of the heart.

1.2 Central nervous mechanisms of autonomic control of the heart

The central circuits responsible for autonomic regulation of the heart consist of the vagal preganglionic groups of neurones near the dorsal surface of the medulla oblongata and within the nucleus ambiguus which project via the vagus nerve to the heart, and the sympathoexcitatory (presympathetic) networks within the brainstem and hypothalamus which provide tonic excitatory drive to the sympathetic preganglionic neurones in the spinal cord which in turn innervate the heart.

1.2.1 Vagal preganglionic neurones

Electrophysiological and histological studies using tracer dyes injected retrogradely into the heart ganglia or anterogradely into the medullary neurones respectively showed that the vagal preganglionic cardiac neurones mainly arise from the posterior ventrolateral nucleus ambiguous (NA) and the dorsal vagal motor nucleus (DVMN) (reviewed in Coote 2013).

The larger NA group of vagal preganglionic neurones receive phasic baroreceptor and chemoreceptor input and projects via myelinated B fibres whilst the smaller group of DVMN neurones conducts via the slower non-myelinated C fibres and have a more irregular non-respiratory dependent discharge pattern independent of baroreceptor and chemoreceptor input (Jones et al. 1995; Garcia Perez & Jordan 2001; Jones 2001).

There is some disagreement with regards to the innervation of these fibres at the level of the heart. Using different fluorescent tracers, Cheng et al showed that DVMN and NA terminals target separate populations of neurones in the intrinsic cardiac ganglion (Cheng et al. 2004). However, Jones (Jones 2001) has suggested that B and C fibres converge on the same postganglionic neurones but at present there is no direct evidence supporting this. Postganglionic efferents synapse via cholinergic muscarinic receptors to the atria and cardiac conduction tissue of the heart including the sinoatrial node (SAN) and atrioventricular node. There is increasing evidence that the ventricular myocardium is also innervated by parasympathetic cholinergic (Deighton et al. 1990; Syrota et al. 1985) and non-cholinergic efferents (Brack et al. 2007; Brack et al. 2011) directly influencing ventricular rhythm and contractility (Casadei 2001). Selective stimulation of the unmyelinated C fibres of the DVMN affects atrioventricular conduction and force of ventricular contraction and also reduces heart rate, but it has a slower onset and different pharmacology to that seen following stimulation of the B fibres in the vagus nerve (Jones et al. 1995; Garcia Perez & Jordan 2001; Jones 2001).

Cardiac and respiratory functions are integrated centrally. Respiratory related fluctuations in heart rate, also known as respiratory sinus arrhythmia, are the result of respiratory modulation on the activity of NA either via direct input from central respiratory neurons or by reflex inputs that are activated by lung inflations (Spyer & Gilbey 1988).

1.2.2 Pre-sympathetic circuits in the brainstem

Sympathetic vasomotor activities are generated by the sympathetic preganglionic neurones in the spinal cord, which receive inputs from sympathoexcitatory (presympathetic) networks within the brainstem and the hypothalamus. Neurones in the presympathetic network include, from rostral to caudal, the paraventricular nucleus of the hypothalamus, the A5 cell group of the pons, the raphe nuclei, the rostral ventrolateral medulla (RVLM), rostral ventromedial and midline medulla, and the A1 cell group (Strack et al. 1989, Granata et al. 1986). This network of neurones integrates peripheral sensory and central command inputs, relay between each other and signal in descending pathways to the sympathetic preganglionic neurones in the IML. In this manner, they regulate sympathetic activity in response to a variety of physiological and behavioural states (Spyer 1994). For example, the raphe nuclei have been shown in rats to project directly to sympathetic preganglionic neurones in the IML (Bacon et al. 1990) and cause sympathetic activation of brown adipose tissue and vasoconstriction in tail artery to effect thermogenesis in response to pyogenic stimuli (Nakamura 2005).

The RVLM is the best studied of all the presympathetic vasomotor neurones. It consists of a chemically heterogenous group of cells. The largest group is the C1 cells which are catecholaminergic as they contain tyrosine hydroxylase (TH) and phenylethanolamine *N-methyl* transferase, enzymes required for the synthesis of adrenaline (Ross et al. 1981, Ross et al. 1983). RVLM neurones are also immunoreactive for a number of other peptides including 5-hydroxytryptamine (5-HT), neuropeptide Y (NPY), substance P, enkaphalin and thyrotrophin releasing hormone (Charlton et al. 1987, Helke et al. 1993, Hirsch & Helke 1988, Sasek & Helke 1989, Strack et al. 1989). The proportion of C1 cells in the RVLM has been estimated at about 70% (Schreihofer et al. 1997, Sartor & Verberne 2003).

The other presympathetic neurones containing PNMT but not TH are the noradrenergic A5 and A1 groups of cells. The A5 group is located rostral to

the RVLM in the pons and is one of the main sources of noradrenergic input to the sympathetic preganglionic neurones (Byrum and Guyenet 1987, Bruinstroop et al. 2012). It is thought to play a role in mediating cardiorespiratory response to activation of the hypothalamic defence area (Lopez-Gonzalez et al. 2013) and to nociception (Clark & Proudfit 1993). The A1 group of cells are noradrenergic neurones located at the caudal half of the ventral lateral medulla (CVLM) extending down to the spinomedullary junction (Ross et al. 1981). They are interspersed with C1 neurones. The A1 cells project predominantly to a number of supraspinal sites including the RVLM and PVN (Woulfe et al. 1990) and are involved in glucoprivic feeding (Li et al. 2009), and central fluid and cardiovascular homeostasis (West et al. 1981) (Figure 1.1).

1.2.3 RVLM and the cardiovascular system

The RVLM is a source of dense projection to the intermediolateral cell column (IML) (Amendt et al. 1979, Dampney et al. 1982) and contributes significantly to the generation of sympathetic vasomotor tone since in anaesthetised experimental animals acute bilateral inactivation or ablation of the RVLM neurones leads to a fall in arterial pressure and sympathetic activity to the levels observed after transection of the spinal cord or during ganglionic blockade (Guertzenstein & Silver 1974; Feldberg & Guertzenstein 1976). Conversely, activation by electrical stimulation or chemical excitation of this region profoundly increases sympathetic nerve activity and the arterial blood pressure (Dampney et al. 1982; Guyenet 2006). In addition, baroreceptor stimulation inhibited RVLM activity and this correlated to reductions in sympathetic vasomotor activity (Barman & Gebber 1985, Brown & Guyenet 1985). A large fraction of these neurones were later identified as C1 cells by intracellular and juxtacelular labeling methods (Lipski et al. 1995, Schreihofer & Guyenet 1997).

The specific role of C1 neurones to arterial pressure control was studied in conscious rats after administration of ribosome inactivating toxin anti-dopamine beta hydroxylase-saporin (anti-DβH-sap), which causes selective

destruction of catecholaminergic cells, to the RVLM (Madden & Sved 2003, Madden et al. 2006). Only modest reductions of mean arterial pressure (~10 mmHg) were observed in conscious rats despite very large reductions in C1 cell numbers (~80%) and substantial collateral damage to the A5 noradrenergic neurones (Madden & Sved 2003). In these rats, plasma catecholamine levels were only marginally lower than in controls, suggesting a small drop in resting sympathetic tone. However, following hydralazine-induced hypotension there was a substantial attenuation in the rise of plasma norepinephrine, vasopressin, and oxytocin. There was also significant attenuation in HR and arterial pressure response to baro- and chemoreflex challenges. These findings suggest that the RVLM contributes significantly in sympathoexcitatory reflexes such as the baroreceptor reflex, and the carotid chemoreceptor reflex. A seperate group replicated these findings in rats with presympathetic C1 neurons (and A5 neurons) destroyed by injecting the same toxin into the spinal cord (Schreihofer et al. 2005), sparing the bulbospinal barosensitive non-C1 RVLM neurons (Schreihofer & Guyenet 2000). In these rats, there were no significant effects on resting arterial pressure or HR. However, sympathoexcitatory responses evoked by electrical stimulation of the RVLM were signficantly attenuated, as were the baroreflex and the increase in sympathetic nerve activity elicited by carotid body stimulation (Schreihofer & Guyenet 2000). Taken together, these studies demonstrate that chronic lesions of the C1 neurons with anti-DβH-sap only modestly decreases resting arterial pressure and resting sympathetic nerve activity, but permanently and substantially reduces the neuroendocrine response to hypotension and hypoxia.

The RVLM has also been implicated in cardiovascular pathologies such as hypertension and heart failure. For example, the development of hypertension in spontaneous hypertensive rats (SHRs) was attenuated when the activity of the RVLM was depressed using a lentiviral construct (Geraldes et al 2014). Marina et al used a different lentiviral vector to disrupt purinergic signaling in the RVLM in rats with myocardial infarction-induced heart failure (Marina et al 2013). They found that expression of the viral construct bilaterally in the RVLM led to lower plasma noradrenaline concentration and

attenuated the progression of LV remodelling and heart failure secondary to myocardial infarction.

1.2.4 The sympathetic baroreceptor reflex pathway

The baroreceptor reflex describes the changes in sympathetic outflow in response to perturbations in arterial BP and is often used to study the central neurotransmitter system regulating sympathetic outflow.

The contribution of the RVLM to the baroreflex operation (the sympathetic cardiac, respiratory, and neuroendocrine responses elicited by hypotension via a reduction in the activity of arterial baroreceptors) is summarised in Fig. 1.2. Baroreceptor afferent neurons terminate at the nucleus tractus solitaries (NTS), which process and integrate these inputs and projects via glutamatergic neurons to the CLVM.

CVLM is the site at which the excitatory signals from baroreceptor afferent nerves are converted to inhibitory inputs to the RVLM. CVLM neurons are tonically active, even in the absence of baroreceptor input and use GABA as a neurotransmitter. These sympatho-inhibitory interneurons project rostrally and bilaterally to the RVLM and generate inhibitory post-synaptic potentials (IPSP)s (reviewed in Pilowsky & Goodchild 2002).

Sympatho-activation secondary to hypotension is hence due to a process of ‘disinhibition’ of RVLM C1 cells via a pathway that consists minimally of three neurons: baroreceptor afferent neurons, glutamatergic neurons located in the NTS and projecting to the CVLM and CVLM GABAergic interneurons which synapse with C1 neurons (Figure 1.2).

Both the CVLM and the RVLM also receive inputs from nearby respiratory (Botzinger) regions and respiratory modulation of sympathetic activity is known to occur (Pilowsky et al. 1996; Miyawaki et al. 2002). Hypotension also activates breathing by stimulating the central respiratory pattern generator and triggers the corticotrophin releasing hormone (CRH)

/adrenocorticotropic hormone (ACTH)/corticosterone cascade, presumably through direct projections from RVLM C1 neurons to the PVN (Guyenet et al. 2013).

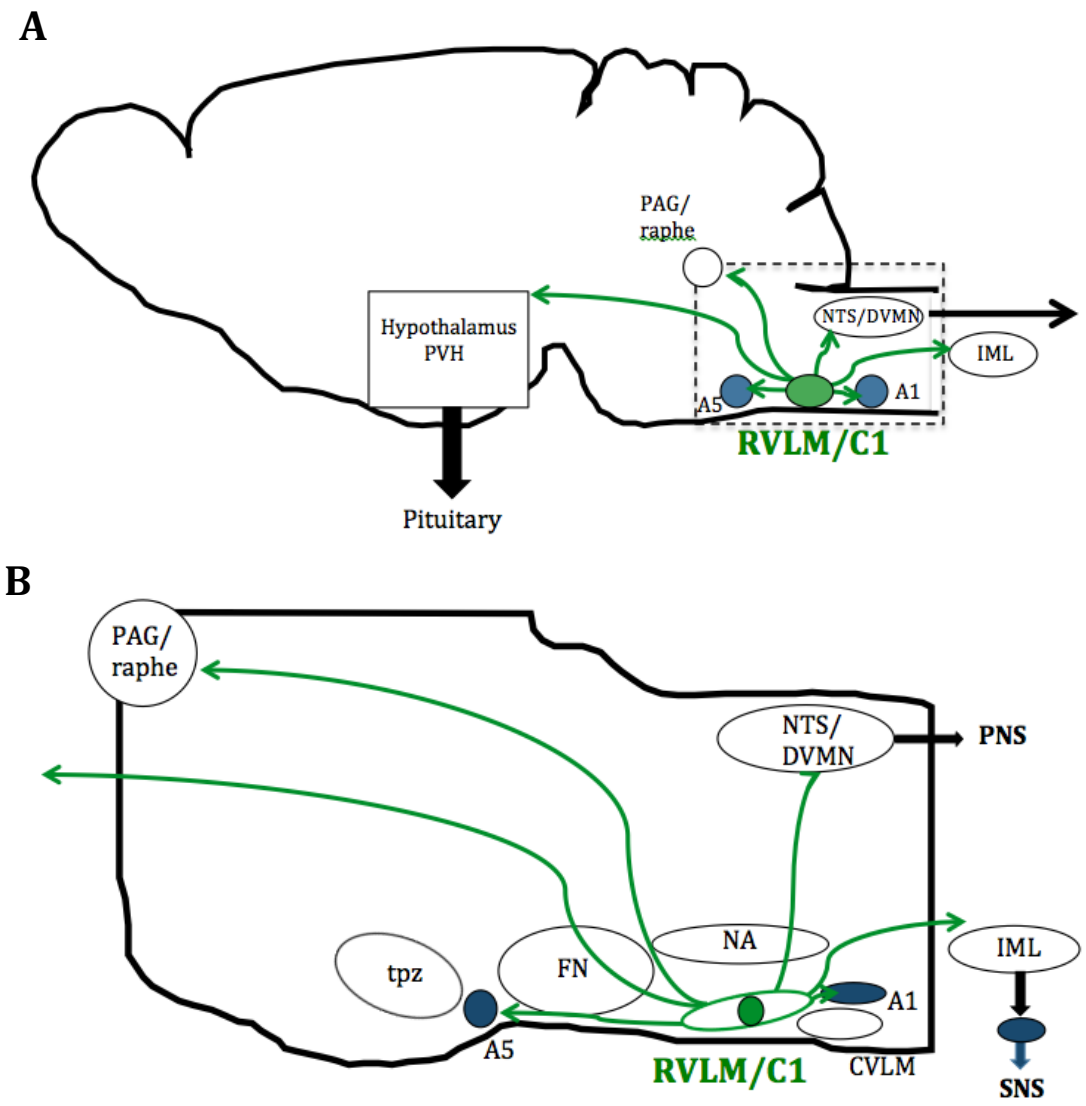

Figure 1.1 Location and principal projections of the rat RVLM/C1 neurones

(A) Schematic representation of the location and main axonal projections of the RVLM/C1 neurons (parasagittal view). **(B)** Higher resolution view of the pontomedullary region outlined in **(A)** showing the location of the C1 cells in relation to nearby anatomical structures. The C1 neurons (in green) project to lower brain stem noradrenergic neurons (A1, 5 in blue), selected serotonergic neuron-rich regions (dorsal raphe), the dorsal vagal complex (nucleus of the solitary tract and dorsal vagal motor nucleus, NTS/DVMN), and the intermediolateral cell column (IML). The main rostral targets are the periacqueductal grey matter (PAG), and, in the hypothalamus, the paraventricular nucleus (PVH). RVLM, rostral ventolateral medulla; FN, facial motor nucleus; NA, nucleus ambiguus; tpz, trapezoid body; CVLM, caudal ventrolateral medulla; PNS, parasympathetic nervous system; SNS, sympathetic nervous system. (Adapted from Guyenet et al. 2013)

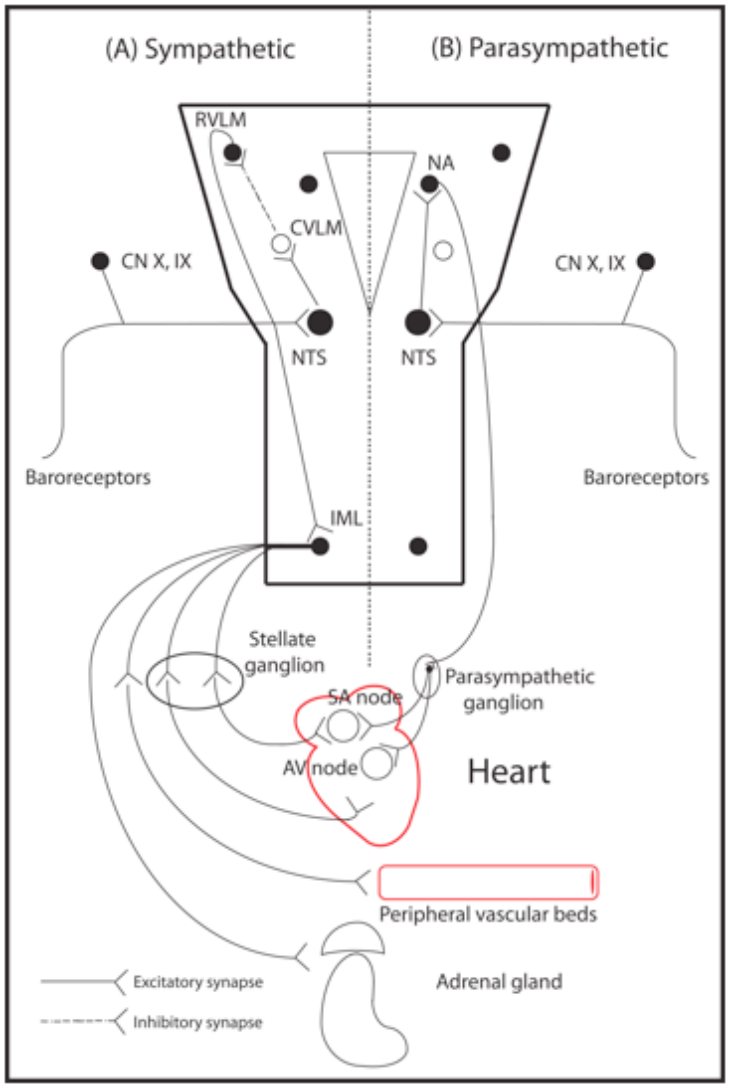

Figure 1.2 Schematic drawing of main peripheral and central pathways involved in autonomic cardiovascular regulation

(A) Sympathetic baroreflex arm: Baroreceptor afferent neurons in the periphery transmit baroreceptor information via a glutamatergic synapse to the nucleus tractus solitaries (NTS) in the dorsal medulla oblongata. NTS neurons project to and excite inhibitory neurons in the caudal ventrolateral medulla (CVLM). CVLM neurons in turn project and inhibit (via a GABAergic synapse) presympathetic neurons in the rostral ventrolateral medulla (RVLM). Spinally projecting presympathetic RVLM neurons make direct connections with sympathetic preganglionic neurons in the intermediolateral (IML) spinal column, which generate sympathetic outflow to the effector organs. (B) Parasympathetic control of heart rate: NTS neurons receive baroreceptor information and relay it via a glutamatergic pathway to the nucleus ambiguus (NA). Cardioinhibitory neurons in the NA project to the heart via the vagus nerve, which mediates its effect via muscarinic receptors in the heart (adapted from Pilowsky & Goodchild 2002).

1.3 G-proteins

G-proteins mediate signal transduction for the G-protein coupled receptors (GPCRs), which make up the majority of mammalian membrane-bounded receptor systems. GPCRs are key modulators of disease pathogenesis and some 30-40% of all therapeutic agents used in clinical practice target certain GPCRs.

Heterotrimeric G-proteins are composed of $\alpha\beta\gamma$-subunits, which dynamically interact with GPCRs within the plasma membrane, as part of the G-protein cycle. Heterotrimeric G proteins can be divided into 4 primary families based on their α subunits: $G\alpha_{i/o}$, $G\alpha_{s}$, $G\alpha_{q/11}$ and $G\alpha_{12/13}$. $G\alpha_{s}$ and $G\alpha_{q/11}$ are excitatory G proteins that act predominantly via adenlyate cyclase (AC) and phospholipase C (PLC) respectively. $G\alpha_{i/o}$ subunit are known as inhibitory G proteins, are sensitive to pertussis toxin, and can be further subdivided into 4 main subtypes based on their α subunit isoforms: $G\alpha_{i1}$, $G\alpha_{i2}$, $G\alpha_{i3}$ and $G\alpha_{O}$ ('O' for other). $G\alpha_{12/13}$ proteins predominantly activate the small G protein Rho and through RhoA and its downstream effectors affect the actin cytoskeleton, cell migration and invasion and other complex cellular processes (reviewed in Birnbaumer 2007a)(Table 1.1).

GPCRs can also be modulated at the receptor or effector level; for instance, members of the regulator of G-protein signaling (RGS) family of proteins can accelerate activation or deactivation of G-proteins, and may alter receptor-effector coupling (Birnbaumer 2007b)

Gα subunit classes	Main subclasses	Gene	Expression	Effectors
$G\alpha_S$ class	$G\alpha_S$	*GNAS*	Ubiquitous	AC ↑
$G\alpha_{i/o}$ class	$G\alpha_{i1}$ $G\alpha_{i2}$ $G\alpha_{i3}$ $G\alpha_O$	*GNAI1* *GNAI2* *GNAI3* *GNAO*	Widely distributed Ubiquitous Widely distributed Neuronal, neuroendocrine	AC ↓ (directly regulated) GIRK ↑, VDCC ↓ Various other effectors regulated by Gβγ subunit
$G\alpha_{q/11}$ class	$G\alpha_q$ $G\alpha_{11}$	*GNAQ* *GNA11*	Ubiquitous Almost ubiquitous	PLC ↑
$G\alpha_{12/13}$ class	$G\alpha_{12}$	*GNA12*	Ubiquitous	PDZ-RhoGEF/LARG, Btk, Gap1m, cadherin
	$G\alpha_{13}$	*GNA13*	Ubiquitous	P115RhoGEF, PDZ-RhoGEF/LARG, radixin

Table 1.1 The 4 major classes of Gα subunits

Abbreviations: ↑ increase in activity; ↓ decrease in activity; AC, adenylyl cyclase; GIRK, G protein regulated inward rectifier potassium channel; VDCC, voltage dependant Ca^{2+} channel; PLC, phospholipase C; RhoGEF, Rho guanide nucleotide exchange factor. Adapted from (Wettschureck & Offermanns 2005)

1.3.1 Inhibitory G proteins and autonomic modulation of heart rate

Heart rate modulation via adrenergic and muscarinic mechanisms operating at the level of the heart is well studied. The current paradigm for the mechanism underlying SAN automaticity involves a complex interaction between activity of the voltage-gated ion channels/exchangers in the plasma membrane (also referred to as the 'membrane clock') and the rhythmic calcium release from the sarcoplasmic reticulum (the 'calcium clock') (Lakatta & DiFrancesco 2009). The key membrane ion channel thought to be involved in pacemaker setting is the hyperpolarisation activated cation currents or 'funny' currents (I_h/I_f) channel (DiFrancesco 2010), and pacemaker activity is further modulated by K^+, Na^+ and Ca^{2+} currents. In addition, recent studies suggest that rhythmic local calcium releases from the sarcoplasmic reticulum (SR) modulated by protein kinase A (PKA) also contribute to pacemaker activity by activating inward Na^+/Ca^{2+} exchanger currents during late diastolic depolarisation (Maltsev & Lakatta 2008) (Figure 1.3). GPCRs can hence modulate heart rate by acting directly on the I_h/I_f channel or by regulation of intracellular calcium cycling.

The release of noradrenaline from the sympathetic nerve endings or the release of adrenaline from the adrenal medulla into the circulation modulates activity of the SAN by binding to β-adrenoreceptors. The stimulatory cascade mediated by Gαs is activated and this leads to stimulation of AC and the generation of cyclic adenosine monophosphate (cAMP). Increased cAMP can directly modulate I_h/I_f leading to increased rate of pacemaker depolarisation. However, increased cAMP can also activate PKA, which can modulate intracellular calcium handling proteins such as phospholamban and the ryanodine receptor to modulate rate. Both of these actions will increase the heart rate.

Acetylcholine (ACh) is released from the terminals of the vagal postganglionic neurones and binds to the muscarinic (M2) receptors, leading to the activation and dissociation of inhibitory G-protein heterotrimers. The resulting βγ-dimer directly activates the G-protein coupled inward rectifying

potassium (GIRK) channel to cause membrane hyperpolarisation, slowing pacemaker depolarisation and sinus rate. Furthermore, the activation of the inhibitory Gα subunit will inhibit AC and thus modulate I_h/I_f and the calcium handling proteins as detailed above. RGS proteins interact with the inhibitory Gα subunit to switch off this pathway through GTPase accelerating protein (GAP) activity and allow the heterotrimer to reform (Figure 1.4).

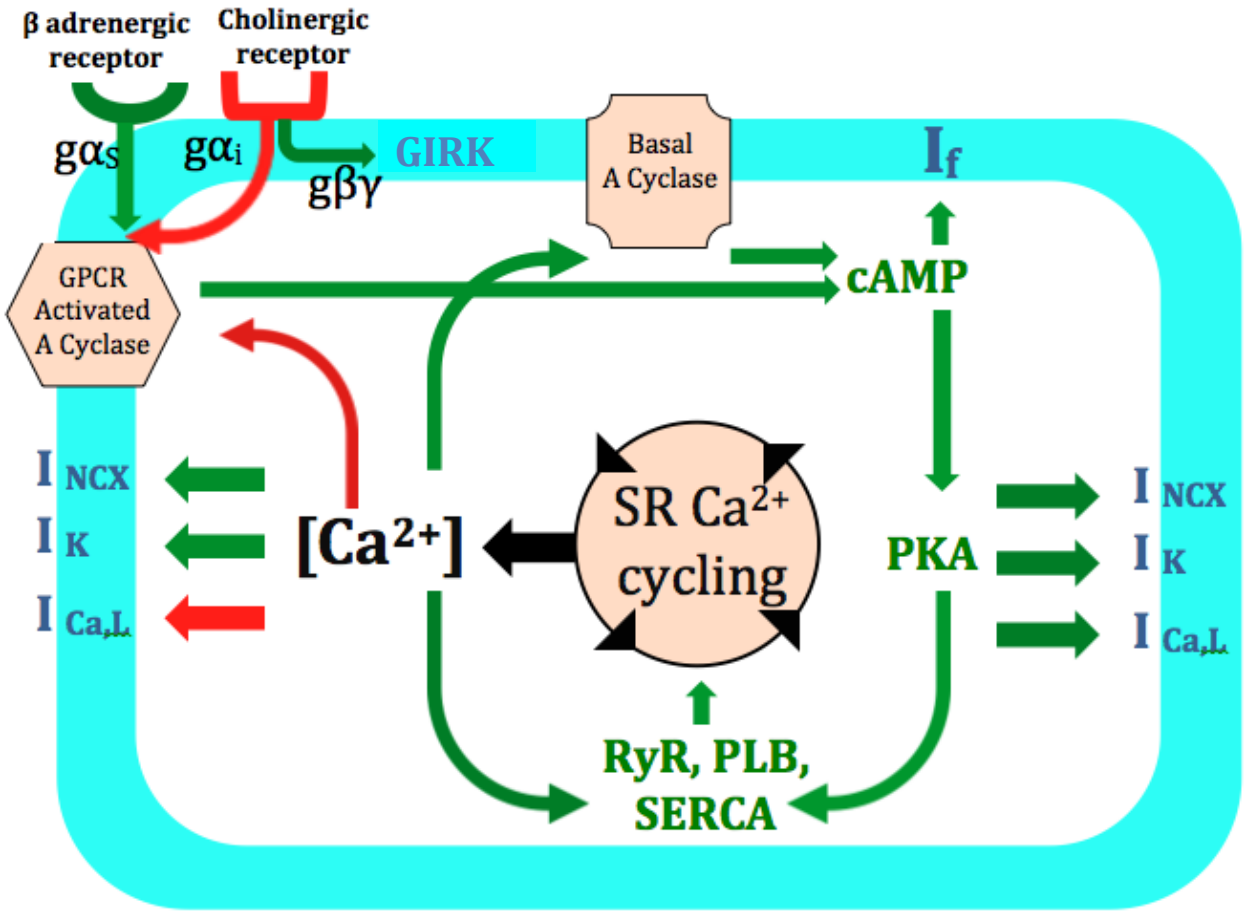

Figure 1.3 Interplay between the membrane and the calcium 'clock' in regulation of SAN automaticity

Schematic illustration of the interplay of Ca^{2+}, basal Ca^{2+}-activated adenylyl cyclase (Basal A Cyclase), GPCR activated adenylyl cyclase (GPCR Activated A Cylcase), cyclic AMP (cAMP) and protein kinase A (PKA), in the context of sarcoplasmic reticulum Ca^{2+} cycling (modulated by activities of ryanodine receptor (RyR), phospholamban (PLB) and sarco/endoplasmic reticulum Ca^{2+}-ATPase (SERCA)), hyperpolarization activated cation/funny current (I_f), L-type Ca^{2+} ($I_{Ca,L}$), Na^+/Ca^{2+} (I_{NCX}) exchanger, and inward rectifier K^+ (I_K) and acetylcholine mediated inward rectifying K^+ (*GIRK*) membrane currents. Spontaneous but rhythmic local submembrane Ca^{2+} releases during late diastolic depolarisation (DD) activate I_{NCX}, causing the DD to increase exponentially to achieve the threshold for $I_{Ca,L}$ activation and the generation of the next AP. Modulatory actions of GPCR signaling via β adrenergic and muscarinic cholinergic receptors are shown by green (stimulatory) and red (inhibitory) arrows. Adapted from (Lakatta & DiFrancesco 2009).

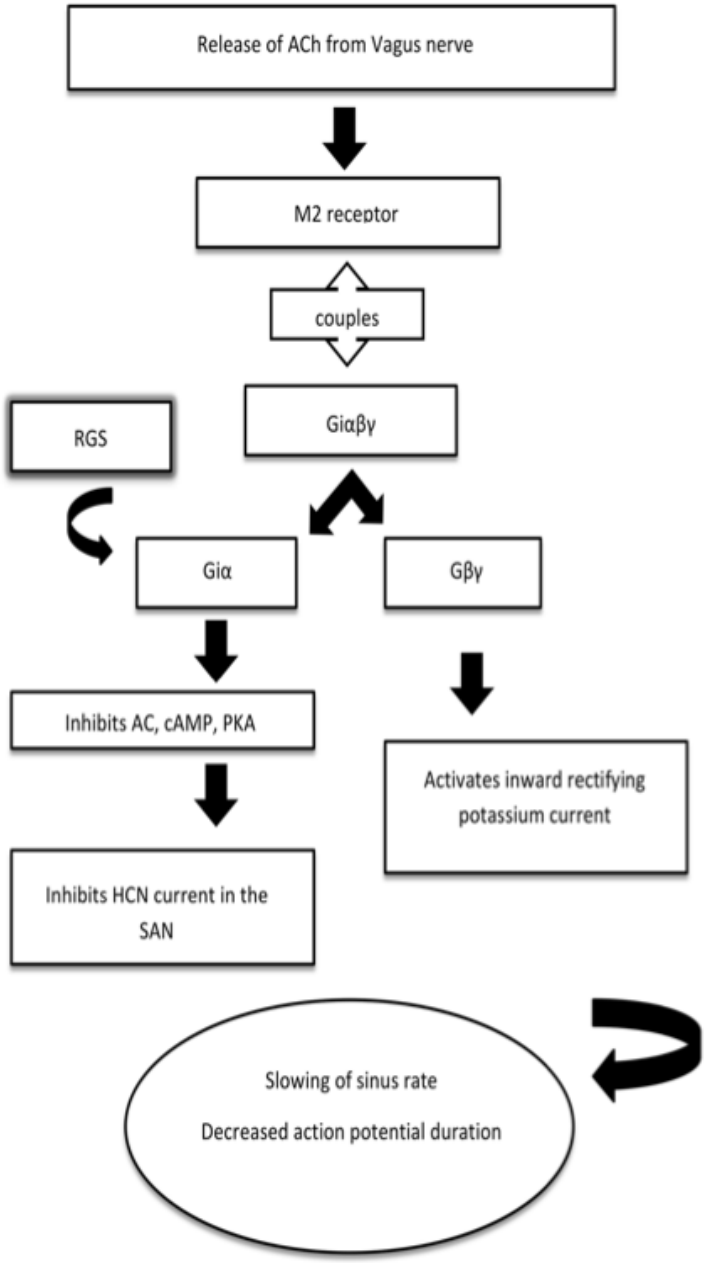

Figure 1.4 A simplified schematic for the mechanism of heart rate regulation by inhibitory G proteins

Acetylcholine (Ach) released from the vagus nerve binds to the muscarinic (M2) receptor, which is coupled to the inhibitory G protein. The α-subunit inhibits cyclic AMP (cAMP) whilst βγ-dimer activates the G protein coupled inward rectifying potassium (GIRK) channel to slow the sinus rate, and decrease the action potential duration. Regulators of G protein signaling (RGS) interact with the α-subunit to switch off this pathway through GTPase accelerating protein activity and allow the heterotrimer to reform. AC, adenylyl cyclase; cAMP, cyclic AMP; PKA, protein kinase A; HCN, hyperpolarization-activated cyclic nucleotide-gated channel (from Ang 2012).

1.3.2 G-proteins specificity

Do specific G-proteins carry out unique functional roles or does the system have significant redundancy? Inhibitory G-proteins are characterised by their sensitivity to PTX, which adenosine di-phosphate (ADP) ribosylates the proteins and uncouples them from receptors. In vitro studies using PTX insensitive $G\alpha_{i/o}$ isoforms suggest that most GPCR's couple well with a number of isoforms (Leaney et al. 2000).

Zuberi et al studied whether specific isoforms of the inhibitory G-proteins differentially modulate heart rate *in vivo* (Zuberi et al. 2008). Mice with global knock out (KO) of $G\alpha_{i1}$ and $G\alpha_{i3}$ combined, $G\alpha_{i2}$ and $G\alpha_{O}$ were implanted with telemetry probes. Heart rate dynamics were then analysed in the time and frequency domain in awake and unrestrained mice. The influences exerted on the heart by the autonomic nervous system can be measured indirectly by the analysis of the beat-to-beat variation of heart rate ("heart rate variability", HRV). In man R-R interval shows characteristic patterns of variability with a low frequency (LF) component (> 6 second cycle length) determined by sympathetic and parasympathetic drive and a high frequency (HF) component (2.5 to 6 second cycle length) governed by parasympathetic input (Stauss 2003). Such analysis has also been applied to the mouse but there is less agreement on the contribution of the different arms of the autonomic nervous system to the frequency components (Thireau et al. 2007). $G\alpha_{i2}$ deficient mice were found to be generally tachycardic with preservation of diurnal variation, had loss of HF power when HRV was analysed and displayed patterns similar to that seen after application of GIRK channel blocker TertiapinQ or muscarinic receptor blocker atropine. There was also an attenuated bradycardic response to muscarinic receptor agonist carbachol. Mice with global deficiency in $G\alpha_{i1,3}$ were similar to wild type (WT) but $G\alpha_{O}$ showed a different phenotype that is discussed below.

These observations correlated with the findings by Fu et al, where mice with a G184S knockin point mutation in the switch I region of $G\alpha_{i2,}$ preventing the binding of RGS proteins and deactivation of $G\alpha_{i2,}$ displayed marked

enhancement of muscarinic agonist-induced bradycardia (Fu et al. 2007). There is, however, one conflicting study suggesting that $G\alpha_O$ but not $G\alpha_{i2}$ mediates muscarinic influences on the heart (Duan et al. 2007).

$G\alpha_{i2}$ and $G\alpha_O$–mediated signalling has also been implicated in the muscarinic inhibition of β-adrenoreceptor activated voltage gated L-type calcium channels in the heart. Using a model of ventricular myocytes isolated from global $G\alpha_{i2}$ and $G\alpha_{i3}$ knockout mice, Nagata et al demonstrated reduced calcium channel currents with carbachol following isoproterenol stimulation in $G\alpha_{i3}$ knockout mice and littermate controls but not in $G\alpha_{i2}$ knockout mice (Nagata et al. 2000). Using a similar experimental strategy in $G\alpha_O$ knockout mice, Valenzuela demonstrated similar impaired muscarinic regulation of L-type calcium channels in ventricular myocytes lacking $G\alpha_O$ but no difference in potassium current compared to wild type controls (Valenzuela et al. 1997).

Differential coupling of G protein subtypes to adenosine A1 and muscarinic M2 receptor mediated heart rate slowing was also demonstrated *in vitro* using RGS insensitive $G\alpha_O$ and $G\alpha_{i2}$ ES derived cardiomyocytes (Fu et al. 2006). The RGS-insensitive $G\alpha_O$ homozygous knock-in cells demonstrated enhanced adenosine A1 and muscarinic M2 receptor-mediated bradycardic responses. In contrast, RGS-insensitive $G\alpha_{i2}$ homozygous knock-in cells showed enhanced responses to activation of M2 but not A1 adenosine receptors. Blocking GIRK channels largely abolished the mutation-induced enhancement of the M2 receptor-mediated response but had a minimal effect on A1 responses.

Taken together, the evidence suggests that M2 mediated GIRK channel activation is coupled preferentially to the $G\alpha_{i2}$ subunit whereas coupling to voltage gated L-type calcium channel appears to be less specific with both $G\alpha_O$ and $G\alpha_{i2}$ implicated.

1.4 Contributory effect of inhibitory G proteins signalling in the central nervous system

As described above, *in vitro* and *in vivo* studies appear to suggest inhibitory G protein specificity at the level of the heart. What is less known is the role and specificity of inhibitory G proteins in the central nervous mechanism of cardiovascular autonomic regulation.

1.4.1 Inhibitory G proteins in the central nervous system

$G\alpha_{i1}$, $G\alpha_{i2}$ and $G\alpha_{i3}$ are ubiquitously expressed in all tissues of the body but $G\alpha_O$ protein expression is restricted mainly to the central and peripheral nervous systems, endocrine cells and cardiomyocytes (Wettschureck & Offermanns 2005). Expression of $G\alpha_O$ is greatest in the brain where it is estimated to constitute around 1% of all membrane proteins (Sternweis & Robishaw 1984). Mice lacking the α subunit of G_O are smaller and weaker than their littermates, have greatly reduced life expectancy and display numerous neurological abnormalities including hyperalgesia, tremors, seizures, and increased motor activity with an extreme turning behavior (Jiang et al. 1998). $G\alpha_{i/o}$ coupled receptors can cause pre- or post-synaptic inhibition either via GIRK channels or by inhibiting calcium channels to mediate an effect on the central nervous system (van den Pol 2012).

GIRK channels are widely distributed in neuronal and endocrine tissues and play key roles in generating late IPSPs and modulating hormone release in addition to their cardiac functions described above. In the central nervous system, GIRK channels hyperpolarize neurons in response to activation by peptides and neurotransmitters including GABA, adenosine, somatostatin, 5-Hydroxytryptophan (5-HT) and opioids, and are composed of heterotetramers of Kir3.1, Kir3.2 and Kir3.3 and homotetramers of Kir3.2 (Lüscher et al. 1997; Lüscher & Slesinger 2010).

The regulation of neurotransmitter release at presynaptic terminals is another important mechanism underlying the modulation of synaptic transmission in

the nervous system. Inhibitory regulation of neurotransmitter release occurs via $G\alpha_{i/o}$-coupled receptors such as GABA-B receptors, α2-adrenoceptors, adenosine A1, μ- and δ-opioid receptors, or endocannabinoid CB1-receptors. The Gβγ subunit of these receptors directly inhibits the presynaptic calcium channels to block action potential-evoked Ca^{2+} entry (Dolphin 2003). There is some evidence showing selectivity of inhibitory G-protein coupling to voltage-gated Ca^{2+} channels in the central nervous system (Ewald et al. 1989; Caulfield et al. 1994).

Finally, signalling via $G\alpha_O$ has also been implicated in vesicular glutamate transporter within the central nervous system (Winter et al. 2005) and GAP43 receptor signalling for neuronal path finding (Strittmatter et al. 1990).

1.4.2 Inhibitory G protein signalling in the RVLM

As described previously, there is a tonic GABAergic input to RVLM neurons which is mediated via CVLM neurones. GABA can mediate its inhibitory actions on the RVLM via the ionotropic GABA-A receptor or the $G\alpha_{i/O}$ linked metabotropic GABA-B receptor. The distribution Gα proteins in the rostral C1 cells of the RVLM, and the noradrenergic A1 and A5 groups of presympathetic neurones was studied by Parker et al (Parker et al. 2012). Using quantitative RT-PCR, the most ubiquitously expressed Gα proteins after $G\alpha_S$ were the inhibitory G proteins $G\alpha i_2$ and $G\alpha_O$. Both $G\alpha i_2$ and $G\alpha_O$ were found to be expressed in around 80%, 90% and 100% of C1, A1 and A5 cells respectively.

Initial studies focused on GABA-A mediated inhibitory mechanisms in the RVLM. Electrophysiological findings indicate that GABA exerts its inhibitory action on RVLM neurons preferentially via ionotropic GABA-A receptor activation. Pharmacological blockade of GABA-A receptors in the sympathoexcitatory region of the RVLM almost entirely eliminates the action of the caudal inhibitory vasomotor neurons and results in a large increase in sympathetic activity and blood pressure (Tagawa et al. 2000; Schreihofer et al. 2005). Conversely, bilateral microinjection of the GABA-A agonist,

muscimol, into the RVLM in anesthetized rats results in a large fall in mean arterial pressure, HR and sympathetic activity (Willette et al. 1983; Horiuchi & Dampney 1998; Fontes et al. 2001; Schreihofer et al. 2005), suggesting that GABA-A receptors mediate a powerful inhibitory input over RVLM neurons.

However, the discovery of specific, high affinity GABA-B antagonists (Dutar & Nicoll 1988) has led to an emerging body of evidence demonstrating its physiological role in the CNS (Misgeld, Bijak & Jarolimek 1995). In anaesthetised rats, iontophoresis of the GABA-B agonist, baclofen, inhibits RVLM bulbospinal barosensitive cells (Li & Guyenet 1995) and produces significant hypotension (Amano & Kubo 1993). Moreover, GABA-B receptor specific antagonists 2-hydroxy-saclofen and CGP-35348 were shown to induce a reversible increase in HR and BP when microinjected into the RVLM and were able to antagonise the depressor response of the GABA-B specific agonist baclofen but not the GABA-A specific agonist muscimol (Avanzino et al. 1994). These data suggest that the $G\alpha_{i/o}$ linked GABA-B receptor may play a role in the inhibitory signalling to the RVLM.

The α2a adrenoceptor, which also signals via $G\alpha_{i/O}$, is also expressed in the RVLM and at least in part mediates the hypotensive effect of centrally acting antihypertensive agents such as clonidine (Link et al. 1996, McMillan et al. 1996). Electron microscopy study using dual immuno-labelling of α2a adrenoceptor and tyrosine hydroxylase (TH) expressing cells in the RVLM have shown that α2a adrenoceptor is mainly expressed on non-catecholaminergic cells and may act as a heteroceptors providing inhibitory pre-synaptic input to C1 neurones of the RVLM (Milner et al. 1999).

Finally, inhibitory influence on the RVLM may also be mediated by adenosine A1 receptors (Thomas & Spyer 1996), δ opioid receptors (Hood & Woods 2004) and endocannabinoid CB-1 receptors (Li et al. 1995). It is likely that the co-expression of inhibitory ionotropic and metabotropic receptors in the RVLM allows for both phasic and tonic regulation of sympathetic output given the differences in receptor kinetics (Misgeld, Bijak & Jarolimek 1995). The different neurotransmitter and neuromodulators involved in inhibitory

signaling may also reflect the different synaptic inputs projecting to the RVLM as detailed above.

It is important to note that the concept of $G\alpha_{i/O}$ signaling at the RVLM as a purely restraining inhibitory influence on excitatory inputs maybe an overly simplistic one. For example, pre-synaptic inhibition of GABA-ergic inputs would result in disinhibition and an overall increase in RVLM discharge. This may in part explain the paradoxical excitatory actions of exogenously applied adenosine to the RVLM, which can be blocked by the ionophoresis of bicuculline, a specific GABA-A antagonist (Thomas & Spyer 1999).

1.4.3 In vivo evidence supporting the role of inhibitory G proteins and central nervous mechanisms of autonomic regulation of the heart

In vivo studies manipulating the expression of inhibitory G proteins and its subtypes either directly with knockout models or indirectly by manipulation of their regulatory proteins such as the RGS proteins have shed some light on their physiological importance and relative contribution to the central nervous control of the heart. Autonomic balance *in-vivo* has been quantified by indirect methods such as catecholamine sampling and analysis of HRV. The baroreceptor reflex is the prototypical cardiovascular reflex studied and its sensitivity is commonly assessed experimentally by computation of baroreflex set point and gain from ambulatory BP recordings, although more direct methods have been described (Young & Davisson 2011; Ma et al. 2002).

Interestingly, mice overexpressing RGS insensitive $G\alpha_{i2}$ were tachycardic during the daytime, have enlarged heart and increased contractile function on echocardiography. Along with reduced viability, growth retardation and multiple neurological deficits, the cardiovascular phenotype observed in these mice was attributed to increased central sympathetic tone (Huang et al. 2006). To study the cardiac specific effect of enhanced $G\alpha_{i2}$ signalling, isoproterenol-stimulated beating isolated perfused hearts of these mice were

studied and showed the expected enhancement of muscarinic mediated bradycardia (Fu et al. 2007).

Mice deficient in RGS_2 were found to be hypertensive but with normal HR suggestive of resetting of baroreceptor sensitivity. There was an associated increase in urinary catecholamine secretion and reduction in both low-frequency and high-frequency power of HRV suggesting increased central sympathetic tone (Gross et al. 2005). This along with data on the RGS insensitive $G\alpha_{i2}$ mice described above implies that overactivity of inhibitory G proteins may contribute to increased central sympathetic tone.

Albarran-Juarez et al studied the haemodynamic response of anaesthetized mice with global KO of $G\alpha_{i1}$, $G\alpha_{i2}$ and $G\alpha_{i3}$ receptor subtypes to the α_{2a} receptor agonist medetomidine (Albarran-Juarez et al. 2009). There was no difference in HR and BP response and correspondingly no difference in noradrenaline release from the prefrontal cortex or the cardiac atria suggesting functional redundancy of the receptor subtypes investigated in modulation of α_{2a} receptor signaling.

In Zuberi et al's study of a limited number of global $G\alpha_O$ knockout mice (Zuberi et al. 2008), in addition to the neurological abnormalities previously described, the mice were found to be tachycardic with loss of diurnal rhythm and fairly selective loss of the LF component of HRV with preserved total power. However, carbachol still had a negative chronotropic effect. This is suggestive of increased central sympathetic tone.

There hence appears to be a contradictory effect of over- and under-expression and function of inhibitory G proteins and its effect on sympathetic tone and central autonomic regulation of the heart. This is not surprising given the complex effects of inhibitory G protein signalling in the central autonomic circuits as described above and the global nature of the knockout models used in previous studies.

Mice with global deletion of a particular G protein often have reduced viability and are difficult to work with and it can be unclear at which level compromised signaling is contributing to the phenotype observed. Use of more refined temporal and spatial conditional deletion strategies would circumvent some of the problems and help define the relative role of inhibitory G proteins and its subtypes in the central and peripheral autonomic control of the heart. For example, by inducing conditional deletion of $G\alpha_O$ in the cardiac conduction tissue and central nervous system of the adult mice the developmental issues faced in global knockouts are circumvented. In addition, generation of mice with specific central autonomic phenotype would also allow the investigation of the role of central autonomic tone per se in mediating cardiac pathophysiology such as ventricular arrhythmia and circumvent the problem of compensation.

1.5 Summary

It is clear that actions of inhibitory G proteins and their associated RGS proteins at multiple levels play a critical role in the mechanisms of autonomic control on the activity of the cardiovascular system. There is also an emerging body of evidence demonstrating isoform specificity of these G proteins *in vivo*. $G\alpha_{i2}$ is implicated in mediating parasympathetic influences on the heart, most likely by coupling M2 receptors at the level of the conduction tissue of the heart.

What is less clear is their role in autonomic traffic in the central autonomic circuits. There is conflicting evidence with regards to G proteins specificity in the central nervous system and if so, the identity and location of the isoform which is important centrally.

From limited *in vivo* studies, it appears that inhibitory G proteins have an important role in mediating sympathetic tone to the heart, with loss of inhibitory G protein signalling resulting in increased sympathetic tone and sympatho-vagal imbalance and $G\alpha_O$ being implicated as possibly an important subtype in the central nervous system. There is a large body of evidence supporting the importance of the RVLM in autonomic regulation of the cardiovascular system and cardiovascular reflexes in health and disease states. The RVLM receives inhibitory inputs and there is evidence that inhibitory G proteins are involved.

We hence postulate that signalling via $G\alpha_O$ in the RVLM may be important in central autonomic regulation of cardiovascular control. For comparison, we would first study the role of $G\alpha_O$ signalling in the cardiac conduction tissue.

Cardiac excitability and susceptibility to arrhythmia appears to be influenced by the prevailing autonomic tone and is currently an area of intense clinical interest. Therefore we would also aim to study whether altered $G\alpha_O$ signalling in the RVLM also lead to alterations in cardiac excitability if it does indeed have an effect on autonomic regulation of cardiovascular control.

1.6 Hypothesis and aims

1.6.1 Hypothesis

$G\alpha_O$-mediated signalling within the presympathetic circuits of the rostral ventrolateral medulla oblongata (RVLM) but not in the cardiac conduction tissue, contributes to autonomic control of the heart. $G\alpha_O$ deficiency in the RVLM alters cardiovascular reflexes and electrical properties of the heart.

1.6.2 Aims

1. To determine the role of $G\alpha_O$-mediated signalling at the level of the cardiac conduction system in regulation of heart rate.

2. To determine the role of $G\alpha_O$-mediated signalling within the presympathetic circuits of the RVLM in the central nervous mechanisms of autonomic control of the heart.

3. To determine whether loss of $G\alpha_O$-mediated signalling within the presympathetic circuits of the RVLM leads to changes in cardiac excitability and predisposes the heart to ventricular arrhythmias.

In the following chapters, I shall first describe the methods used to generate mice with specific knockout of $G\alpha_O$ proteins in tissues of interest and the experiments used to profile their cardiovascular autonomic and electrophysiological phenotypes. I will then present and discuss the data obtained to address the aims stated above.

Chapter 2

Materials and methods

2.1 Introduction

2.1.1 The transgenic mouse model

Whilst *in vitro* methodologies such as patch clamping has contributed greatly to our understanding of molecular and cellular mechanisms of arrhythmia (Benians et al. 2003; Leaney et al. 2004), these technologies do not address how modification of cellular events affect 'complex' electrophysiological properties that occur in the setting of integrated animal physiology such as neuro-cardiac feedback within the autonomic nervous system. Transgenic technology allows for manipulation of gene expression and the study of cardiovascular physiology and pathophysiology at the molecular level in a whole intact organism, allowing a more integrated approach in the understanding of cardiovascular function compared to the 'reductionist' approach of studying cell and tissue cultures.

In this respect, the mouse has become the transgenic animal model of choice. Two complementary strategies are used to engineer the transgenic mice. The first approach involves injection of transgene constructs directly into the nucleus of fertilized single cell embryos. Thus the endogenous gene is not affected, and the expected phenotype will not be detectable unless the product of the transgene is dominant. In addition, neither insertion site nor copy number can be controlled and this can lead to insertional mutagenic events or atypically high levels of expression. An alternative method relies on homologous recombination of electroporated DNA sequences into pluripotent embryonic stem (ES) cells. The modified DNA sequence is inserted into the endogenous genetic site and replaced the normal sequence. The genetically modified ES cells are then selected out and introduced into blastocysts in order to generate chimeric embryos. Mice incorporating genetic modification into the germline then act as founders to transmit the engineered genetic modification into subsequent progeny. Although much more expensive and time consuming, the genetic event is precise and occurs at a single site, allowing for recessive mutations and null or site-specific mutant alleles to be studied under the control of the endogenous promoters (Yutzey & Robbins

2007). This approach has been applied extensively to study the function of G-proteins as most of them can be fully inactivated or human mutations can be incorporated into the mouse genome (Jiang et al. 1998; Boknik et al. 2009).

Limitations associated with these approaches are mainly due to the pluripotent nature of germline mutation resulting in the targeted defect being present in all cell types that express the gene (so called ‘global’ knock out or knock in). As a result, the resulting phenotype studied may not be solely due to genetic modification in the cells/tissue/organs of interest. In addition, as these mutated genes are expressed from the embryonic stage of development, long term compensatory changes/gene remodelling may potentially mask the role of a particular gene/protein of interest (gene redundancy) (Stieber et al. 2003) or in some cases result in embryonic lethality (Jiang et al. 1998).

To overcome these problems, temporal and spatial gene targeting approaches have been developed to produce genetic manipulation driven by promoters which are tissue and time specific. A commonly used technique to achieve this is the Cre-LoxP technology (Sauer 1998). Briefly, the gene of interest is flanked by LoxP constructs which in the presence of Cre recombinase enzyme results in deletion of the gene (Figure 2.1). Temporal and spatial specificity can then be achieved by targeted expression of Cre recombinase. Various approaches have been used to produce specific Cre recombinase expression such as using tissue specific promoters in combination with drug inducible constructs (Hoesl et al 2008; DeGeorge et al. 2008) and the use of viral vectors (Marina et al. 2011).

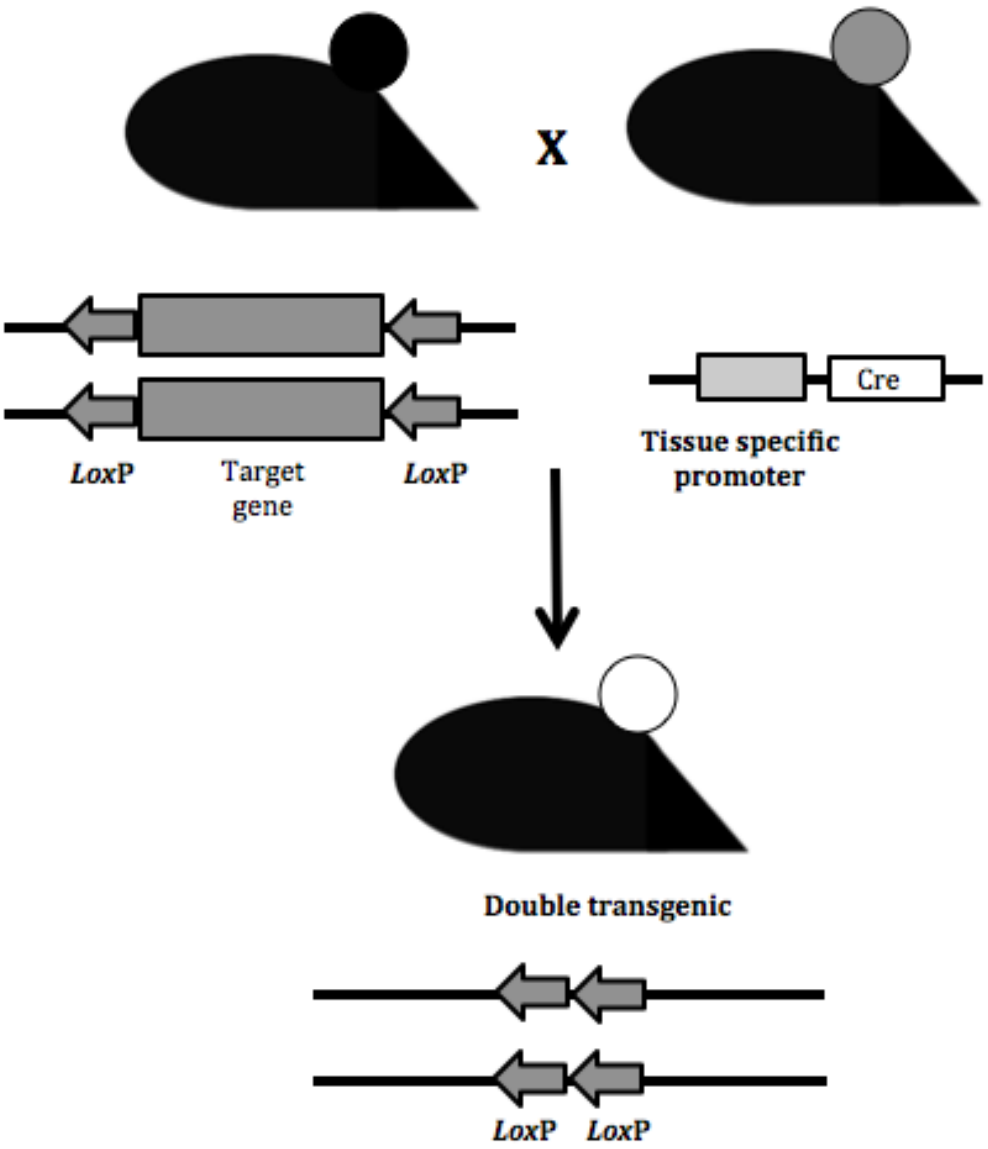

Figure 2.1 Conditional gene deletion by Cre recombinase

Crossing a loxP-modified mouse with a Cre transgenic generates a double-transgenic mouse in which the loxP-modified gene has been deleted in those tissues where Cre transgene has been expressed. In the diagram above, Cre is expressed in the ears (shaded) of the Cre transgenic so that deletion of the loxP-modified target gene is confined solely to the ears (white) of the double transgenic. Adapted from (Sauer 1998)

2.1.2 Autonomic and electrophysiological phenotyping of transgenic mouse models

Increasingly sophisticated methods of integrative physiological investigations and analyses have permitted the investigation of complex neurocardiac-regulatory and cardiac eletrophysiological processes in ways not possible before.

The central nervous system is important in both short- and long-term control of arterial BP. Many investigators have focused on the central mechanisms and brain regions involved in the neurogenic control of blood pressure as a way to study central autonomic regulation of the cardiovascular system. This involves direct and indirect methods of measuring arterial BP and baroreflex sensitivity (Young & Davisson 2011).

Electrophysiological phenotyping of transgenic mice has contributed significantly to our understanding of cardiac impulse propagation and arrhythmogenesis (Gehrmann & Berul 2000), complementing existing techniques of cellular imaging, patch clamping and molecular biology to give us a broad range of experimental tools to study cardiac electrophysiology.

Studying murine cardiac electrophysiology has required the miniaturization of instruments and techniques originally developed for human studies. These include the recording of surface electrograms, programmed electrical stimulation of the heart in the whole mouse and electrophysiological mapping in perfused mouse hearts.

Table 2.1 provides summary of the main experimental approaches currently used for the *in vivo* assessment of neuro-cardiac regulatory control and cardiac electrophysiological phenotyping in the mouse.

Modality	Technique	R	C	Notes	Pros	Cons
Electrocardiogram	Surface ECG electrodes	Yes	No	Needle electrodes placed on surface of chest to record surface ECG.	Cheap, readily available	Unable to obtain data from conscious freely moving animal
	Implantable telemetry probes	Yes	Yes	Small re-usable probes implanted into the subcutaneous space or peritoneal cavity. Can be used to record surface ECG or other biological parameters such as BP.	Data from conscious freely moving animal	Expensive. Need time for adequate recovery post surgery.
Programmed electrical stimulation	Transoesophageal catheters	Yes	No	Placement of bipolar electrodes in the oesophagus directly behind the atria allows for PES of the atria and induction of arrhythmia.	Able to repeat in recovered animal. Relatively cheap.	Large stimulus artefacts. Unable to study ventricle.
	Epicardial catheters	No	No	Placement of electrodes directly onto the epicardial surface of the atria and ventricle for PES and arrhythmia induction. Open chest surgery required.	Assessment of atria and ventricle. Relatively cheap.	Not recoverable. Very invasive and high mortality.
	Endocardial catheters	No	No	Placement of closely spaced multipolar electrodes endovascularly into the atrium and ventricle for PES and arrhythmia induction.	Less invasive. Assessment of all chambers.	Not recoverable. Technically challenging. Expensive.
Electrical mapping of the perfused heart	Optical dye mapping	No	No	Optical dye mapping in isolated Langendorff perfused heart	Highest spatial and temporal resolution.	Technically challenging. Use of exciation-contraction uncouplers may confound. Low sensitivity of the voltage sensitive dyes. In vitro conditions.
	Multi-electrode array	No	No	High density mapping using an array of closely spaced bipolar electrodes.	Direct recording of cellular electrical activity. Can combine with optical imaging (eg calcium imaging).	Expensive. Relatively lower spatial resolution. Limited array size.

Table 2.1 Summary of experimental methodologies for *in vivo* study of cardiac electrophysiology

Reviewed in (Young & Davisson 2011) and (Gehrmann & Berul 2000). R, Recoverable; C, Conscious experimental model (without use of any sedation or anaesthetic agents); PES, programmed electrophysiological stimulation.

2.1.3 Limitations

It is important to note that different mouse strains show considerable differences in baseline autonomic and electrocardiographic parameters (Wehrens et al. 2000; Waldeyer et al. 2009) and in processes such as baroreflexes and chemoreflexes in (Tankersley et al. 2000; Campen et al. 2004). Hence, it is important to use appropriate controls with similar genetic background in assessing the role of a genetically modified gene.

In addition, given the difference in body size, mass and basal metabolic rate, the cardiac index in mice is ten folds higher than in humans with resultant scaling of cardiac indices such as HR, stroke volume and blood volume although mean arterial pressure is the same (Janssen & Smits 2002). However, differences in murine cardiac physiology cannot be explained simply by scaling. For example, mice can only raise their maximum cardiac output over a small range whereas humans can increase theirs by a factor of 5-6. This is because murine heart is operating close to the maximum limit even at baseline (Kaese & Verheule 2012).

Although similar ion channels are expressed in mice and human hearts, their contributions to cardiac pacemaking and action potential morphology may also be different. For example, in the human ventricle, the rapid and slow delayed outward rectifier K^+ currents are predominantly responsible for phase 3 repolarization whilst in mice it is mediated by transient outward K^+ currents, a slowly inactivating K^+ current, and a non-inactivating steady state current resulting in much faster repolarization (reviewed in Kaese & Verhaule 2012).

It is hence important to take these differences into account when interpreting data obtained from mouse models.

2.1.4 Objectives

In this methods chapter, I aim to:

1. Describe the transgenic mouse lines developed and used, the strategies used to generate conditional knockout models in the heart and the brain, the PCR based genotyping method, the real time PCR method used for gene expression quantification, and immunohistochemistry techniques used.

2. Describe ECG and BP telemetry hardware and its application to study heart rate dynamics and BP profile under both physiological resting conditions and during pharmacological treatments.

3. Describe the methods of whole body plethysmography in conjunction with BP telemetry recordings to assess respiratory and cardiovascular responses evoked by hypoxic and hypercapnic stimuli.

4. Describe the methods of baroreflex sensitivity assessment in an *in vivo* anaesthetised preparations.

5. Describe the methods of programmed electrical stimulation of the heart to evaluate ventricular effective refractory period and susceptibility to ventricular arrhythmias.

2.2 Mice strains and generation of conditional knockout mice

2.2.1 Transgenic mouse lines and breeding strategy

Mice were maintained at the UCL animal core facility under the U.K. Home Office guidelines relating to animal welfare. All breeding programs and procedures were in accordance to the Animals (Scientific Procedure) Act 1986. All experimental work was covered by project licences 70/6732 and 70/6630 and personal licence PIL 70/23104.

All mice were kept in a temperature controlled environment (21-23°C) with 12hr day/12hr night light cycle. Animals were allowed access to standard rodent chow and water *ad-libitum*. Mice were studied between 10-12 weeks of age weighing between 20-30 grams.

The Cre/LoxP approach described previously (Sauer 1998) was used to target the gene of interest in mice. Mice on a Sv129 background with coding exons 5 to 6 of the $G\alpha_O$ allele on chromosome 8 (here on referred to as $G\alpha_O$ flx/flx) and exons 2 and 4 of the $G\alpha_{i2}$ allele on chromosome 9 (here on referred to as $G\alpha_{i2}$ flx/flx) flanked by loxP sites were obtained from our collaborator Professor Lutz Birnbaumer. These mice were initially generated using homologous recombination techniques in mouse ES cells. Gene targeting strategies and confirmation of selective deletion of $G\alpha_O$ and $G\alpha_{i2}$ at protein level from various tissues including the brain and the heart using western blot approaches have previously been published (Ustyugova et al. 2012).

2.2.2 Conditional gene deletion in the cardiac conduction tissue

The hyperpolarisation activated cyclic nucleotide gated cation channel (HCN4) gene codes for the channel responsible for pacemaker currents I_h/I_f and is expressed in cardiac conduction tissue with high specificity (Herrmann et al. 2011). Mice on a C57/Bl6 background expressing a tamoxifen inducible Cre driven by the HCN4 promoter (here on referred to as HCN4-KiT Cre)

were kindly donated by Professor Andreas Ludwig. Briefly, the tamoxifen-inducible CreER^{T2} construct was 'knocked in' into the pacemaker HCN4 locus. After administration of tamoxifen, highly selective and efficient recombination is triggered in the sinoatrial and atrioventricular node as demonstrated by Hoesl et al using western blot analysis and immunohistochemistry (Hoesl et al. 2008).This allows highly specific spatial and temporal (by timing tamoxifen administration) targeting of gene deletion in cardiac conduction tissue.

By intercrossing HCN4-KiT Cre with $G\alpha_O$ flx/flx mice, heterozygotes ($G\alpha_O$ flx/wt) mice containing the HCN4-KiT Cre transgene were produced. These were then crossed with $G\alpha_O$ flx/wt mice to obtain $G\alpha_o$ flx/flx HCN4-KiT Cre mice and all other genetic combinations were used as controls. $G\alpha_{i2}$ flx/flx HCN4-KiT Cre mice were derived using the same process.

To activate Cre expression in mice with the HCN4-KiT allele, tamoxifen (1mg/25g/day made up in sunflower oil, i.p.) was administered for 5 days and the experiments were performed after 10 days to allow for adequate Cre recombinase activity (Hoesl et al. 2008).

2.2.3 Targeting gene deletion in the central nervous system

Using a similar strategy as above, we sought a Cre line that is expressed in the central nervous system. Nestin is a class 6 intermediate filament primarily expressed by neural stem cells. It is expressed from day 7 of intrauterine development and is also expressed in other organs and tissues including striated muscle, cardiac muscle, the adrenals, and others (Gilyarov 2008). Due to a lack of a better alternative at the time, we compromised with this Cre line as an initial approach.

Mice on a C57/Bl6 background expressing Cre driven by the nestin promoter were obtained from the Jackson's Laboratory (ME, USA) (Tronche et al. 1999) and were crossed using a similar strategy as above to generate $G\alpha_o$flx/flx nestin Cre mice and controls.

2.2.4 Targeted gene deletion in the central nervous system using Cre expressing viral vectors

Due to limitations of the nestin Cre approach as discussed above, we used a parallel strategy with direct delivery of Cre expressing viral vectors to the brainstem. This allows precise spatial and temporal targeting.

Mice were anaesthetised with a mixture of ketamine (75 mg/kg, i.p.) and medetomidine (1 mg/kg, i.p.). Animals were placed in a stereotaxic apparatus (Kopf Instruments, CA, USA) in a prone position. The position of the head was adjusted in a flexed position and incision and blunt dissection was performed to expose the atlanto-occipital membrane. An incision was then made to the atlanto-occipital membrane to allow direct visualization of the calamus scriptorius, which was used as the reference point, and the viral vectors were delivered to the desired anatomical location.

Microinjections were made through glass micropipettes pulled through capillary tubing (WPI Inc, FL, USA) using a P-97 Flaming/Brown micropipette puller (Sutter Instruments, CA, USA) with the settings Pressure=500, Heat=500, Pull=50, Velocity=20 and Time=90. The tip of the glass micropipette was broken off using a Dumont 5-SF forcep (WPI Inc, FL, USA) and heat treated over a flame. Solutions were ejected using pressurized air delivered using a 10ml syringe and volumes determined by observation of movement of the fluid meniscus using a microscope fitted with an eye-piece graticule. Volumes injected were between 100 to 150 nanolitres delivered over 5 minutes per injection site. The co-ordinates used were determined in dedicated preliminary trials using microinjections of fluorescent beads with subsequent histological analysis to verify the sites of delivery and is detailed in Chapter 4.

The viral vector chosen was an adenoviral vector, Ad Cre/GFP, to drive the expression of Cre and green fluorescent protein (GFP) under the control of a cytomegalovirus (CMV) promoter (Cre/GFP AVV) (López et al. 2008). A similar adenoviral viral vector, VQAd CMVeGFP-2.6del, to drive the

expression of GFP only (GFP AVV) (LaVallie et al. 2006) was used as a control. Both viral vectors were purchased from Viraquest (IA, USA). Titres of the Cre/GFP AVV and control GFP AVV stock used were 6×10^{10} pfu and 3×10^{10} pfu respectively. The stock solution was diluted prior to the injections (titre of injected virus were determined in a separate set of experiments detailed in Chapter 4).

Anaesthesia was reversed with atipemazole (1 mg/kg, i.p.). The mice were studied 7 to 14 days after the injections as Cre expression should reach maximal in this period when AVV constructs are used (Haskell et al. 2003).

2.2.5 Genotype procedure

Mice were ear marked and tail tips (~2mm) were snipped with scissors after application of local anaesthesia by spraying with ethyl chloride and the samples were placed in 1.5 ml eppendorf tubes. Lysis buffer (150 µl; 3.35ml 2M Tris-HCL pH 8.8, 1.66ml 1M $(NH_4)_2SO_4$, 1.34ml 0.5M $MgCl_2$, 0.5ml Triton X-100, 92.2ml H_20, 1ml β-mercaptoethanol) was added and the samples were heated to 100^oC for 10 minutes to denature proteins. Samples were then cooled and 5 µl of proteinase K (20 mg/ml) was added at 55^oC for 12 hours to cause protein digestion. Samples were then re-heated to 100^oC for a further 10 minutes to terminate proteinase activity and then spun down at 10000 rpm for 5 minutes to sediment tail debris. For PCR genotyping 1-2µl of sample (containing genomic DNA) was used.

$G\alpha_O$ loxP (floxed allele) genotyping was performed using the following primers:

GNA_oF1B 5'- AAGAA TAGAA CCTAG GACTG GAGG - 3' and
GNA_oR 5'- GCAGA CAAGT GAACA AGTGA AACCC - 3'.

A hotstart PCR strategy was used to detect the presence of a 1868bp band corresponding to WT $G\alpha_O$, a 2142bp band corresponding to the $G\alpha_O$ loxP (floxed) allele and a 442bp band produced after Cre recombinase activation.

$G\alpha_{i2}$ loxP (floxed allele) genotyping was performed using the following primers:

$G\alpha_{i2}$LOXF 5’ – GGAGCCTGGACTTTGCTTCTGACC - 3’,
$G\alpha_{i2}$LOXR 5’- GGCTATGATCCCAAAACTCCCCG - 3’ and
$G\alpha_{i2}$LOXF2 5’- GTGGTAAGCCTGTGTGTTTGTGAGAG - 3’.

A hotstart PCR strategy was used to detect the presence of a 400bp band corresponding to WT $G\alpha_{i2}$, a 500bp band corresponding to the $G\alpha_{i2}$ loxP (floxed) allele using $G\alpha_{i2}$LOXF and $G\alpha_{i2}$LOXR respectively, and a 400bp band produced after Cre recombinase activation, using $G\alpha_{i2}$LOXF2 and $G\alpha_{i2}$LOXR.

Identification of HCN4-Kin Cre expression was determined using the following primers:

CreF 5’- ATGAC AGACA GATCC CTCCT ATCTC C - 3’ and
CreR 5’- CTCAT CACTC GTTGC ATCAT CGAC - 3’.

The presence of the Cre transgene was determined by the presence or absence of a 300bp band.

Identification of nestin Cre expression was determined using the following primers:

oIMR1084 5’- GCGGT CTGGC AGTAA AAACT ATC - 3’ and
oIMR1085 5’- GTGAA ACAGC ATTGC TGTCA CTT - 3’,

The presence of Cre transgene was determined by the presence or absence of a 100bp band.

This is summarised in Figure 2.2.

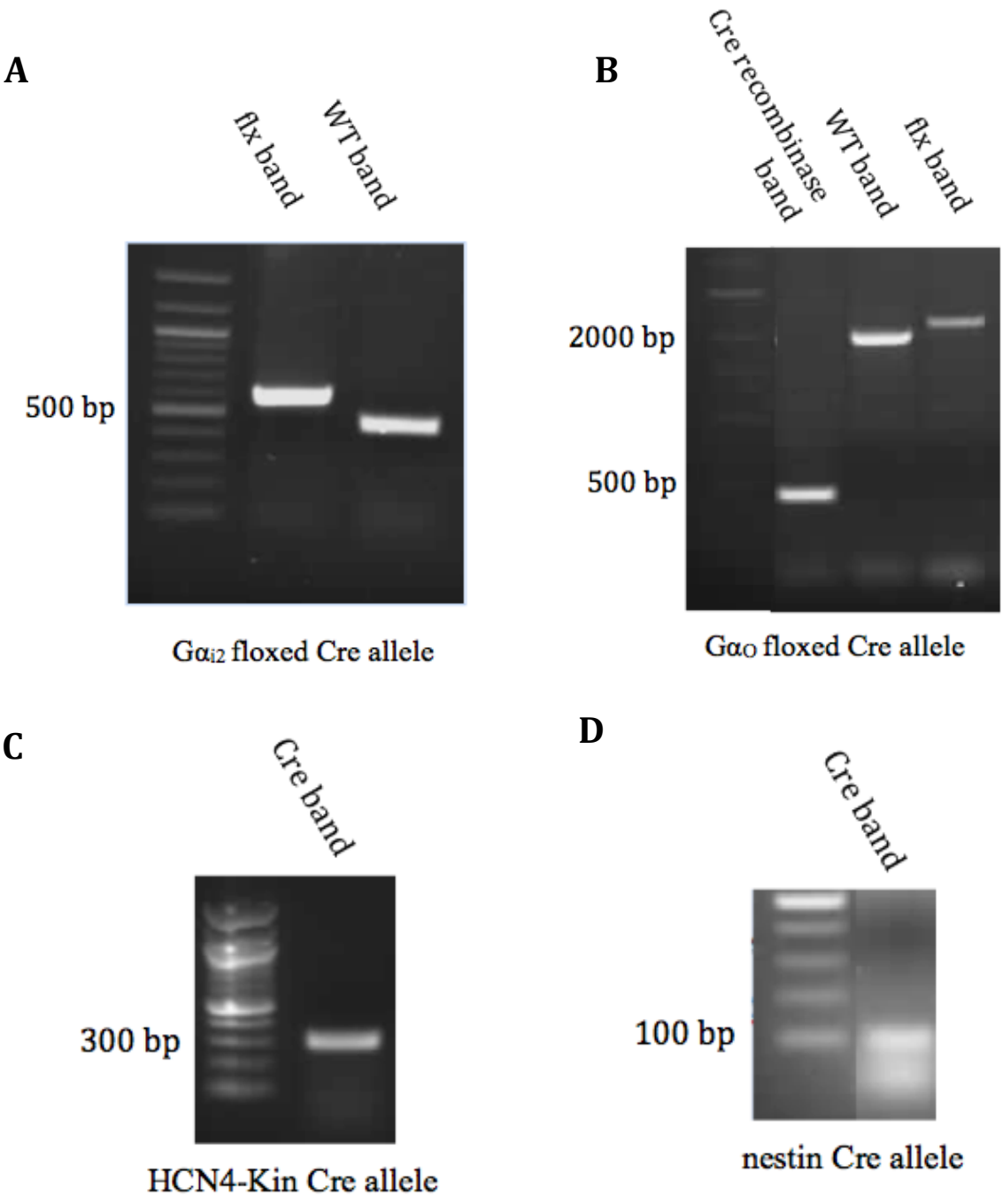

Figure 2.2 PCR products identified during genotyping procedure

(A) $G\alpha_{i2}$ floxed Cre mice; (B) $G\alpha_{O}$ floxed Cre mice; (C) HCN4-Kin Cre mice and; (D) nestin Cre mice.

2.2.6 Quantification of gene expression in tissues by quantitative real time PCR (RT-PCR)

Mice were terminally anaesthetised (ketamine, 100mg/kg, i.p.; xylazine, 10mg/kg, i.p.), tissues under study were harvested and immediately immersed in RNA*later* solution (600 µl) (Qiagen, CA, USA). RNA was then extracted using the RNAeasy Mini Kit (Qiagen, CA, USA) and converted to cDNA using the high capacity RNA-to-cDNA reverse transcriptase kit (Applied Biosystems, CA, USA). Quantitative PCR (qPCR) was then performed on the cDNA samples using the TaqMan gene expression assay kit (Applied Biosystems, CA, USA) with primers directed to exon 5 of $G\alpha_O$, exons 2 to 3 of $G\alpha_{i2}$ and GAPDH, which was chosen as the reference house-keeping gene. Relative gene expression was quantified using the comparative C_T method (Schmittgen & Livak 2008).

For mice injected with Cre/GFP and GFP AVV viral constructs in the brainstem, the location of injection was confirmed by the presence of green fluorescence near the ventral surface of the brainstem (visualized using 395nm light) and the tissue was then punch biopsied with a Uni-Core device (core diameter 1.25mm; Harris, USA) and processed as described above. Further details and images are provided in Chapter 4.

2.2.7 Immunohistochemistry

Mice were perfused transcardially with 0.9% NaCl solution followed by 50 mL of 4% paraformaldehyde (PFA). Brainstems were then removed, post-fixed for 12 h in 4% PFA at 4°C and cryoprotected in 30% sucrose. Medulla oblongata was sectioned using a freezing microtome, and a series of coronal sections (30 µm) was collected and stored in an anti-freeze solution at -20°C for subsequent histological processing. Sections were immunostained for detection of tyrosine hydroxylase (TH; marker of catecholaminergic neurones). Tissue was incubated in sheep anti-TH antibody for 24 h (1:250; Abcam, Cambridge, UK). Secondary antibodies were donkey anti-sheep

Alexa Flour 568 (1:1000; Invitrogen, CA, USA). The slices were examined and images were taken using a confocal microscope.

2.3 ECG and BP telemetry in conscious mice

Surface ECG and arterial BP recordings were obtained from mice using surgically implanted telemetry devices (Data Sciences International, MN, USA). Using this technology, continuous ECG and BP measurements can be obtained in freely moving animals, removing potential confounders of animal restraint and anaesthesia, under normal physiological conditions, following drug provocation or under hypoxic/hypercapnic conditions in a plethysmography chamber.

ECG signal reflects the electrical potential difference between two adjacent electrode pairs. This bio-potential signal was sampled at 2000Hz from electrode pairs placed in an ECG lead II configuration and transmitted to a receiver mat by radio-wave and digitised using the PowerLab platform (ADInstruments, Dunedin, NZ). Commercially available software (Dataquest ART v3.0, Data Sciences International, MN, USA and LabChart Pro v4.0, ADInstruments, Dunedin, NZ) was used to analyse ECG recordings to obtain ECG parameters including PR, QRS and corrected QT intervals. Heart rate (HR) was calculated from the R-R interval, and heart rate variability (HRV) was derived by fast fourier transformation (FFT) analysis of HR over a pre-determined time period (described in more detail below).

Systemic arterial BP was continuously sampled at 2000Hz by gel filled catheters with the tip placed in the aorta. Systolic, diastolic and mean arterial blood pressures were obtained. HR was also obtained from the intervals between systolic peaks, although these measurements are not as accurate as that obtained from ECG tracings.

2.3.1 General surgical preparation

Surgery was performed in mice of at least 20g in weight, as survival was found to be compromised in smaller animals. Anaesthesia was induced with 5% isoflurane entrained with oxygen-enriched air and then maintained with 1.7% isoflurane delivered via a nose cone. Analgesia (10mg/kg Rimadyl [Carprofen], i.p, Pfizer Animal Health, NY, USA) and prophylactic antibiotics (5uL 1% enorfloxacin, i.p.) were given. The mice were then secured with a masking tape in a supine position on a sterile drape rested on a heating mat set to support animal's body temperature at ~37°C. The area of incision was swabbed with 70% ethanol solution as disinfectant. The mice were then draped and surgery was then carried out in an aseptic manner. After the surgery, 200-300μL of warm 0.9% NaCl solution was given i.p. for post-operative hydration. The mice were then returned to their individual cages placed on warming mats for surgical recovery. Additional analgesia was administered 8-12 hourly after the surgery as necessary.

2.3.2 Implantation of the ECG telemetry probes

A midline laparotomy was performed, with the skin, muscle layer and peritoneum carefully divided by blunt dissection with due care to haemostasis throughout. A murine telemetry probe (model TA-F20, Data Sciences International, MN, USA) was then placed in the abdominal cavity taking care not to disturb or compress bowel loops or other visceral organs. Attached to the main probe housing are two insulated electrodes and the device was implanted within the peritoneal cavity with the leads exiting the body of the device in rostral direction. Two small stab incisions were made within the peritoneal membrane either side of the midline incision to allow for the extrusion of the electrodes out of the peritoneal cavity and the peritoneal membrane was sutured close. Two further incisions were then made in the overlying skin of the chest, one in the anterior right shoulder position and another near the cardiac apex to allow for placement of the ECG leads in a lead II configuration. The ends of the electrodes were cut to an approximate length to allow for placement of the positive lead near the right shoulder and

the negative lead at the level of the cardiac apex. A small sheath of insulation was removed from the electrode tips to expose the wire within. The leads were then subcutaneously tunnelled from the abdomen to their respective positions and the bare wire of the electrode tips was sutured onto the exposed chest wall muscle, ensuring good contact with the tissue. All incisions were then closed with interrupted sutures.

2.3.3 Implantation of the BP telemetry probes

A midline anterior cervical incision was made and the underlying salivary glands were carefully parted by blunt dissection. The left sternocleidomastoid muscle was then retracted to expose the left carotid artery. The left carotid artery was carefully dissected out and 2 silk ties were placed at the cranial and caudal end of the artery. The artery was tied off at the cranial end just distal to the bifurcation and blood flow in the artery was transiently occluded by gentle retraction of the tie sling at the caudal end. The carotid artery was then cannulated with the gel-filled catheter of the BP telemetry probe (model PA-C10, Data Sciences International, MN, USA) and the tip of the catheter was slowly advanced by about 5 mm (so that the tip of the catheter was placed within the aorta) and the catheter was then carefully secured. A subcutaneous pocket was then created in the abdomen and the body of the probe was then tunnelled into this pocket via the same cervical incision. The wound was then closed.

2.3.4 Serial HR/BP measurements and circadian rhythm

All animals were allowed to recover for a minimum of 10 days prior to recording (Thireau et al. 2007). Experiments were performed in a temperature-controlled environment (21-23°C) with 12hr/12hr light/dark cycle and the animals were allowed to acclimatise to the experimental conditions for at least 48 hours prior to experiments. Housing cages were placed onto receiving mats and telemetry probes were turned on with the aid of a magnetic wand. For serial HR/BP measurements, 15s samples were taken every 30 minutes over 2 days using a ‘scheduled sampling’ protocol. From

this data set, it was possible to evaluate diurnal changes in HR/BP between day and night and also calculate the mean HR/BP. HR can be derived from BP recordings by the following equation:

HR= 60000/pulse interval (interval between successive systolic peaks in milliseconds)

2.3.5 Assessment of heart rate variability

Heart rhythm shows beat-to-beat variations between successive R-R intervals and is largely due to autonomic modulation of the pacemaker activity of the sino-atrial node. Heart rate variability (HRV) is the measure of such R-R interval variability and can be used as a non-invasive measurement of autonomic tone, and can be used specifically to determine the parasympathetic contribution to HRV (Wickman et al. 1998). Measurement of HRV has prognostic implications (Stauss 2003).

HRV recordings were taken between 12-2 pm only (during “lights on” to simulate daylight). Mice being nocturnal animals are active during the night and rest/sleep during the day. Therefore, we determined HRV during ‘midday’ in order to evaluate heart rate dynamics at a time when parasympathetic tone is expected to be highest.

Changes in R-R intervals were assessed from ECG tracings continuously streamed over 20 minutes (divided into ten 2 min-long epochs) at 2000Hz. Data was then imported into LabChart v4.0 (ADInstruments, Dunedin, NZ) and analysed using a HRV analysis extension module. Raw tracings were carefully inspected and recording artefacts were manually removed. A threshold R-wave-sensing algorithm was then applied to detect all R-R intervals. Ectopic beats were defined as those that were 2 times above or below the average R-R interval; these beats were excluded from the analysis, while averaged or interpolated beats were not used to replace them. The data set of consecutive R-R intervals (typically over 12000 sinus beats per recording) was then mathematically analysed both the linear time and

frequency domains, as has been applied by others to analyse HRV in the mouse (Ecker et al. 2006, Gehrmann et al. 2000; Uechi et al. 1998).

2.3.6 Time domain analysis

Time domain measurements (Table 2.2) determine simple variance of R-R intervals over the entire length of recording. Although relatively simple, time domain analysis has been equated prospectively with clinical outcome in man (Nolan et al. 1998).

2.3.7 Frequency domain analysis

Frequency domain analysis was performed using fast fourier transform (FFT) using 1024 spectral points and a half overlap within a Welch window. Conversion of R-R intervals by FFT produces a power spectral density (PSD) plot which reports frequency ranges (x-axis) plotted against the total number of events occurring at a particular individual frequency (y-axis).

Frequencies previously demonstrated to be accurate for the analysis of mouse ECG were used to divide signal into three major components, very low frequency (VLF < 0.4 Hz), low frequency (LF 0.4–1.5 Hz), and high frequency (HF 1.5–4.0 Hz), which are scaled up 10x from frequencies used in humans (Gehrmann et al. 2000, Just A et al. 2000). Variability for individual frequency components is determined by integral sum of the area under the curve between pre-specified frequency cut-offs and is also described as the 'power' of the respective frequency ranges. Normalization to exclude VLF was also performed. Normalized low frequency (nLF) = LF/(TP-VLF) x 100 and normalized high frequency (nHF) = HF/(TP-VLF) x 100.

There has been controversy regarding the physiological significance of the different frequency bands. In humans, there is general acceptance that the HF component is reflective of parasympathetic tone modulating HR variation with respiration and LF component reflects combined sympathetic and parasympathetic influences (Pagani et al. 1986, Malliani et al. 1991, Stauss

et al. 2003). Guidelines recommending standard HRV analysis techniques have been established for humans in (Task Force of the European Society of Cardiology and the North American Society of Pacing and Electrophysiology 1996).

The data available in mice however appears conflicting. Experiments using pharmacological challenges and transgenic methods have shown that attenuation of parasympathetic tone or increase in sympathetic activity leads to a general decrease in power across the spectral range including both HF and LF components (Gerhmann et al. 2000, Uechi et al. 1998). Wickman et al studied HRV in GIRK4 knockout mice with loss of vagal mediated GIRK channel function and found selective loss of LF power (Wickman et al. 1998). Interestingly, in these studies mice were found to have little or no resting vagal tone and high resting mean HR (ranging from 580 to 724 beats per minute). All mice were studied less than 1 week after surgical instrumentation.

In contrast, a number of studies have shown selective loss of HF component with attenuation of parasympathetic tone (Baudrie et al. 2007, Just et al. 2008, Zuberi et al. 2008). Mice were allowed to recover for greater than a week and it was noted that they have significant resting parasympathetic tone and lower resting mean HR (ranging from 400 to 662 beats per minute) compared to studies described above.

It is hence important to interpret HRV data in the context of experimental conditions. Variables including surgical recovery time, sampling time and duration, housing conditions and ambient temperature can all affect autonomic tone and resulting HRV parameters (Thireau et al. 2007, Swoap et al. 2008). Frequency domain indices used in this study are summarised in Table 2.3 and have previously been validated (Zuberi et al. 2008).

Variable	Unit	Statistical measure
SDNN	ms	Standard deviation of all NN intervals.
SDANN	ms	Standard deviation of the averages of NN intervals in all 5 min segments of the entire recording.
RMSSD	ms	The square root of the mean of the sum of the squares of differences between adjacent NN intervals.
SDNN index	ms	Mean of the standard deviations of all NN intervals for all 5 min segments of the entire recording.
SDSD	ms	Standard deviation of differences between adjacent NN intervals.
NN50 count		Number of pairs of adjacent NN intervals differing by more than 50ms in the entire recording. Three variants are possible counting all such NN intervals, pairs or only pairs in which the first or the second interval is longer.
pNN50	%	NN50 count divided by the total number of all NN intervals.

Table 2.2 Time domain indices of HRV analysis

Summary of indices obtainable using time domain analysis for heart rate variability (HRV). NN is the normal-to-normal intervals between successive QRS complexes during sinus rhythm obtained during a continuous ECG recording. Adapted from (Malik et al. 1996).

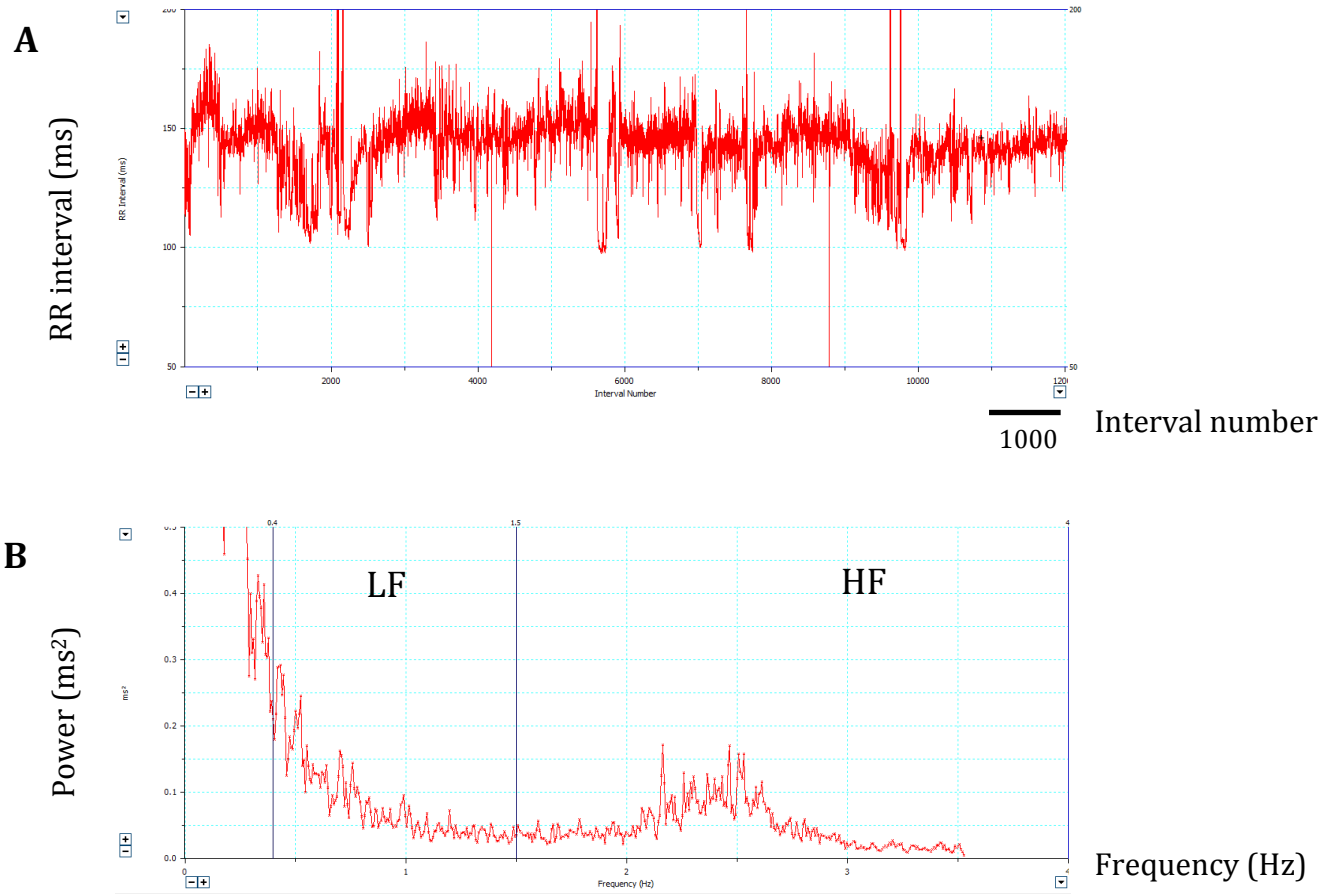

Figure 2.3.1 Representative plot of RR interval against time and power spectral density transformation

Screenshots showing (A) plot of RR interval against time and (B) power spectral density transformation. The R-R interval data set is converted into frequency domain by fast fourier transform to generate a power spectral density plot. Characteristic frequency peaks can be seen in both the LF (0.4-1.5 Hz) bandwidth and in the HF (1.5-4.0 Hz) range. The HF band is a selective marker of parasympathetic tone.

Power (ms^2)	Frequency range (Hz)	Interpretation
Total Power (TP)	<4.0	Total variability over all defined frequency ranges
Very Low Frequency (VLF)	<0.4	Significance unclear in the mouse
Low Frequency (LF)	0.4-1.5	Combined sympathetic and parasympathetic influence
High Frequency (HF)	1.5-4.0	Parasympathetic modulation

Table 2.3 Frequency domain indices

Table summarises the frequency bandwidths obtained from power spectral density analysis used in this thesis.

2.3.8 Pharmacological manipulations

Pharmacological manipulations to antagonize or activate parasympathetic and sympathetic influences were employed to determine their relative contributions to the modulation of heart rate and heart rate dynamics. Table 2.4 summarises the drugs and doses used. All drugs were administered intra-peritoneally between 12 to 2 pm. The prevailing autonomic tone is dependent on the time of day with vagal tone highest during the daytime when mice are resting. This specific period was chosen for drug administration to standardise experimental conditions at a time when murine vagal tone should be highest.

HR and BP recordings were taken before and after administration of the compounds, as described previously. A baseline of 30 minutes recording was obtained prior to administration of a particular drug and a further 60 minutes recording was then obtained after the drug was given. The raw traces obtained before and after drug administration were manually inspected. An average over 5 minute of stable recording was taken for the baseline and an average over 5 minute during the peak effect after administration of the drug was taken as the post drug reading (Figure 2.3.2).

Drug	Dose	Route	Mode of action
Carbachol	0.5mg/kg	ip	Muscarinic M2 receptor agonist
2-Chloro-N6-cyclopentyladenosine (CCPA)	0.1mg/kg	ip	A1 receptor agonist
Atropine	0.5-1 mg/kg	ip	Non-specific muscarinic receptor antagonist
Propranolol	1 mg/kg	ip	Non-specific β adrenoceptor antagonist
Atenolol	1 mg/kg	ip	β adrenoceptor antagonist which is more selective for β1 receptor

Table 2.4 Drugs used for pharmacological manipulation of autonomic influences to the heart

Summary of drugs used for pharmacological manipulations to antagonize or activate parasympathetic and sympathetic influences to the heart. ip, intraperitoneal.

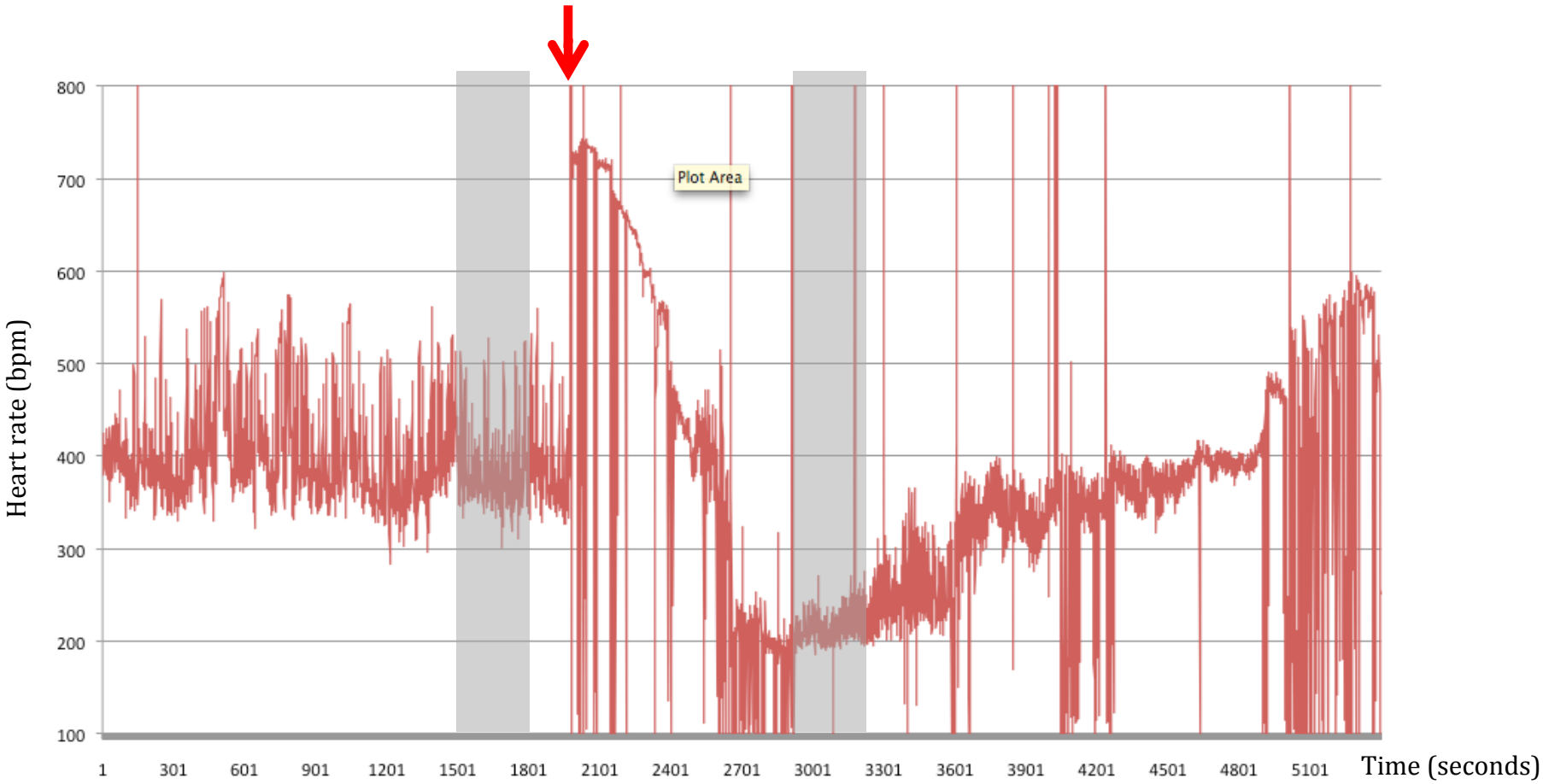

Figure 2.3.2 HR response to pharmacological challenge

A representative raw tracing obtained from ECG telemetry recording of HR plotted over time before and after pharmacological challenge with carbachol 0.5mg/kg ip. Red arrow indicates time of drug administration. Note stress-induced increase in HR when animal is handled during drug administration. Shaded areas represent intervals where averaged values of HR pre and post drug administration were obtained.

2.4 Whole body plethysmography

Mice with telemetry probes implanted were also subjected to hypoxic and hypercapnic conditions and respiratory rate (f_R, breaths minute^{-1}) and tidal volume (V_T, ml kg^{-1}) were measured by whole body plethysmography as described in detail previously (Onodera et al. 1997; Rong et al. 2003). Simultaneous continuous recordings of BP, HR, f_R and V_T data during hypoxic and hypercapnic challenges were obtained.

All experiments were performed at room temperature (22-24°C). The mouse was placed in a Plexiglass recording chamber (~200ml) that was flushed continuously with a mixture of 79% nitrogen and 21% oxygen (unless otherwise required by protocol) at a rate of ~1 L min^{-1}. Concentrations of O_2 and CO_2 in the chamber were monitored on-line using a fast-response O_2/CO_2 monitor (Morgan Scientific, MA, USA). The plethysmography chamber was placed on top of a telemetry receiving mat and simultaneous telemetry data was obtained as described above. Figure 2.4.1 shows the experimental set-up used.

The animals were allowed at least 20 minutes to acclimatise to the chamber environment at normoxia/normocapnia (21% O_2, 79% N_2 and <0.3% CO_2) before measurements of baseline ventilation and BP telemetry data were taken. Hypoxia was induced by lowering the O_2 concentration in the inspired air down to 10% for 5 minutes. After 5 minutes, the O_2 concentration was then brought back up to 21% for a further 5 minutes. In separate experiments, normoxic hypercapnia was induced by titrating CO_2 into the respiratory mixture up to a level of 3% or 6% (lowering N_2 accordingly) for 5 minute at each CO_2 level.

The chamber pressure signal was amplified, filtered and recorded and analysed offline using the Spike 2 software (Cambridge Electronic Design, Cambridge, UK). The measurements of f_R and V_T were taken during the last 2 minutes before exposure to the stimulus and during the 2 minute period at the end of each stimulus, when breathing has stabilized. Hypoxia- or

hypercapnia- induced changes in the f_R, V_T and minute ventilation (V_E) ((f_R x V_T)/1000; L min^{-1} kg^{-1}) were averaged and expressed as means ± SEM. Similarly, the BP and calculated HR data measurements were taken during the same time intervals, averaged and expressed in the same manner.

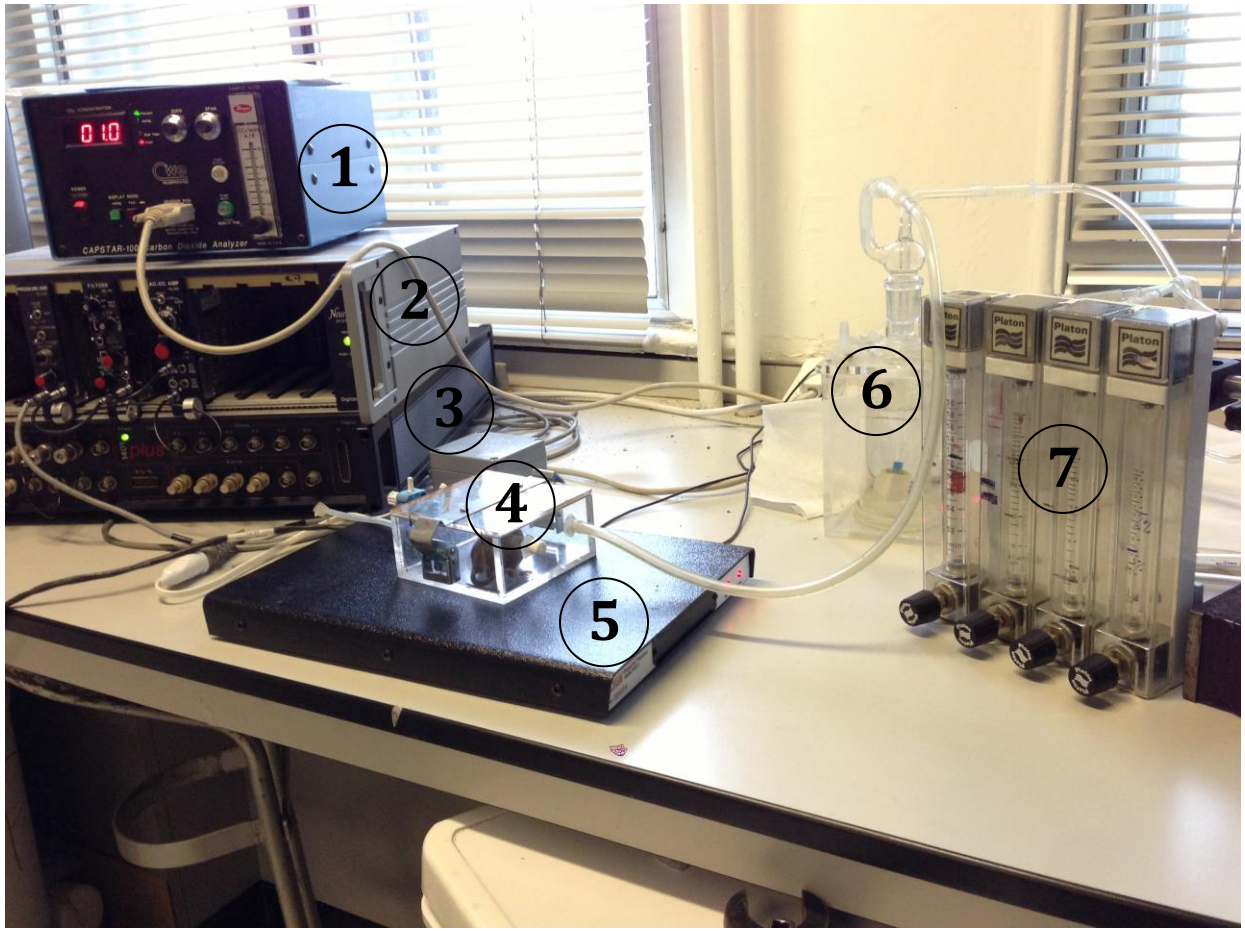

Figure 2.4.1 Plethysmography experimental set-up

From left to right; 1. CO_2 analyser; 2. Signal digitiser, amplifier and filter; 3. 1401 interface console; 4. Plexiglass plethysmography chamber; 5. Telemetry receiver mat; 6. Gas humidifier chamber; 7. Gas mixer.

2.5 Anaesthetised *in vivo* preparations

Mice were anaesthetised with urethane (1.3 mg/kg i.p.) and the depth of anaesthesia was monitored using the stability of BP, HR, and lack of flexor responses to a paw-pinch with supplemental doses of anaesthesia given as required. Body temperature was maintained at 37.0±0.2°C using a servo-controlled heating pad. Needle electrodes were placed in a lead II configuration to record surface ECG (sampled at 2 kHz, amplified x50-100, and filtered to a bandwidth between 5 to 100 Hz with 50Hz notch filtering).

A cervical midline incision was performed and trachea was cannulated with polyethylene tubing (PE-90) to facilitate ventilation in spontaneously breathing mice. For the assessment of baroreflex sensitivity, the right and left internal jugular veins were cannulated with polyethelene tubing (PE-10) for administration of test drugs. The left internal carotid artery was cannulated with saline filled polyethylene tubing (mechanically stretched PE-10 connected to PE-50) connected to a pressure transducer to measure the arterial blood pressure (sampled at 2kHz).

In some mice undergoing *in vivo* cardiac electrophysiological studies, the 1.1 french size EPR-800 catheter (described below) was introduced into the heart via the right internal jugular vein with the tip of the catheter located at the right ventricular apex. Correct placement of the catheter tip was confirmed by the presence of ventricular signals recorded from the distal electrical bipoles of the catheter.

2.6 Analysis of baroreflex function

Two main methods to determine the baroreflex sensitivity in man and experimental animal models which include analysis of contributions from all the arterial baroreceptors are the ramp and the steady state methods. The ramp method estimates the slope of the reflex sensitivity from a linear fit of a unidirectional fast ramp change in arterial BP, usually assessed by injecting a vasopressor drug (Smyth et al. 1969). However, there are limits to the extent

HR can be altered by changes in the arterial BP which is not recognized by this method. Ultimately, HR reaches a plateau and changes in the slope can occur from movement of the basal BP-HR point in relation to this plateau. The second, steady state approach takes into consideration the change in slope of the baroreflex curve as HR reaches plateau in response to both increases and decreases in BP. By extending the limits of BP changes in both directions from the basal value this method describes a sigmoidal relationship between changes in HR and BP. The advantage of this method is that the slope is estimated from the centre of the curve and is therefore independent of changes to basal HR. In addition, it provides information about the effector responses i.e. the contributions of both the sympathetic and the parasympathetic influences (Head & McCarty 2002). A modification of the steady state protocol developed by Head and McCarty was used.

Changes in systemic arterial BP were induced by boluses of phenylephrine (0.5-2.5 mg kg^{-1} iv in 2-10 µL normal saline) or sodium nitroprusside (0.1-1 mg kg^{-1} iv in 1-10µL normal saline). The drugs were administered by varying the volume of injection delivered via two separate venous catheters in the left and right internal jugular veins respectively. Using this method, the need to flush the catheter was avoided and very small volumes of injectate were used to minimise the effect of volume on the haemodynamic response.

After surgical preparation as described above, the animal was allowed to stabilize over a 30-minute period. Randomly selected doses of the two drugs were then sequentially given to evoke increases in arterial BP (with phenylephrine) followed by BP decreases (with nitroprusside). The doses of both drugs were adjusted to produce changes in BP that were small (5-20 mmHg), medium (21-35 mmHg) or large (36-50 mmHg) with sufficient time between injections to allow both BP and HR to return to baseline. Increases in blood pressure greater than 50 mmHg were avoided as this can evoke vagal bradycardia, which has been shown (in rabbits) to involve cardiac rather than arterial baroreceptor activation (Hood & Woods 2004).

Data were recorded using a 1401 interface and Spike 2 software. The peak changes in arterial BP and HR were determined following application of each drug and in total, 10-15 data points were obtained across the range of BP-HR for each the animal (Figure 2.6.1). The changes from basal values (ΔBP-ΔHR) were then calculated for each pair of data points and scaled back to absolute BP and HR by the average of all basal values recorded. This allows for best fit as described by Head et al (Head & McCarty 2002).

The data points were then fitted to the following logistic equation with MatLab R2010b (MathWorks, MA, USA) using a least squares interative routine developed by Varuna De Silva at University of Surrey (Appendix A):

$$\mathbf{HR} = P1 + P2 / [1 + e^{P3(\mathbf{BP}-P4)}]$$

where P1 = lower HR plateau, P2 = HR range, P3 = a curvature coefficient which is independent of range and P4 = BP_{50}, i.e. the BP at half the HR range. The average baroreflex gain (BRG) or slope of the curve between the two inflection points is given by BRG = -P2 ×P3/4.56 and the upper plateau = P1 + P2 (Figure 2.6.2).

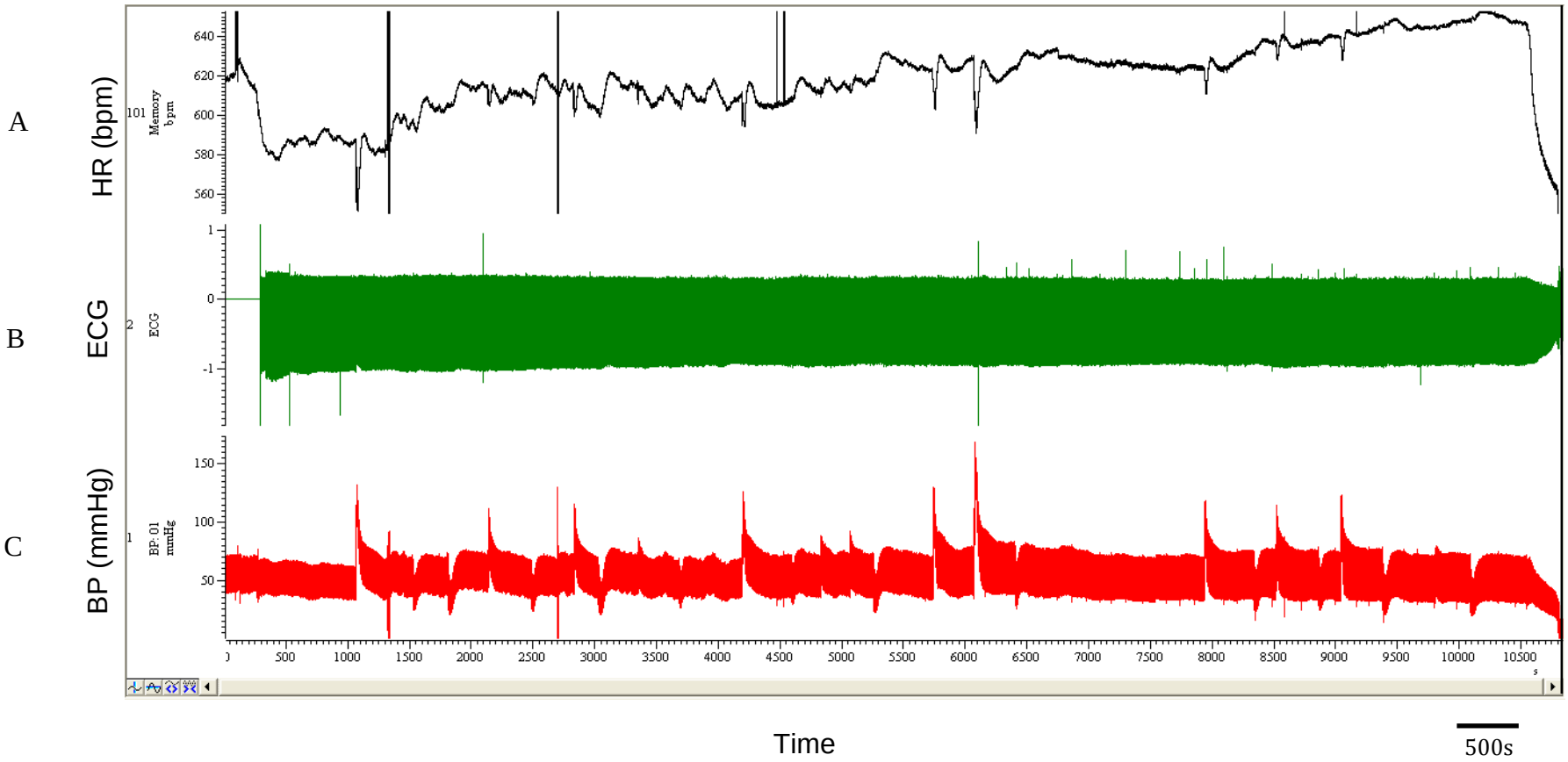

Figure 2.6.1 Tracings obtained from urethane anaesthetised *in vivo* preparation used to determine baroreflex function

Screenshot of tracings obtained during urethane anaesthetised *in vivo* preparation. From top to bottom (A) HR averaged over 10 seconds derived from RR interval of ECG trace; (B) ECG trace obtained from surface electrode; and (C) arterial BP trace obtained invasively from a fluid filled cannula in the right internal carotid artery over time in seconds. The peaks and troughs on the arterial BP trace follows alternating administration of intravenous phenylephrine and sodium nitroprusside.

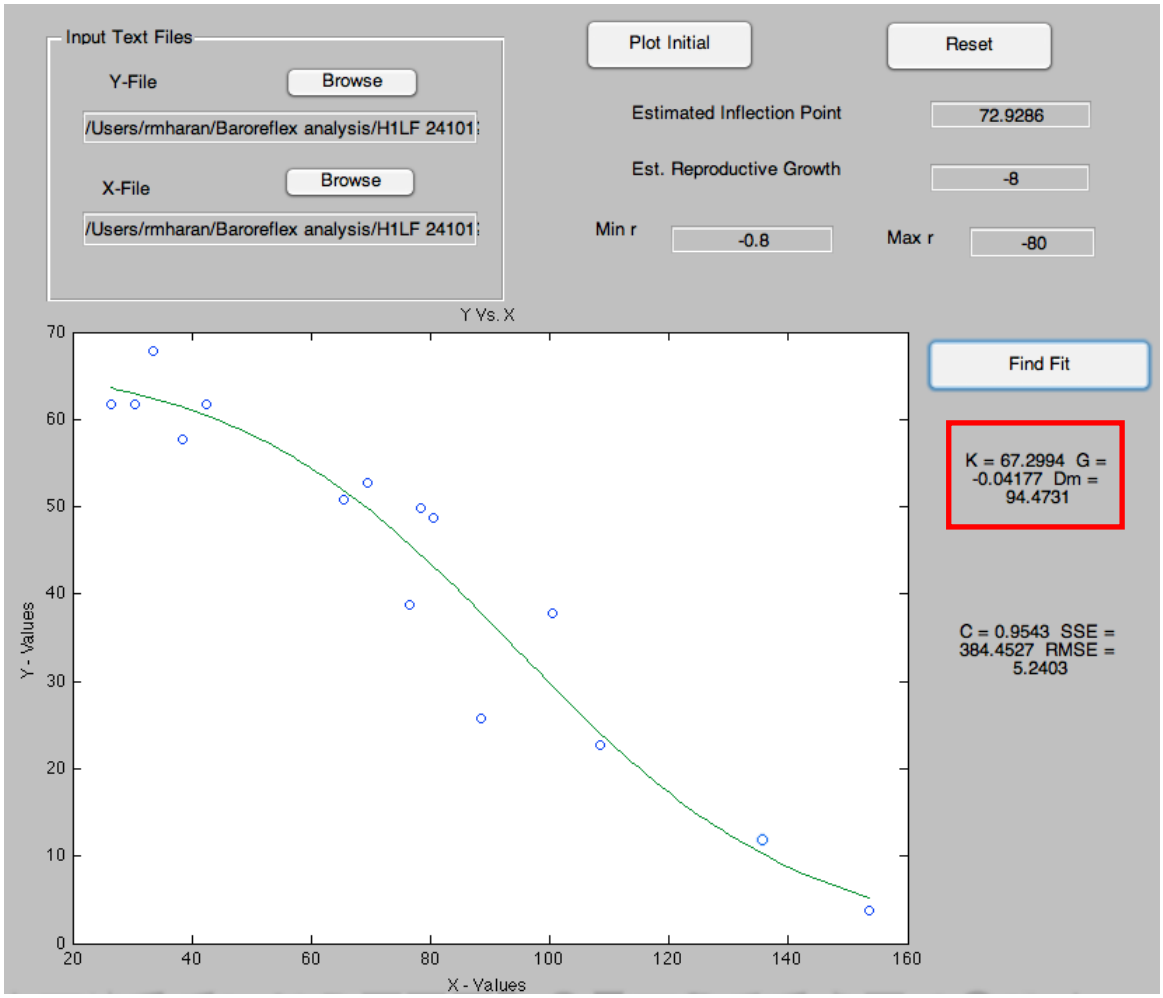

Figure 2.6.2 Derivation of baroreflex curve

Screenshot of MatLab program used to derive a best fit sigmoidal curve to the HR and BP data points obtained from the urethane anaesthetised *in vivo* preparation. The Y axis represents HR-HR $_{min,}$ and the X axis represents arterial systolic BP. The program solves for the equation y = K./(1+exp(-G*(x-Dm))) with the solution shown in the red box. The baroreflex gain (BRG) or slope of the curve between the two inflection points is hence given by BRG= -K x G/4.56.

2.7 *In vivo* cardiac programmed electrical stimulation

The minimally invasive cardiac electrophysiological (EP) assessment is a procedure performed in clinical cardiology and involves the placement of electrophysiological catheters capable of recording and delivering electrical stimuli directly onto cardiac endo- or epicardial surfaces.

Cardiac pacing can be performed where an external electrical stimulus is applied directly to the myocardium adjacent to catheter between the electrode bipoles. The electrical current delivered can be modulated by the voltage and pulse duration. When sufficient energy is delivered (i.e. when 'threshold' is reached), localised myocardial depolarisation will occur (i.e. 'electrical capture') and an electrical wavefront can then spread via cardiac gap junctions from the field of stimulation to the rest of the heart. Provided the pacing stimulus rate is faster than the intrinsic heart rate, externally controlled cardiac pacing will occur.

Pacing at different locations within the heart can provide important information regarding cardiac conduction and electrophysiological properties. Cardiac pacing can also be delivered in a programmed manner (programmed electrical stimulation, PES) where a basic pacing train delivered at a fixed interval is then supplemented with one or multiple extra stimuli at progressively shorter intervals.

The cardiac EP study protocols and PES have recently been adapted by our laboratory (Zuberi et al. 2010) to study *in vivo* cardiac electrophysiology in transgenic mice following earlier work by other groups (Gehrmann & Berul 2000; Kovoor et al. 2001). The recording system is based on the Powerlab platform (Figure 2.7.1). All electrical inputs are delivered to the Powerlab receiver hardware, which shows a multichannel display of various inputs on the Labchart v4.0 software interface. Surface ECG signals in the lead II configuration are filtered and amplified using an amplifier (BioAmp). Intracardiac electrograms are recorded using an EPR-800 electrophysiological catheter (ADInstruments, Dunedin, NZ). EPR-800 has 8

equally spaced electrode poles and each pole is attached to an individually insulated micro-wire with a unique input/output connection. Pacing generated by the S88 Grass stimulator (Grass, USA) can also be delivered using the EPR-800. Two separate bipole recordings can be obtained simultaneously or one bipole can be used to record an intracardiac signal whilst the other pair is used to deliver pacing. Recordings are filtered and amplified using a separate dual Bioamp connected to the Powerlab device. When correctly placed within the right heart, the distal poles of the catheter are in the right ventricle whilst the more proximal poles are in the right atrium and this can be seen from the recorded local intracardiac electograms (Figure 2.7.2).

2.7.1 Invasive cardiac electrophysiology study protocol

Once suitable catheter position is obtained the S-88 stimulator is turned on and pacing is attempted. When reliable electrical capture is obtained, the stimulator output voltage is reduced whilst keeping the pulse duration fixed at 10 ms until capture is lost and then voltage is increased incrementally until reliable capture is obtained again. This is the threshold (the minimum output required for reliable capture) and pacing output is then set at twice the pacing threshold voltage to ensure reliable electrical capture throughout the study (Figure 2.7.3).

Next, cardiac pacing protocol is performed. I am interested in studying the electrical properties of the ventricular myocardium, specifically changes in the ‘excitability’ of the myocardium following autonomic manipulations. For this purpose, the ventricular effective refractory period (VERP), which is defined as the minimum coupled cycle length at which ventricular pacing (at a rate of 750 bpm/ cycle length of 80 msec) can no longer result in ventricular capture as the ventricular myocardium is in a refractory state. A train of 10 S1 pulses with a cycle length of 86 msec is delivered followed by an S2 impulse at the end of the S1 train. The interval between S1-S2 was progressively shortened until the point at which pacing fails to produce ventricular capture (Figure 2.7.4)

Finally, a ventricular tachycardia (VT) stimulation by burst pacing was performed in order to determine susceptibility of the myocardium to ventricular tachycardia (VT) or ventricular fibrillation (VF) (Maguire et al. 2003). This was achieved by delivering a train of 15 S1 beats at increasingly shorter intervals from 80 ms to 50 ms (12.5 to 20 Hz) in 5 ms increments. A successful study was defined as induced VT that consisted of at least 4 consecutive QRS complexes with different morphology to that recorded in sinus rhythm (Gellen et al. 2008). In some cases, we were also able to detect dissociation of ventricular and atrial electrograms from intracardiac electrograms as an additional marker of VT (Figure 2.7.5).

A

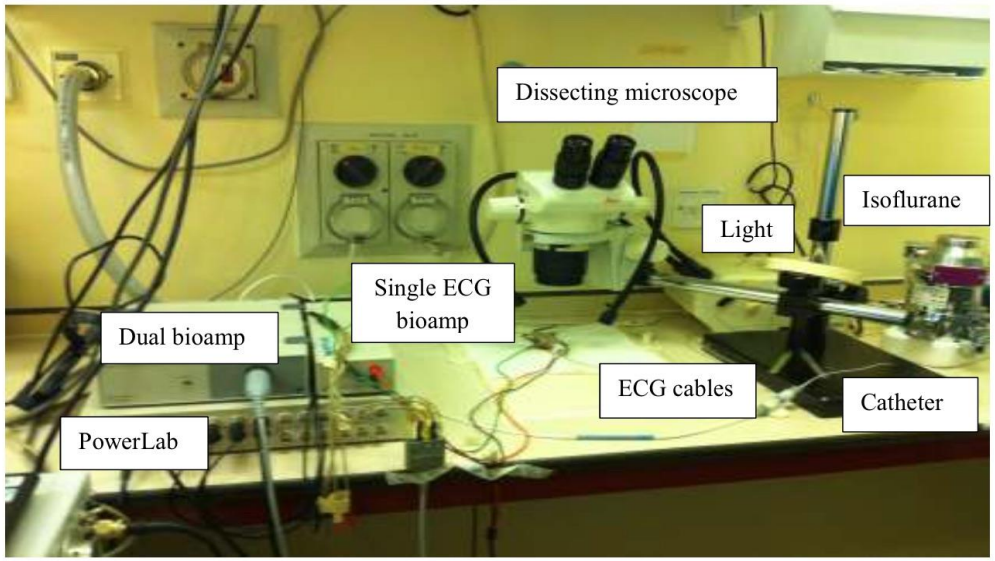

B

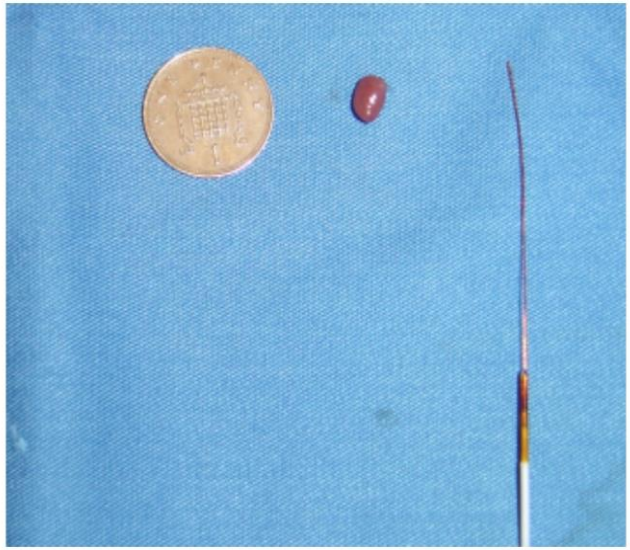

Figure 2.7.1 Equipment used for programmed electrical stimulation

A. Bench set-up for programmed electrical stimulation. B. Close up of EPR-800 octapolar electrophysiological catheter next to a 1 pence coin and a murine heart for size comparison.

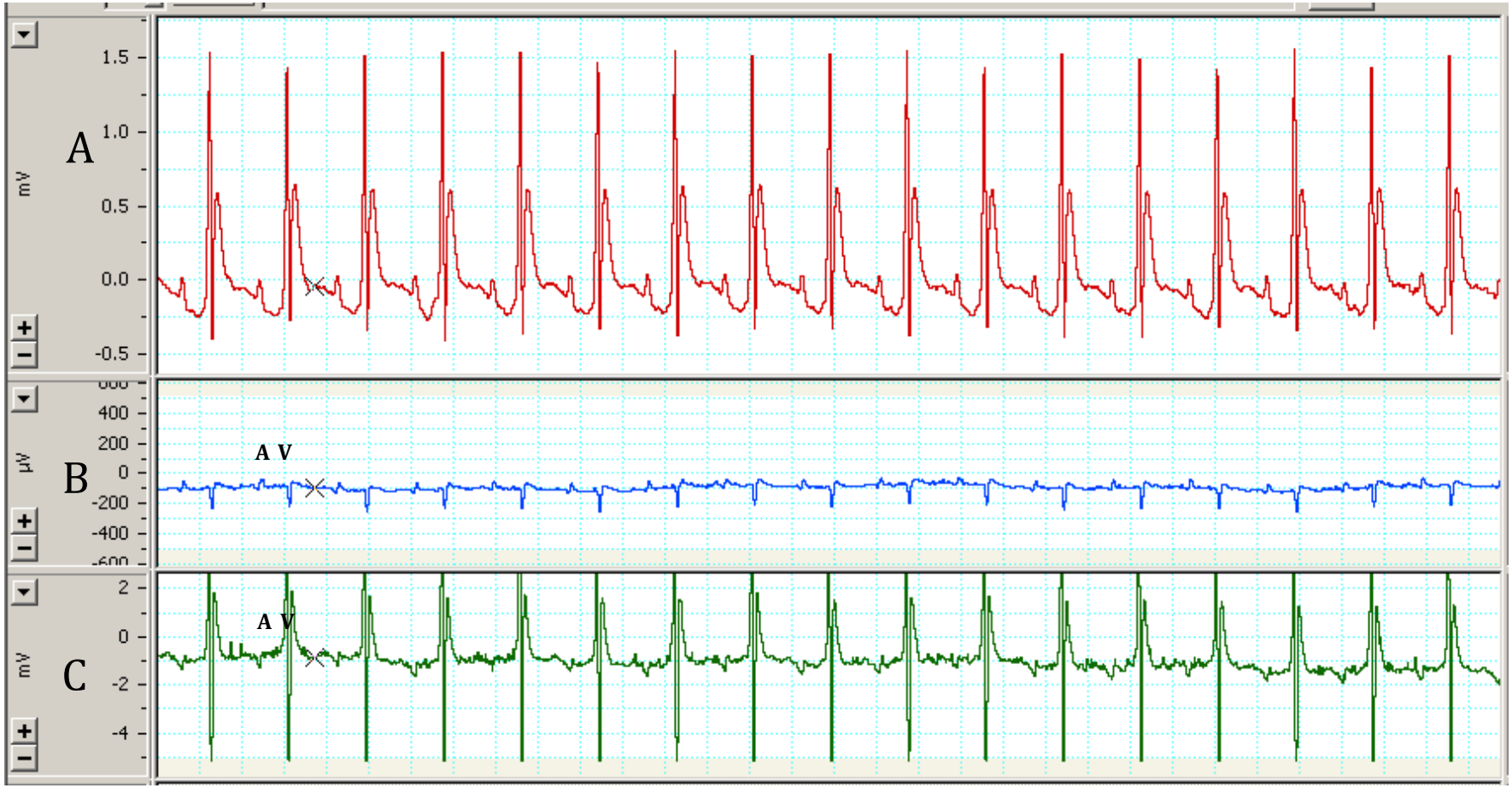

Figure 2.7.2 Intracardiac electrograms showing correct placement of electrodes in the right heart

Screenshot showing: (A) Surface ECG; (B) Atrial (**A**) and ventricular (**V**) electrograms in the proximal poles and; (C) Much larger local **V** electrograms seen in the distal pole.

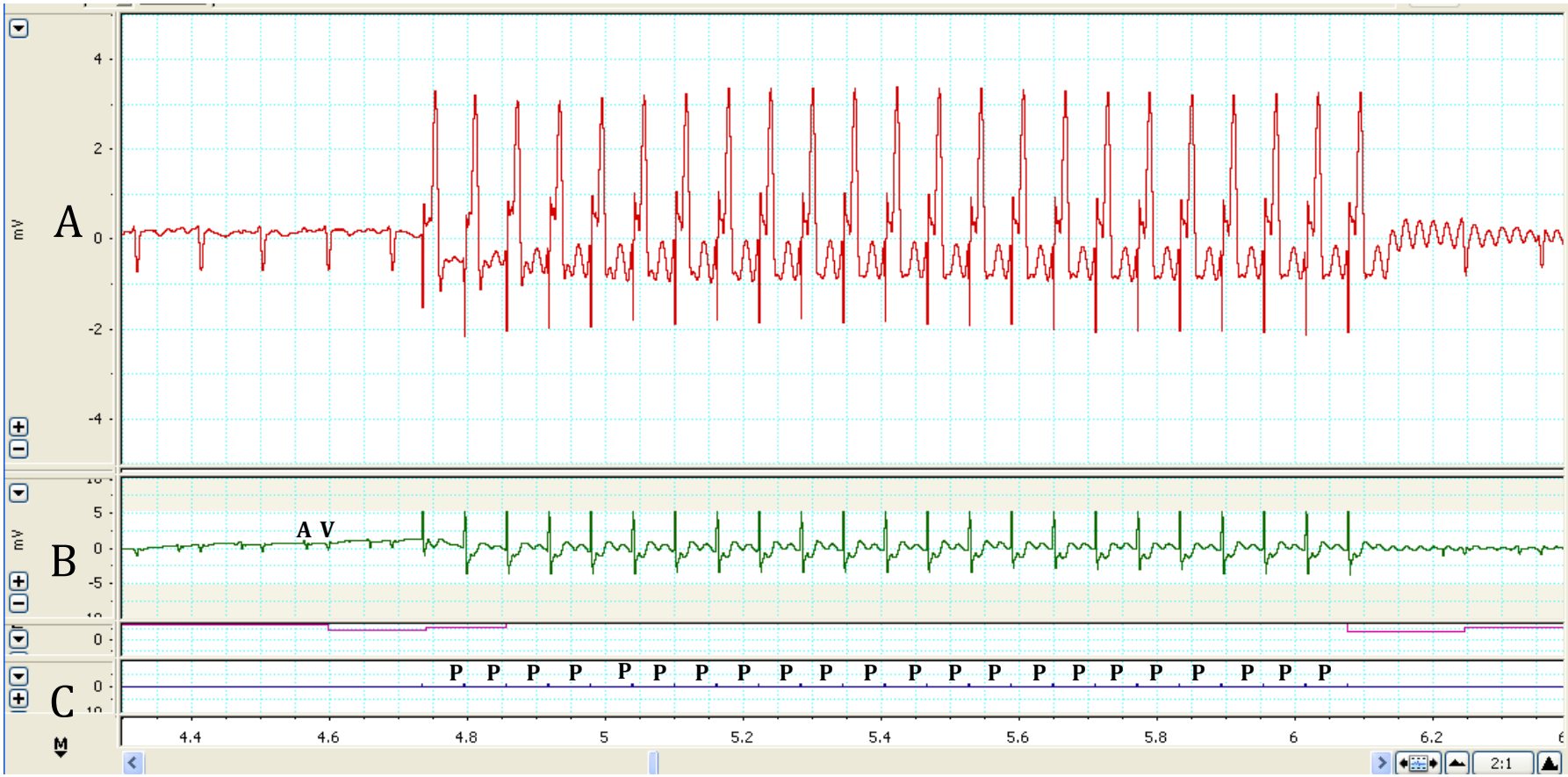

Figure 2.7.3 Intracardiac electrograms during right ventricular pacing

Screenshot showing: (A) surface ECG; (B) Atrial (**A**) and ventricular (**V**) electrograms in the proximal pole. (C) Trace showing delivery of pacing (**P**) stimuli. The distal pole of the catheter is used to pace the right ventricle and ventricular capture can be seen on the surface ECG with broad QRS complexes and also on the recorded local electogram.

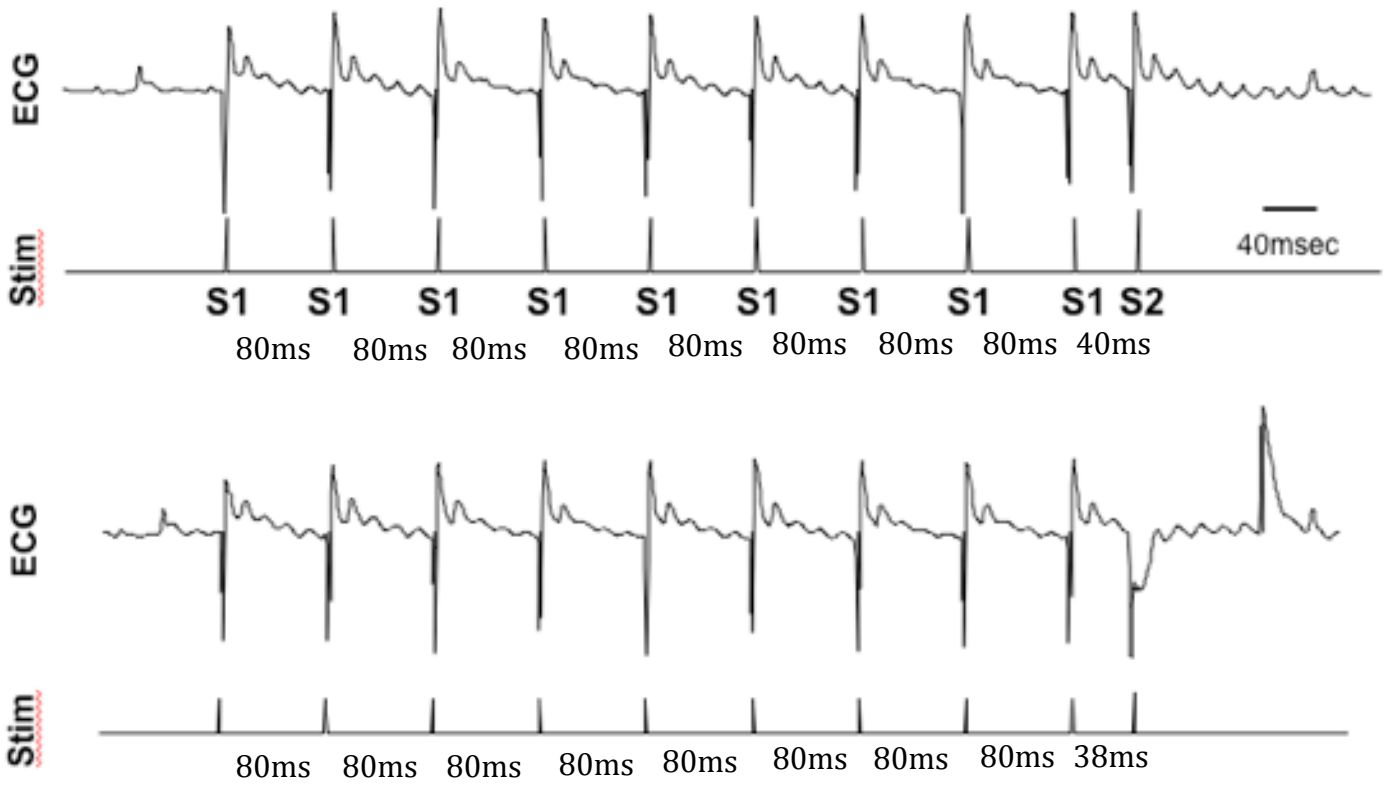

Figure 2.7.4 Determination of ventricular effective refractory period (VERP)

A train of 9 S1 beats (coupling interval 80ms) is delivered followed by an S1-S2 coupling interval of 40ms which still captures the ventricle. The S1-S2 is then further shortened to 38ms. The S2 now fails to capture the ventricle. VERP at 80ms coupling interval, or 750bpm, steady state pacing (expressed as $VERP_{750}$) is hence 38ms.

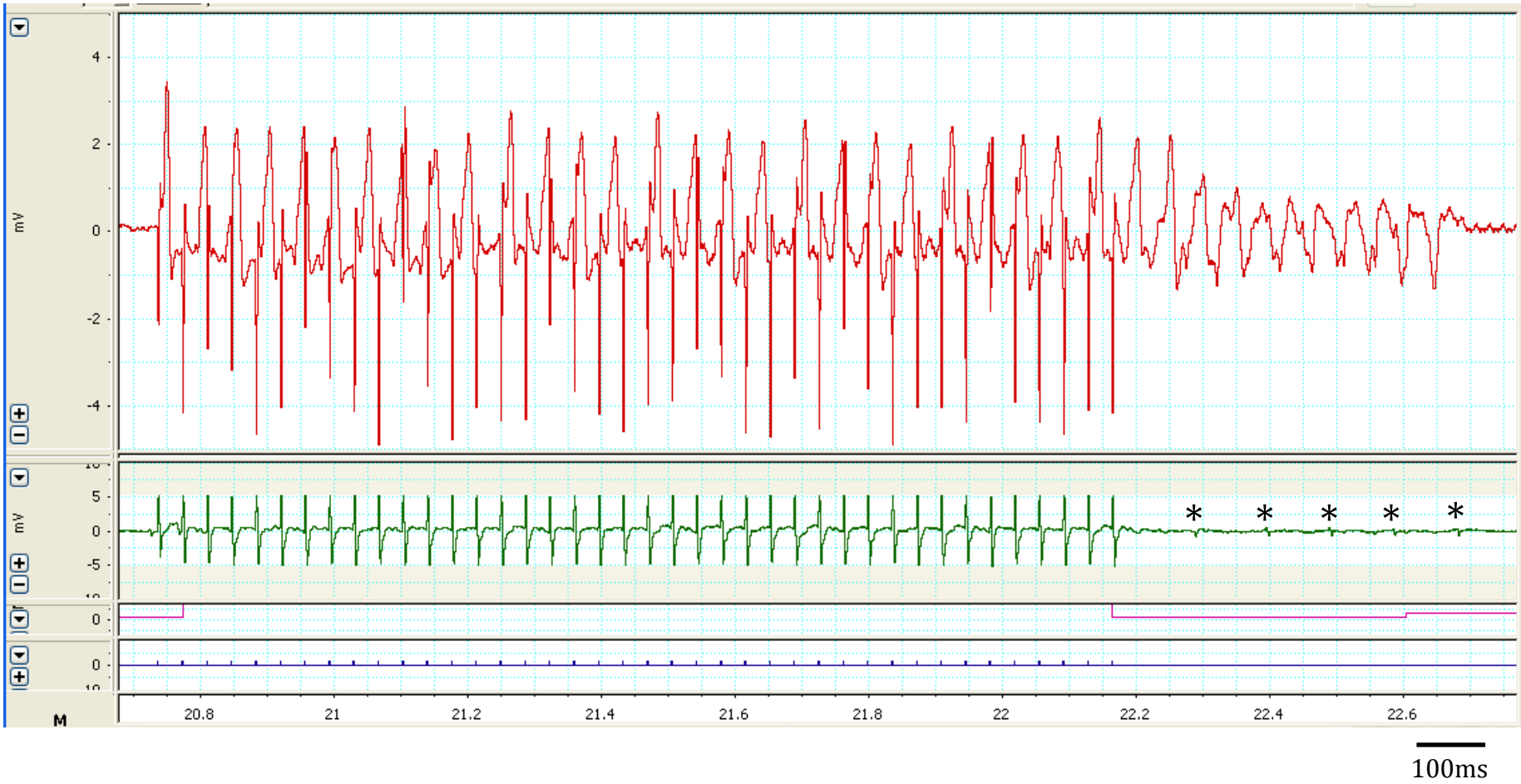

Figure 2.7.5 Burst pacing protocol to determine ventricular tachycardia threshold

An example of burst pacing at 20 Hz from the right ventricle used to induce VT. The induction protocol results in polymorphic ventricular tachycardia. Evidence of AV dissociation can be seen from the regular atrial activation (marked with *) signal recorded simultaneously from the right atrial intracardiac electogram.

2.8 Statistical analysis

Data are reported as means ± standard error of measurement (SEM) unless stated otherwise. For determination of statistical significance between groups, 2 tailed Student's *t* tests were used for parametric data with a normal distribution and the Mann-Whitney U Test was used for non-parametric data. Data with repeated sampling between groups was analysed using analysis of variance (ANOVA) with post-hoc Kruskal-Wallis test to estimate the difference between groups. For data with repeated sampling between multiple groups of unequal sizes or in the presence of missing values, mixed modelling using both fixed and random effects was used to compare the mean effect of each group. All statistical computation was performed using SPSS version 21 (IBM, NY, USA). In all instances, $P<0.05$ was considered significant.

Chapter 3

Results I

$G\alpha_{i2}$ and not $G\alpha_{O}$ protein mediates parasympathetic influences on cardiac conduction tissue

3.1 Introduction

As discussed in Chapter 1, pacemaker setting in the SAN is thought to be an interplay between a membrane and a calcium 'clock'. The membrane 'clock' involves cyclical depolarisation generated by HCN channels (also known as I_f/I_h), whilst the calcium 'clock' involves the cyclic release of Ca^{2+} from intracellular stores via ryanodine receptors, increasing inward sodium-calcium exchanger currents during diastolic depolarization (Lakatta & DiFrancesco 2009).

Vagal input via M2 receptor activation slows down the rate of SAN depolarization by inhibiting AC, leading to a reduction in cAMP level which in turn inhibits the I_f/I_h channel. Reduced cAMP level also leads to negative modulation of downstream effectors such as intracellular Ca^{2+} handling pathways for example phospholamban and the ryanodine receptor, resulting in reduced cycling of intracellular Ca^{2+}. In addition, the free Gβγ subunit released from $G\alpha_{i\backslash o}$ directly activates the GIRK channel leading to membrane hyperpolarization. These responses are all predicated on signaling via the inhibitory $G\alpha_{i\backslash o}$ but current evidence supporting these pathways is largely based on ex-vivo studies of the sinoatrial node and pacemaker cells (Monfredi et al. 2010).

There is currently limited *in vivo* data available on the physiological role and the molecular identity of the inhibitory G protein subtype(s) responsible for mediating parasympathetic influences on the SAN. Previous study using mice with global knockout of $G\alpha_{i1/3}$, $G\alpha_{i2}$ and $G\alpha_O$ genes have showed altered autonomic regulation of HR, but only in mice with global $G\alpha_O$ and $G\alpha_{i2}$ deletions (Zuberi et al. 2008). The relative contribution of these G protein subtypes to autonomic regulation of the SAN activity remains unknown.

In this chapter, I present and discuss the results of the experiments aimed to address the relative contributions of $G\alpha_O$ and $G\alpha_{i2}$-mediated signaling on the activity of SAN and by extension on autonomic regulation of heart rate. Conscious freely moving mice with conditional deletion of $G\alpha_O$ and $G\alpha_{i2}$ in

the conduction system of the heart were used to determine the role of these subunits. Heart rate profile and dynamics were recorded over a 48-hour period, and heart rate responses to autonomic blockade were determined.

3.2 Cardiac conduction tissue specific deletion of $G\alpha_O$ and $G\alpha_{i2}$

$G\alpha_O$ flx\flx HCN-KiT Cre+, $G\alpha_{i2}$ flx\flx HCN-KiT Cre+ (here on referred to as $G\alpha_O$ floxed conduction Cre and $G\alpha_{i2}$ floxed conduction Cre, respectively) mice and their littermate controls were generated. Tamoxifen (1mg/25g/day, i.p.) was administered as previously described. RNA was then extracted from the SAN and ventricular tissues 10 days post administration of tamoxifen and quantitative RT-PCR performed to confirm selective deletion of the respective gene in the cardiac conduction tissue only. Measurements obtained in these mice were normalized to the expression of levels detected in control mice (both after administration of tamoxifen) in the ventricle and the SAN.

There was a significant reduction in relative $G\alpha_O$ and $G\alpha_{i2}$ expression in the SAN but not the ventricle ($G\alpha_O$ floxed conduction Cre SAN relative expression compared to WT = 0.27 (95%CI 0.17- 0.45) ventricle= 0.86 (95%CI 0.71-1.04), and $G\alpha_{i2}$ floxed conduction cre SAN relative expression compared to WT = 0.11 (95%CI 0.09- 0.24), ventricle= 1.04 (95%CI 0.80-1.36); n=3 mice respectively in triplicate for all groups. Genomic DNA was also isolated from the tail, cardiac ventricle and the SA node and PCR was performed which confirmed Cre recombinase mediated deletion of exons 5-6 of Gna_O and exons 2-4 in Gna_{i2} in the SA node but not in the ventricle or tail (Figure 3.2.1).

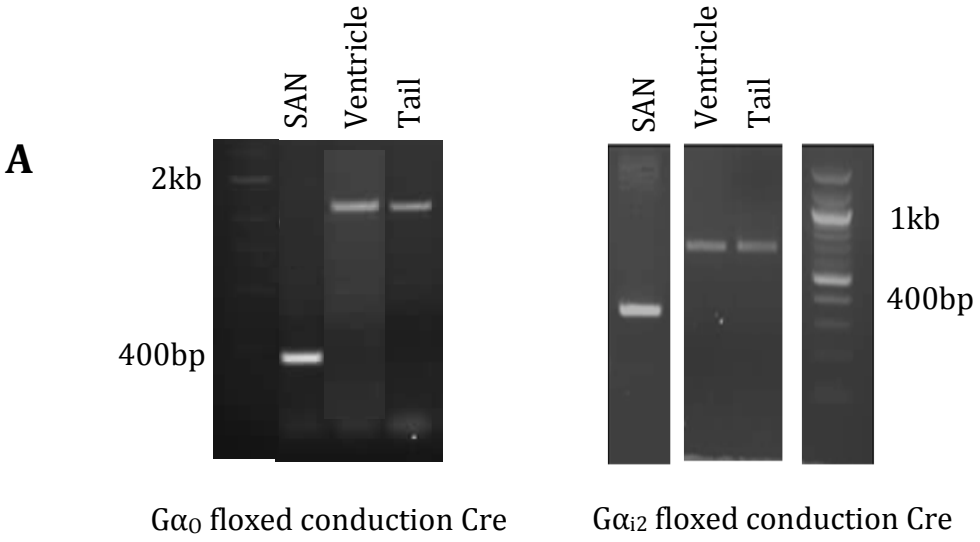

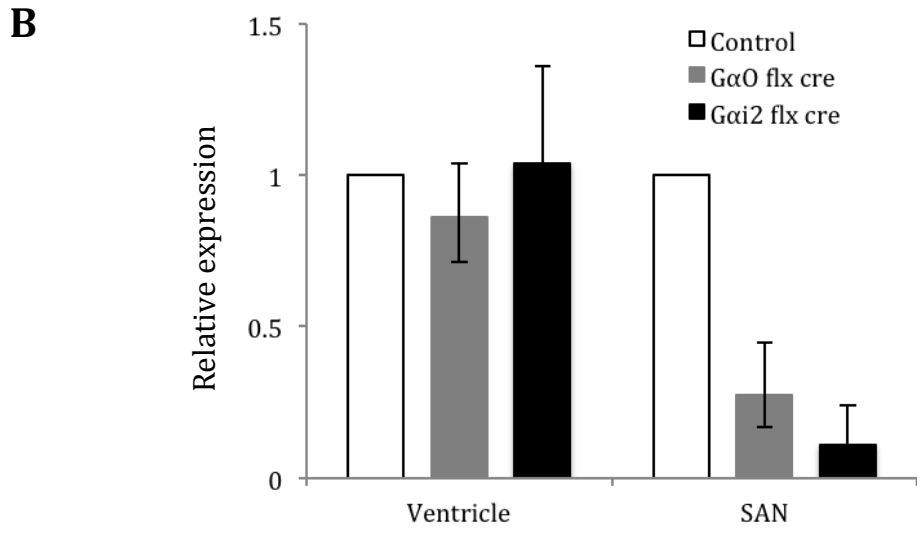

Figure 3.2.1 Conditional deletion of $G\alpha_O$ and $G\alpha_{i2}$ in the SAN

(A) PCR products of DNA obtained from $G\alpha_O$ (left) and $G\alpha_{i2}$ (right) floxed conduction Cre mice after tamoxifen treatment, where the presence of a ~400bp band in the SA node reveals the Cre mediated deletion of floxed allele whilst the other bands from the tail and ventricle samples reveals the non-deleted floxed Cre alleles. (B) Quantitative RT-PCR of SAN and ventricular tissues after tamoxifen treatment for 5 days in $G\alpha_O$ floxed conduction Cre and $G\alpha_{i2}$ floxed conduction Cre mice compared to controls (n=3 in all groups). Data presented as mean ± 95% CI.

3.3 HR profile in mice with selective deletion of $G\alpha_O$ and $G\alpha_{i2}$ in the cardiac conduction tissue

Mice are nocturnal animals and display peak activity during the night and they normally sleep during the day. This pattern of activity is reflected in a clear diurnal variation of heart rate. The 48-hour heart rate profile of $G\alpha_O$ and $G\alpha_{i2}$ floxed conduction Cre mice and their respective controls before tamoxifen treatment were similar and demonstrated this circadian variation (Figure 3.2.2 A).

The heart rate profile of $G\alpha_O$ floxed conduction Cre mice remained unchanged following tamoxifen treatment when compared to control with preserved circadian variation (450±20 bpm day, 570±20 bpm night; vs 468±16 bpm day, 557±16 bpm night, p=0.922, n=5 in both groups). It appears that tamoxifen lowers HR in the $G\alpha_O$ group. However the HR profile is similar between $G\alpha_O$ floxed conduction Cre mice and controls suggesting that the effect is non-specific.

In contrast, daytime heart rate of $G\alpha_{i2}$ floxed conduction Cre mice was significantly higher when compared to the level observed before tamoxifen treatment (546±16 v 499±16 bpm, p=0.009, n=12) and to the level recorded in control mice receiving tamoxifen treatment (546±16 v 474±15 bpm, p=0.008, n=12 and 9 respectively). There was a corresponding loss of circadian variation of heart rate in Gαi2 floxed conduction Cre mice (546±16 bpm day; 564±15 bpm, p=0.094, n=12), These data are summarized in Figure 3.2.2 B.

There were no significant differences in ECG parameters including PR interval, QRS duration and QTc interval between experimental groups before and after administration of tamoxifen (Table 3.1).

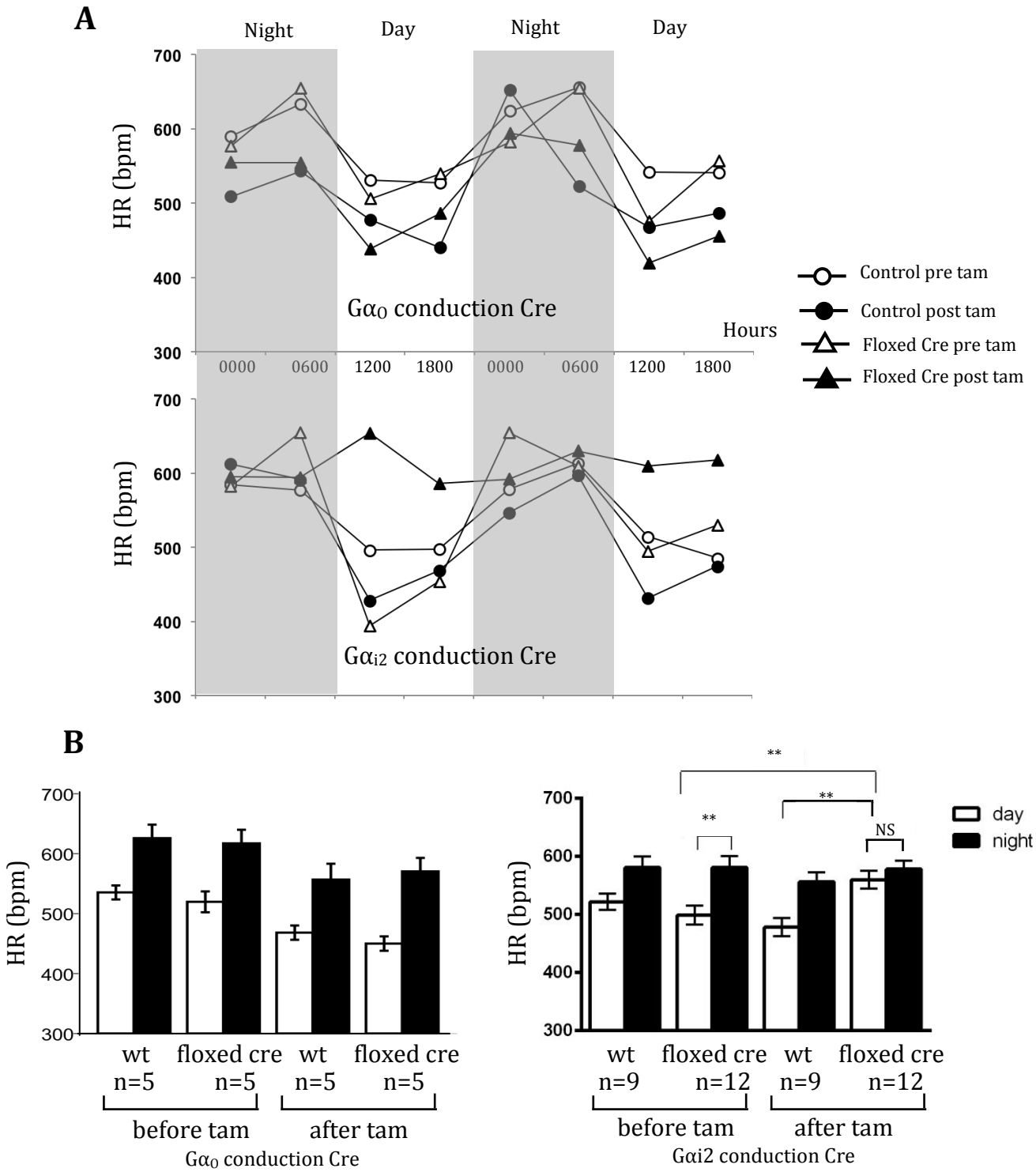

Figure 3.2.2 Day and night HR profile in mice with selective deletion of Gα$_O$ and Gα$_{i2}$ in the conduction tissue of the heart.

(A) Representative HR profile measured in six hourly intervals over a 48-hour period for an individual Gα$_O$ floxed conduction Cre (top) and an individual Gα$_{i2}$ floxed conduction Cre mouse (bottom) compared to a control mouse before and after tamoxifen treatment. (B) Summary data of mean heart rate ± SEM in Gα$_O$ (left) and Gα$_{i2}$ (right) floxed conduction Cre mice and their controls before and after tamoxifen treatments. NS $p \geq 0.05$; ** $p < 0.01$.

3.4 Heart rate variability in mice with selective deletion of $G\alpha_O$ and $G\alpha_{i2}$ in the cardiac conduction tissue

In $G\alpha_{i2}$ floxed conduction Cre mice, treatment with tamoxifen resulted in a clear disturbance in the normal pattern of HRV with selective loss of high frequency power (nHF 43.35±3.09 nu before tamoxifen vs 30.21±1.24 nu after tamoxifen treatment, p=0.013) but preserved low frequency and overall total power (Figure 3.2.3 and Table 3.1). There was no effect of Ga_{i2} deletion when HRV was analysed in time domain (Table 3.1).

In contrast, there was no significant difference in HRV of the $G\alpha_O$ floxed conduction Cre mice both before and after tamoxifen treatment when HRV was analysed by power spectral density analysis or in the time domain (Table 3.1).

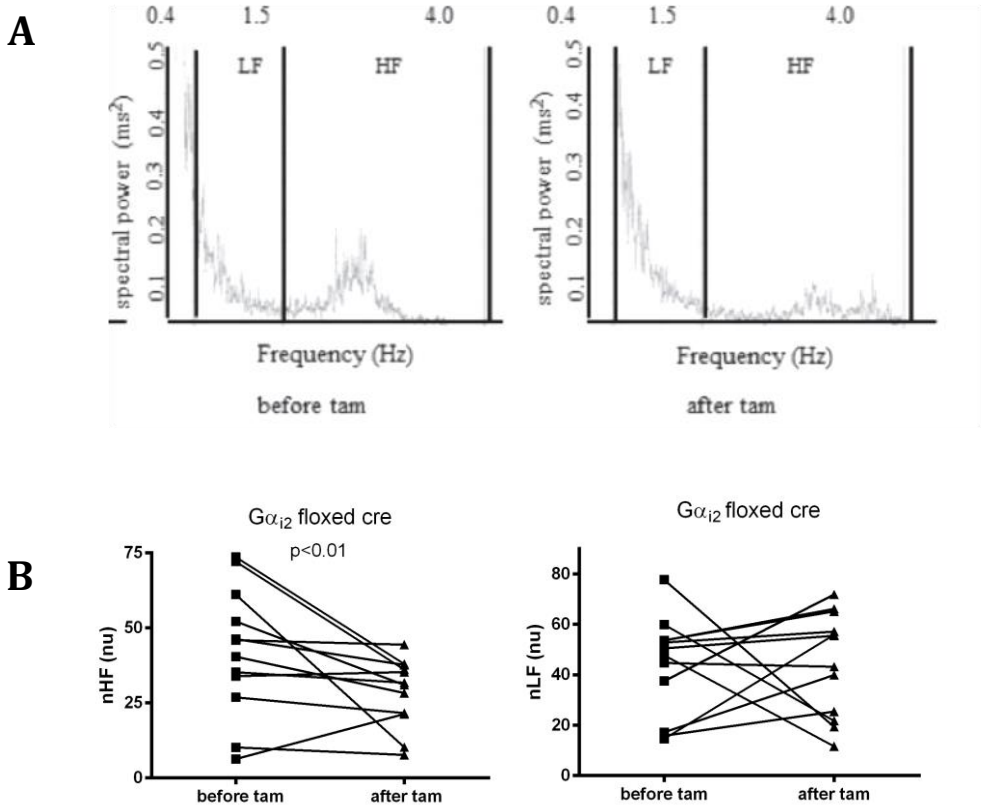

Figure 3.2.3 Loss of HF component of HRV in mice with selective deletion of $G\alpha_{i2}$ in the cardiac conduction tissue.

(A) Representative power spectrum density traces of HRV in $G\alpha_{i2}$ floxed conduction Cre mice before and after tamoxifen treatment. (B) Mean normalised HF component power of $G\alpha_{i2}$ floxed conduction Cre (n=12) and control (n=9) mice before and after tamoxifen administration.

	PR (ms)	QRS (ms)	QTc (ms)	RR (ms)	SDnn (ms)	RMSSD (ms)	TP (ms^2)	LF (ms^2)	HF (ms^2)	nLF (nu)	nHF (nu)
$G\alpha_O$ flx cre pre tam	35 ± 1	8 ± 1	56 ± 2	126 ± 7	27 ± 16	23 ± 10	172 ± 29	40 ± 12	66 ± 19	38 ± 1	63 ± 1
$G\alpha_O$ flx cre post tam (n=5)	37 ± 1	9 ± 1	57 ± 4	116 ± 13	18 ± 8	20 ± 8	118 ± 42	26 ± 13	53 ± 20	40 ± 4	60 ± 4
$G\alpha_O$ control pre tam	36 ± 1	9 ± 1	66 ± 6	125 ± 5	25 ± 5	30 ± 14	181 ± 25	48 ± 8	52 ± 11	49 ± 8	51 ± 8
$G\alpha_O$ control post tam (n=5)	33 ± 1	9 ± 1	60 ± 4	118 ± 5	22 ± 4	35 ± 20	147 ± 73	46 ± 19	70 ± 32	39 ± 4	61 ± 4
$G\alpha_{i2}$ flx cre pre tam	33.1±0.5	10.2±0.6	70 ± 5	120 ± 3	24 ± 8	12 ± 3	215 ± 81	56 ± 9	50 ± 6	48 ± 6	43 ± 3
$G\alpha_{i2}$ flx cre post tam (n=12)	34 ± 1	10 ± 1	69 ± 3	**110 ± 4***	31 ± 7	14 ± 6	130 ± 43	45 ± 8	31 ± 7	45 ± 6	**30 ± 1***
$G\alpha_{i2}$ control pre tam	35 ± 1	10 ± 1	62 ± 4	120 ± 10	12 ± 5	8 ± 1	134 ± 46	25 ± 5	22 ± 6	37 ± 6	33 ± 2
$G\alpha_{i2}$ control post tam (n=9)	36 ± 1	10 ± 1	62 ± 4	124 ± 3	6 ± 6	7 ± 1	218 ± 56	27 ± 3	36.2±7.2	35.4±8.3	48.0±3.6

Table 3.1 Summary data of ECG and HRV parameters in $G\alpha_O$ and $G\alpha_{i2}$ floxed conduction Cre mice and their respective controls.

The comparisons are between mice pre and post tamoxifen (tam) in the each group (repeated measures one way ANOVA).

* $p<0.05$

3.5 Heart rate responses to pharmacological challenges in mice with selective deletion of $G\alpha_O$ and $G\alpha_{i2}$ in the cardiac conduction tissue

To determine the role of $G\alpha_O$ and $G\alpha_{i2}$ in mediating responses triggered by muscarinic and adenosine receptor activation in the cardiac conduction tissue, the chronotropic responses of $G\alpha_O$ and $G\alpha_{i2}$ floxed conduction Cre mice and their respective controls were assessed after administration of carbachol or 2-Chloro-N^6-cyclopentyladenosine (CCPA), before and after treatment with tamoxifen. Both drugs were administered between 12 to 2 pm.

Carbachol (0.5mg/kg, ip), a non-specific muscarinic agonist, and CCPA (0.1mg/kg, ip), a specific A1 receptor agonist, both reduced the heart rate in wild type mice. Similar reductions in heart rate were observed in both $G\alpha_O$ floxed conduction Cre mice and controls (n=5 both groups) and cardiac $G\alpha_{i2}$ floxed conduction Cre mice (n=12) and controls (n=9) following administration of carbachol or CCPA before and after tamoxifen treatment in conscious animals (Figure 3.2.4). No specific conduction block or arrhythmias were observed after administration of either carbachol or CCPA.

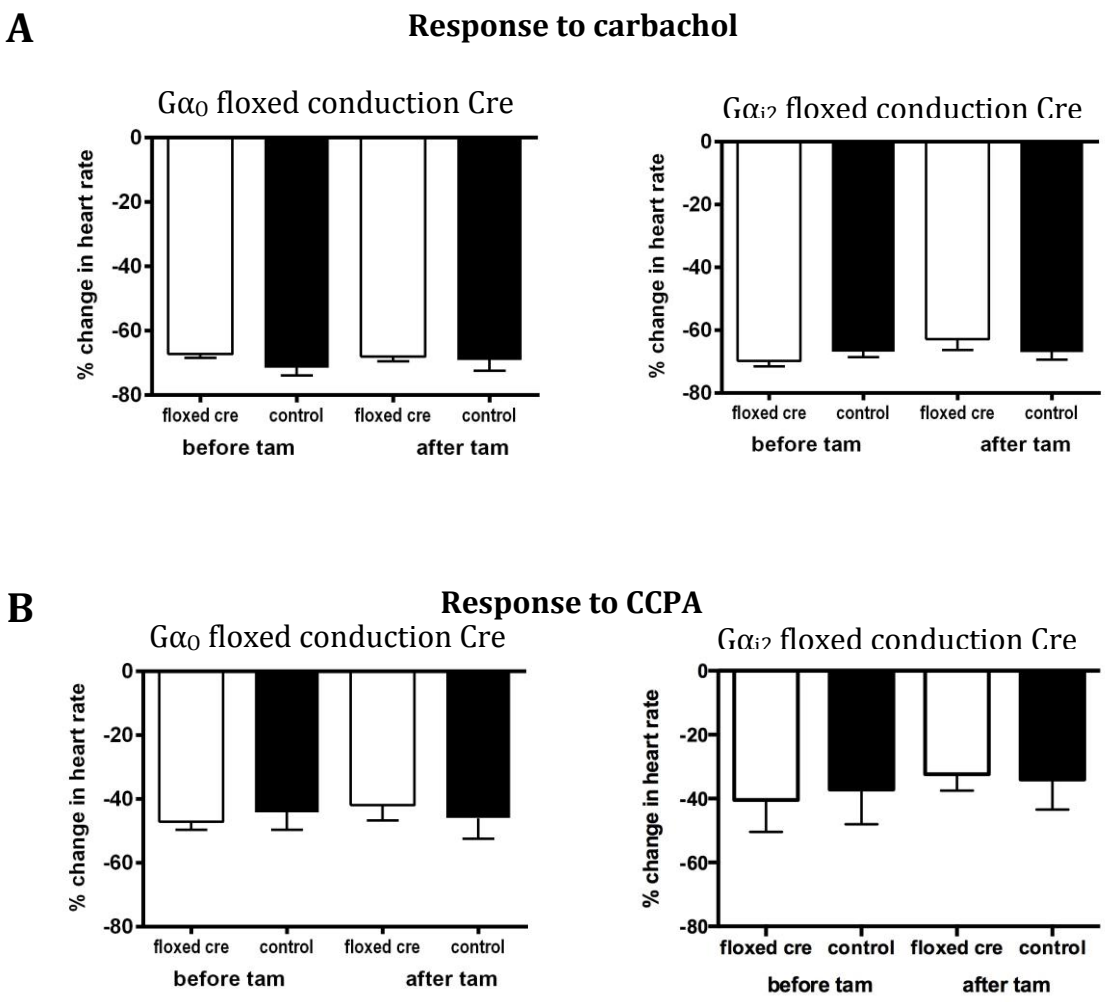

Figure 3.2.4. Assessment of heart rate responses to carbachol and CCPA in mice with selective deletion of $G\alpha_O$ and $G\alpha_{i2}$ in the cardiac conduction tissue.

Summary data illustrating changes in heart rate in $G\alpha_O$ floxed conduction Cre (n=5) and control (n=5) mice (left panel) and in $G\alpha_{i2}$ floxed conduction Cre (n=11) and control (n=9) mice (right panel) induced by carbachol (panel A) and CCPA administration (panel B). Bars represent mean ± S.E.M.

3.6 Intrinsic heart rate in mice with selective deletion of $G\alpha_O$ in the cardiac conduction tissue

Intrinsic heart rate was determined in $G\alpha_O$ floxed conduction Cre mice by combined pharmacological blockade of parasympathetic and sympathetic influences using atropine and propranolol, respectively. Atropine (0.5mg/kg, ip) was first administered and peak change in heart rate was recorded. This was followed by propranolol (1mg/kg, ip) administration and after 30 minutes when the heart rate has stabilized the intrinsic heart rate was determined. Drugs were given between 12 to 2 pm. There was no significant difference between $G\alpha_O$ floxed conduction Cre mice and control animals following pharmacological autonomic blockade with atropine and propranolol, either before or after tamoxifen treatment (Figure 3.2.5).

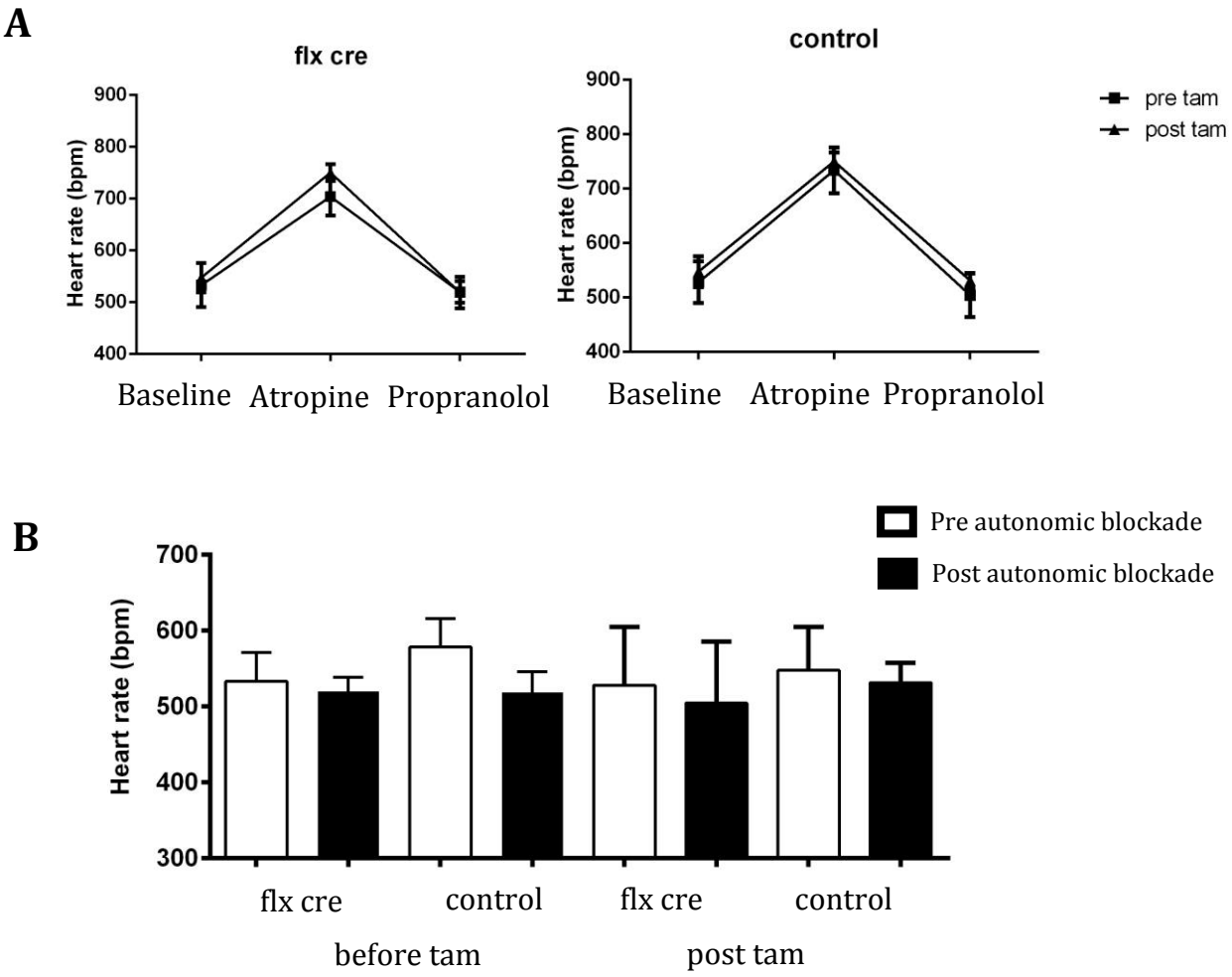

Figure 3.2.5 Combined pharmacological autonomic blockade with atropine and propranolol in $G\alpha_O$ floxed conduction Cre mice to determine intrinsic heart rate.

(A) Changes in heart rate of $G\alpha_O$ floxed conduction Cre (n=5) and control (n=5) mice induced by atropine and after combined atropine (0.5mg/kg, ip) and propranolol (1mg/kg, ip) treatment. (B) Summary data illustrating heart rates of $G\alpha_O$ floxed conduction Cre and control mice before and after pharmacological autonomic blockade. Bars represent mean ± S.E.M.

3.7 Discussion

The aim of the experiments described in this chapter was to determine the role of $G\alpha_O$ and $G\alpha_{i2}$ protein-mediated signalling in the cardiac conduction tissue in the control of heart rate. It was found that mice with selective deletion of $G\alpha_{i2}$ in the cardiac conduction system were tachycardic during the daytime and displayed a loss of circadian variation of heart rate and HF component of HRV. Selective deletion of $G\alpha_O$ in the cardiac conduction system had no effect on heart rate and HRV in mice. Negative chronotropic effects of muscarinic and adenosine receptor activation (systemic injections of carbachol and CCPA) were not affected by $G\alpha_O$ or $G\alpha_{i2}$ deletions in the cardiac conduction system. The intrinsic heart rate was also not affected by $G\alpha_O$ deletion.

3.7.1 HCN4 expression in cardiac conduction tissue and pacemaking cells

Within the murine heart, HCN4 (along with HCN1) was found to be the predominant isoform expressed in cardiac conduction tissue including the SA node (SAN), AV node and His-Purkinje tissues (Herrmann et al 2011). Hence using HCN4 as the promoter to drive Cre expression is expected to result in deletion of $G\alpha_{i2}$ or $G\alpha_O$ along the entire axis of the cardiac conduction system. However, as the SAN is responsible for pacemaking in sinus rhythm, this strategy would still allow us to study the effects of $G\alpha_{i2}$ or $G\alpha_O$ deletion in the SAN on heart rate modulation. Indeed, inspection of ECG traces in our mice has shown sinus rhythm throughout the recordings.

3.7.2 Higher heart rate during daytime and loss of circadian variation of heart rate in mice with $G\alpha_{i2}$ deletion in the cardiac conduction tissue

In mice with conditional deletion of $G\alpha_{i2}$ in the cardiac conduction tissue, HR was higher during the daytime with complete loss of its circadian variation. We interpret this as being due to lack of parasympathetic influences. It is traditionally thought that in mice sympathetic tone dominates the control of

heart rate with little vagal influence at resting conditions (Uechi et al. 1998, Wickman et al. 1998, Gehrmann et al. 2000) . However, autonomic tone is also determined by a number of environmental factors including ambient temperature and levels of physical activity (Thireau et al. 2007; Swoap et al. 2008). It is possible that mice have a certain level of vagal tone under a variety of conditions and there are reports which demonstrated vagal predominance of HR control in mice if appropriate care is taken in housing and recovery of the animals after the surgery (Just et al. 2000, Baudrie et al. 2006, Zuberi et al. 2008).

How does loss of $G\alpha_{i2}$-mediated signaling in the SA node result in increased HR? There are two likely mechanisms as indicated in the Chapter 1. Firstly, loss of inhibitory influence on AC would lead to increased cAMP concentration resulting in increased activity of both the I_f/I_h channel and downstream calcium cycling (membrane and calcium 'clock' respectively) (Robinson & Siegelbaum 2003; Lakatta & DiFrancesco 2009). Secondly, reduction in the direct GIRK activation from the inhibitory G protein would also lead to increased HR (Logothetis et al. 1987).

3.7.3 The effect of selective $G\alpha_{i2}$ deletion in the cardiac conduction tissue on heart rate variability

HRV is a widely used non-invasive technique used to estimate the autonomic influences on the heart and has been used in humans as a prognostic measure in many disparate clinical conditions including ischaemic heart disease, hypertension and cardiac arrhythmias (Malik et al. 1996). The high frequency (HF) component of the HRV is determined by the magnitude of the respiratory sinus arrhythmia and reflects vagal influences whilst the low frequency (LF) component reflects the response of heart rate to short term variations in blood pressure mediated by both sympathetic and vagal inputs (Frenneaux 2004), although the latter assumption remains controversial (Stauss 2003). Higher heart rate during the daytime when vagal tone should be highest together with selective loss of HF component of the HRV supports

a physiological role for $G\alpha_{i2}$ signaling in mediating parasympathetic influences on the SA node.

Interestingly, the heart rate response to carbachol was preserved in mice with conditional deletion of $G\alpha_{i2}$ in the cardiac conduction tissue, which contrasts with the finding in the global $G\alpha_{i2}$ knockout mice where heart rate slowing was significantly attenuated (Zuberi et al. 2008). There are a number of potential explanations for this. Firstly, the carbachol challenge is a significant pharmacological manipulation with the resultant HR reduction well below the physiological levels as HR drops by about 70%. It is also known that the SAN is quite an extensive and heterogenous structure and that the primary pacemaker may move as the strength of the sympathovagal balance changes (Monfredi et al. 2010; Shibata et al. 2001). Thus it is possible that following $G\alpha_{i2}$ deletion the pacemaking site shifts to a small region that is not solely dependent on the deleted G-protein or a site in which Cre mediated deletion is spared due to the expression of other HCN isoforms such as HCN1 (Herrmann et al. 2011).

3.7.4 No effect of selective deletion of $G\alpha_O$ proteins in the cardiac conduction tissue on HR and HRV

In comparison, there were no differences in HR or HRV in mice with conditional deletion of $G\alpha_O$ in the cardiac conduction tissue compared to control animals both at rest and in response to pharmacological challenges. This suggests that the role of $G\alpha_O$-mediated signalling in heart rate regulation at the level of the cardiac conduction tissue of the heart is insignificant.

There was no difference in heart rate following combined autonomic pharmacological blockade after the administration of atropine and propranolol. This lends further evidence that the intrinsic heart rate is not determined by events downstream of G protein signaling at the level of the conduction tissue of the heart.

3.7.5 Comparison of heart rate phenotype in mice with conditional deletion in cardiac conduction tissue versus global deletion of $G\alpha_{i2}$ and $G\alpha_O$ proteins

It was previously demonstrated that mice with global deletion of $G\alpha_{i2}$ are tachycardic and display a clear suppression of HRV in time and frequency domain across all three frequency spectra (Zuberi et al. 2008). The effect of conditional deletion of $G\alpha_{i2}$ in the SA node is consistent, albeit more subtle, with daytime tachycardia and selective loss of HF component of HRV only after normalization to remove variation in VLF (which accounts for the most significant power in the HRV signal). In mice with global deletion of $G\alpha_O$, there was increased heart rate with loss of diurnal rhythm accompanied by selective loss of the LF component of the HRV with preserved total power (Zuberi et al. 2008). In contrast, mice with conditional deletion of $G\alpha_O$ in the cardiac conduction tissue showed no clear HR and HRV phenotype.

3.7.6 Limitations

These results need to be discussed taking into consideration a number of possible caveats. First, non-stationarities in the HRV signal can be a confounding factor as physical activities can result in significant changes in heart rate and HRV (Thireau et al. 2007). However, efforts were taken to minimize this by monitoring the parameters when mice were at rest at defined time during the day for a short recording period. Second, it is important that the mice were allowed to recover for at least 10 days after the surgery and resume normal activity after probe implantation before measurements were made (Kramer et al. 1993).

Extra-cardiac expression of HCN4 has also been found in the nervous system (Brewster et al. 2007, Cho et al. 2009) including spinal inhibitory interneurones (Hughes et al. 2013). Spinal inhibitory interneurons are involved in modulation of sympathetic outflow and deletion of inhibitory G proteins in this region may potentially contribute to the findings. However, given that $G\alpha_O$ is also richly expressed in the CNS (Sternweis & Robishaw

1984, Parker et al. 2012) and no difference was seen in the HR phenotype of HCN4 Cre $G\alpha_O$ flx/flx mice, it is unlikely that this is an important confounder.

Considering that all the experiments were performed in standardised conditions and taking into account the confounding factors mentioned above, the differences in HR and HRV between global $G\alpha_O$ and $G\alpha_{i2}$ knockouts and mice with conditional deletion of $G\alpha_O$ and $G\alpha_{i2}$ in the cardiac conduction system are likely to be real. The likely reason for the observed differences in the conditional and global knockout models is the potential role played by the respective inhibitory G proteins in other mechanisms which contribute to the autonomic control of HR.

3.7.7 Summary

The data presented in this chapter suggest that $G\alpha_{i2}$ is an important signaling protein which mediates vagal influences on the heart at the level of the cardiac conduction tissue, most likely by coupling to M2 cholinoceptors. In contrast, $G\alpha_O$ appears to play no role at the level of the cardiac conduction system and hence the HR phenotype seen in the global $G\alpha_O$ knockout mice is most likely due to its role in other tissues, most likely in the central nervous system, as discussed in Chapter 1. Therefore, I next generated mice with conditional deletion of $G\alpha_O$ in the central nervous system to determine the role of signalling mediated by this protein in the central nervous mechanisms which control the heart.

Chapter 4

Results II

Generation of mice with conditional deletion of $G\alpha_O$ in the central nervous system

4.1 Introduction

I have shown in the previous chapter that mice with conditional deletion of $G\alpha_O$ in the cardiac conduction tissue did not display any abnormalities in heart rate profile or HRV. In this chapter, I shall present the results of the two strategies described in Chapter 2 used to generate mice with conditional deletion of $G\alpha_O$ in the central nervous system to investigate its role in the central nervous mechanisms of cardiac regulation.

Choice of promoter driving the expression of Cre is critical in determining the spatial and temporal specificity of deletion of the target protein when using the Cre/LoxP system. A pan-neuronal approach would allow for a more global assessment of the role of $G\alpha_O$ in the CNS in the generation of sympathetic tone. This approach also has the advantage of being technically easier as all that is required is the crossing of mice with floxed alleles of the gene of interest with the appropriate Cre-expressing mice. However, even accounting for issues of non-specificity of deletion and compensation, any phenotypic changes would be difficult to attribute to any specific signalling pathway within the CNS and the lack of any observable phenotypic changes may be due to the effect of deletion in the different pathways cancelling out each other given the ubiquity of $G\alpha_O$ expression in the CNS.

A targeted approach using viral vectors expressing Cre would allow for precise temporal and spatial deletion of the gene of interest and is a very powerful approach to study the role of a ubiquitous protein like $G\alpha_O$ in specific brainstem circuits of interest. However, the approach is technically challenging and dependent on efficient transfection of the viral vector.

Given the different strengths and weaknesses of each approach we decided to develop and investigate both the pan-neuronal and targeted approaches.

4.2 Nestin Cre approach

A pan-neuronal approach was first used by crossing $G\alpha_O$ flx/flx mice with mice expressing Cre driven by the nestin promoter as described in Chapter 2.

4.2.1 $G\alpha_o$ flx/flx nestin Cre mice display growth retardation and poor survival

Only a few $G\alpha_O$ flx/flx nestin Cre pups were obtained after close to a hundred littermates were genotyped with the other genotype combinations predicted by Mendelian distribution. $G\alpha_O$ flx/flx nestin Cre mice appeared small, had tremors, abnormal gait and did not survive beyond 4-5 weeks of age (Figure 4.2.1).

Figure 4.2.1 $G\alpha_o$ flx/flx nestin Cre mouse at 5 weeks of age

Morphological appearance of a $G\alpha_O$ flx/flx nestin Cre mouse at 5 weeks of age

4.2.2 Nestin Cre expression in the brain and other organs

As $G\alpha_O$ flx/flx nestin Cre mice were generally non-viable and difficult to obtain, I examined whether Cre mediated excision occurred in tissues outside the central nervous system in GαO flx/wt nestin Cre mice. DNA was extracted from brain cortex, quadriceps muscle, ventricular myocardium, liver and tail of euthanized mice and Cre recombinase products were amplified by PCR as previously described.

Cre mediated recombination of GnaO product corresponding to removal of exons 5-6 was found to be present in the brain, skeletal muscle and heart but not in the liver of $G\alpha_O$ flx/wt nestin Cre mice (Figure 4.2.2).

4.2.3 $G\alpha_O$ protein expression in the brain and other organs

The expression of $G\alpha_O$ mRNA in the striated muscle, heart (ventricular myocardium) and brain cortex was then investigated by performing quantitative RT-PCR as described previously.

Quantitative RT-PCR analysis revealed that $G\alpha_O$ flx/flx nestin Cre mice had significantly reduced expression of $G\alpha_O$ in the brain (relative expression 0.60, 95%CI 0.57-0.64) and in the skeletal muscle (relative expression 0.61, 95%CI 0.58-0.65). Interestingly, $G\alpha_O$ expression appears to be up-regulated in the heart with a relative expression of 1.53 (95%CI 1.50-1.54).

Phenotypically normal appearing heterozygotes ($G\alpha_O$ flx/WT nestin Cre) mice showed similar reduction of $G\alpha_O$ expression in skeletal muscle (relative expression 0.64, 95%CI 0.62-0.66), and the heart (relative expression 0.86, 95% CI 0.81-0.97), but preserved expression of $G\alpha_O$ in the brain (relative expression 1, 95%CI 0.94-1.08) (Figure 4.2.3).

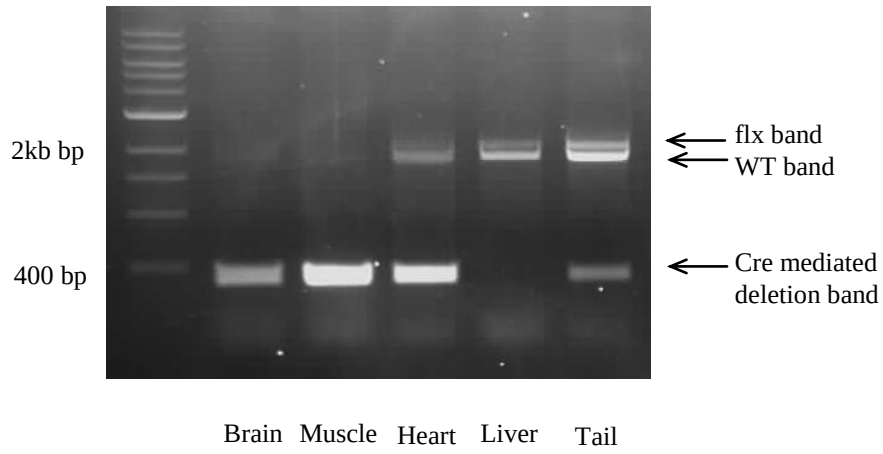

Figure 4.2.2 PCR products of DNA samples obtained from tissues of a $G\alpha_O$ flx/wt nestin Cre mouse

PCR products of DNA obtained from a $G\alpha_O$ flx/wt nestin Cre mouse where the presence of a ~400bp band reveals the Cre mediated deletion of floxed allele whilst the ~2 kb band reveals the non-deleted floxed Cre and WT alleles differentially expressed in various tissues.

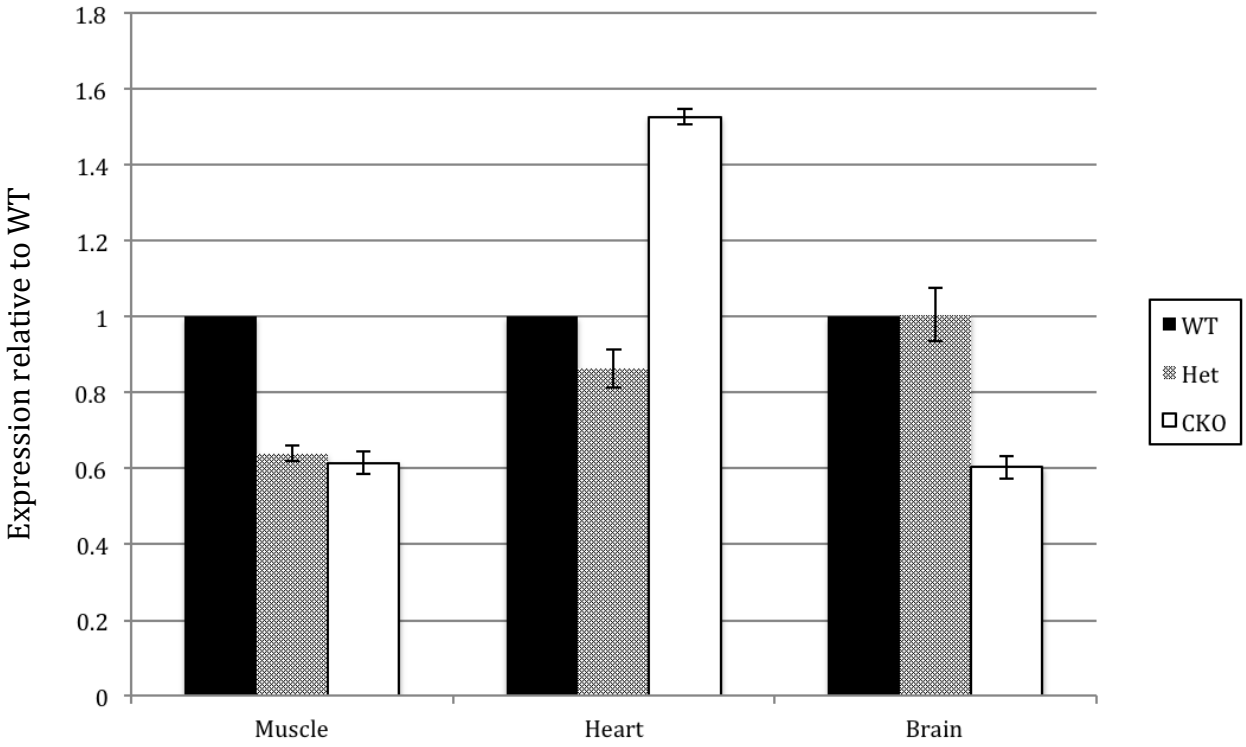

Figure 4.2.3 $G\alpha_O$ expression in GαO floxed nestin Cre mice and controls

Quantitative RT-PCR in the muscle, heart and brain tissues of WT, $G\alpha_O$ flx/WT nestin Cre (Het), and $G\alpha_O$ flx/flx nestin Cre (CKO) mice (n=3 in all groups). Data presented as mean ± 95% CI.

4.3 Targeted approach using Cre expressing adenoviral vector

As discussed in Chapter 1, the RVLM is important in generating sympathetic vasomotor tone, receives inhibitory inputs and is a putative site of action for inhibitory G proteins. Hence for the targeted approach, we chose to target the RVLM with a Cre expressing adenoviral vector (AVV).

4.3.1 Validation of RVLM coordinates by microinjection of fluorescent beads

The exact RVLM coordinates (adapted to our stereotaxic apparatus) in these mice were determined in dedicated preliminary trials using microinjections of fluorescent beads with subsequent histological analysis to verify the sites of delivery, using the brain atlas as reference (Franklin and Paxinos, 2007).

Fluorescent beads (0.2µm *FluoSpheres* amine-modified microspheres in red fluorescence, Invitrogen, CA, USA) diluted in 0.9% Saline at 1:50 concentration were injected using micropipette as described in Chapter 2 to differing depths, distance and angulation relative to the calamus scriptorius (Figure 4.3.1).

From the preliminary trials, the optimum co-ordinates to target RVLM with the microinjection pipette angled at 10 degrees were found to be: 1.4 mm lateral to the midline and 2.4mm ventral from the dorsal surface of the brain (relative to the *calamus scriptorius*).

4.3.2 Targeting the RVLM with adenoviral constructs

One microinjection per side of Cre/GFP AVV (6 x 10^{10} PFU) or GFP AVV (3 x 10^{10} PFU) at 1:50 dilution was delivered using the co-ordinates derived above. Mice were then euthanized and brain harvested and fixed in PFA at 7 to 10 days post injection when expression of AVV has been shown to be maximal (Haskell et al. 2003).

Histological analysis was then performed as previously described with TH staining to identify C1 neurones of the RVLM, looking for co-localisation with GFP expression to verify successful delivery and expression of the AVV constructs in the RVLM (Figure 4.3.2).

A. Bregma -6.2mm, Angulation 11 ^{O}, Lateral 1.3mm, Dorsal-ventral 2.4mm

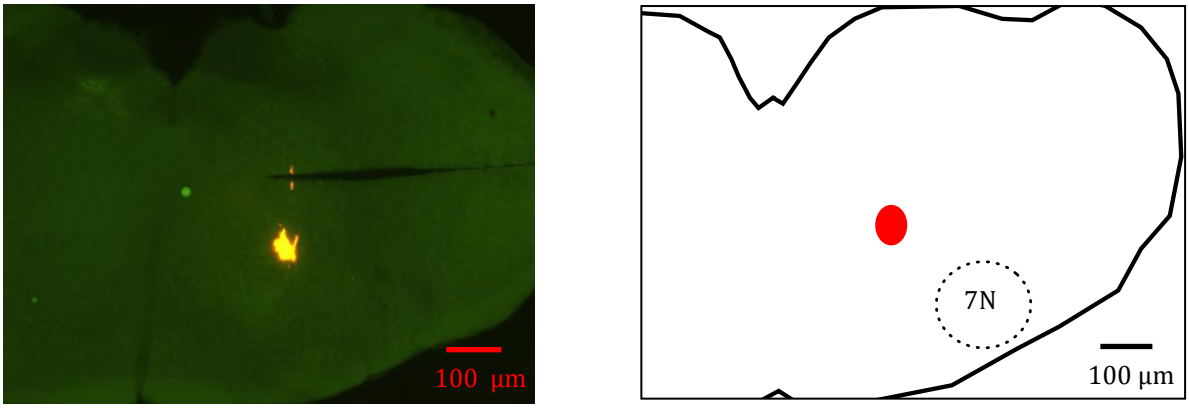

B. Bregma -6.7mm, Angulation 10 ^{O}, Lateral 1.3mm, Dorsal-ventral 2.4mm

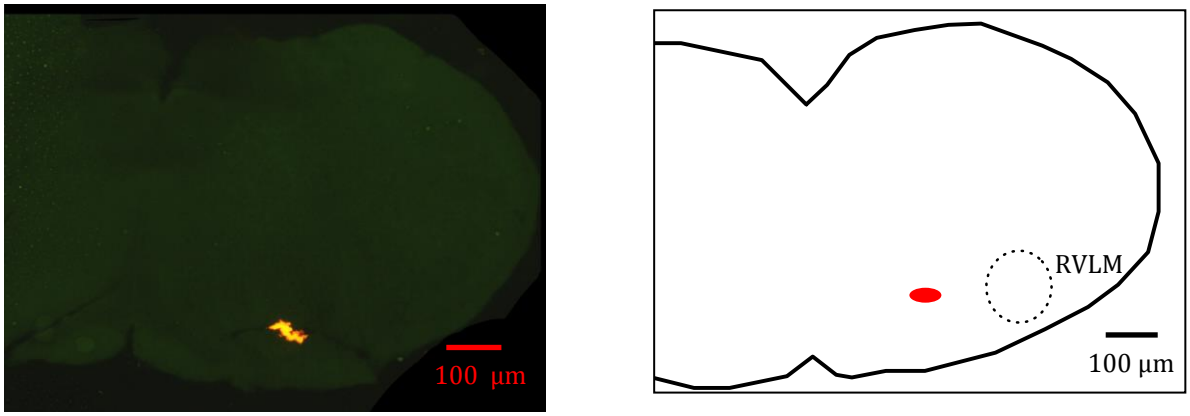

C. Bregma -7.5mm, Angulation 10 ^{O}, Lateral 1.3 mm, Dorsal-ventral 2.2mm

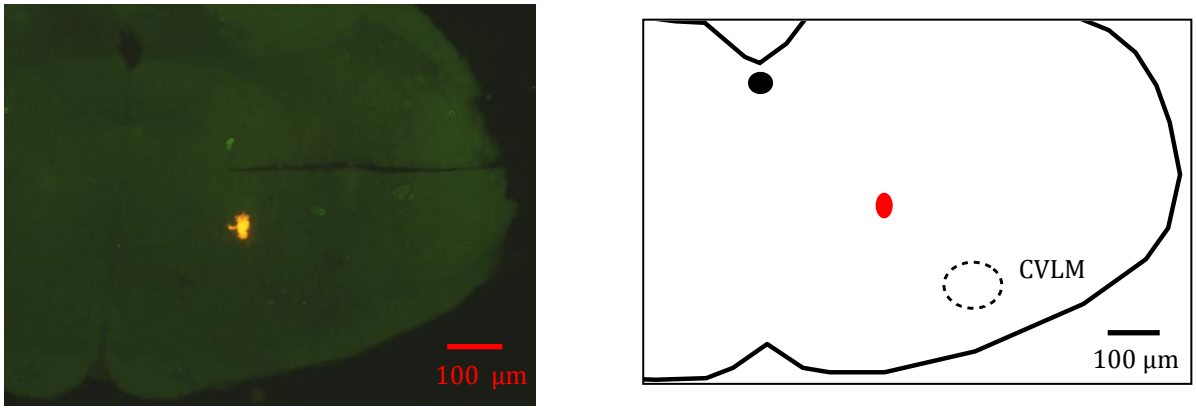

Figure 4.3.1 Determination of stereotaxic co-ordinates using fluorescent beads

Examples of microscopy images (left) and schematic diagrams (right) at 3 levels of the brainstem showing the locations of fluorescent beads following microinjections using different stereotaxic co-ordinates to determine the optimum co-ordinates to target RVLM. Scale bar 100 µm.

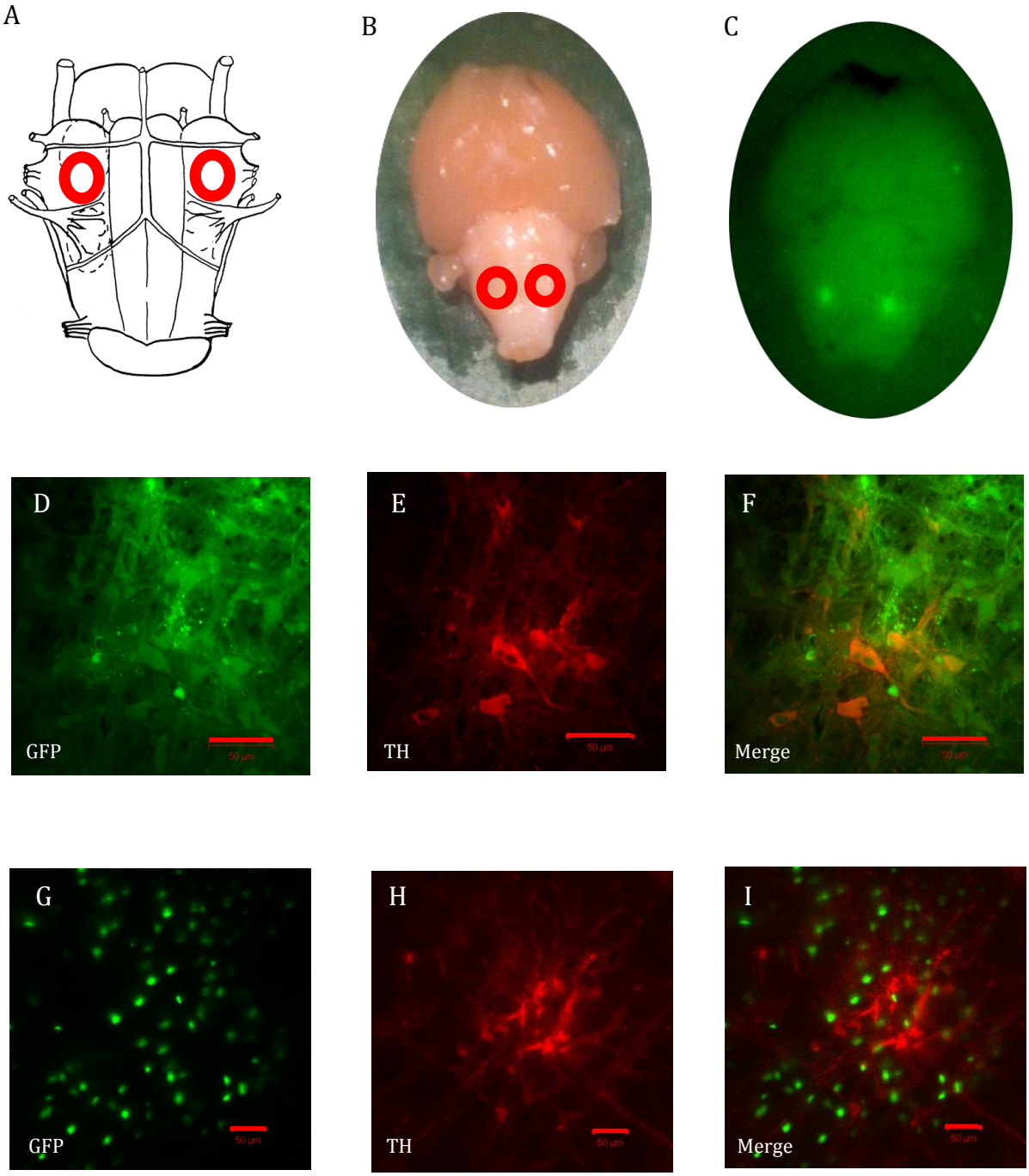

Figure 4.3.2 Targeting RVLM with AVV constructs to express GFP in $G\alpha_o$ flx/flx mice

Anatomical location of RVLM circled in red in: (A) Line drawing of brainstem structures viewed from the ventral surface, and, (B) ventral surface of the mouse brain stem. (C) Fluorescence at sites of injections when ventral surface of brain stem is illuminated with light at the wavelength of 395nm.
Confocal images of tyrosine hydroxylase (TH)-positive neurones (red) expressing GFP (green) in brain slices injected with GFP AVV (1:50 dilution of VQAd CMVeGFP-2.6del $3x10^{10}$ PFU) (D), (E), (H), and Cre/GFP AVV (1:50 dilution of Ad Cre/GFP 6×10^{10} PFU) (G), (H), (I).
Bregma level -6.7mm. Scale bar 50μm.

4.3.3 RT-PCR to validate deletion of $G\alpha_O$ proteins and determine titres of AVV construct to be used

WT and $G\alpha_O$ flx/flx mice were injected with both Cre/GFP AVV (Ad Cre/GFP, 6 x 10^{10} PFU) and GFP AVV (VQAd CMVeGFP-2.6del, 3x10^{10} PFU) at a concentration of 1:50 and 1:100 dilutions. Tissue from the injection sites was then extracted and RT-PCR performed as described in Chapter 2.

There was around 80% reduction of $G\alpha_O$ expression in the brainstems of $G\alpha_O$ flx/flx mice injected with Cre/GFP AVV at dilution of 1:50 (relative expression 0.16, 95%CI 0.11-0.23) and 1:100 (relative expression 0.21, 95%CI 0.18-0.25). Relative expression in mice injected with the control GFP AVV was 0.51 (95%CI 0.45-0.58) and 0.79 (95%CI 0.75-0.82) at 1:50 and 1:100 dilutions respectively (Figure 4.3.3).

In summary, there was good knock-down of gene expression achieved with both 1:50 and 1:100 dilutions of Cre/GFP AVV. However, at 1:50 dilution, there was also some reduction in gene expression with the control GFP AVV. This is most likely due to non-specific inflammation with adenoviral vectors which is well recognised (Naldini et al. 1996). This is minimised with the 1:100 dilution of the GFP AVV.

Given the similar efficacy of gene knockdown with lower inflammatory effects, the 1:100 dilution of AdV constructs was chosen for subsequent experiments to generate mice with knockdown of $G\alpha_O$ in the RVLM of the brainstem.

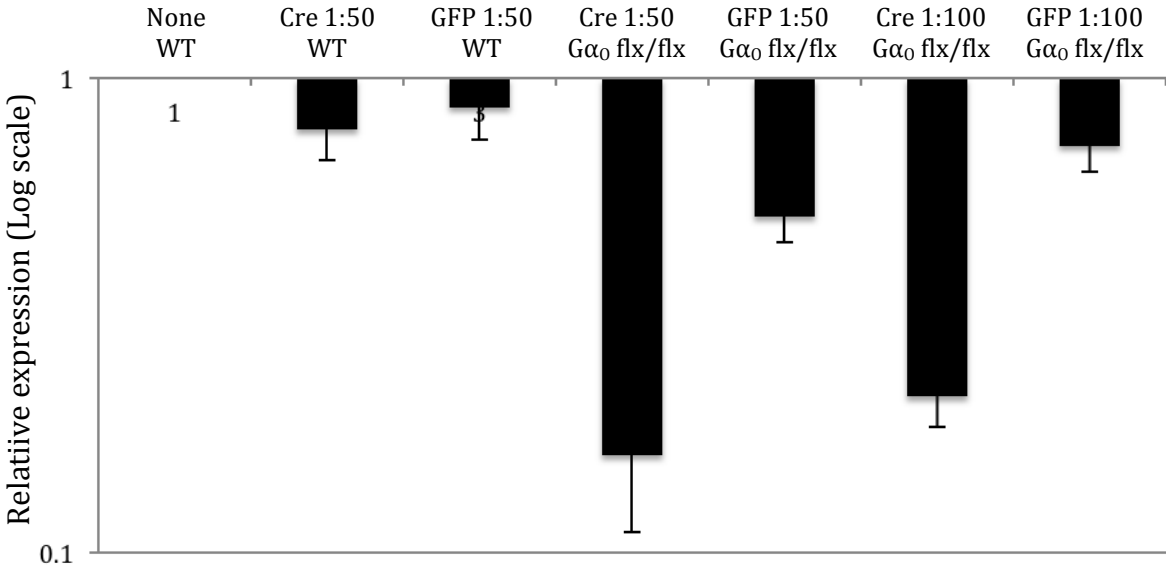

Figure 4.3.3 $G\alpha_O$ expression using different concentrations of adenoviral constructs

Quantitative RT-PCR of brainstem tissue in the brainstem of GαO flx/flx and WT mice injected with Cre/GFP AVV and GFP AVV at 1:50 and 1:100 dilutions (n=3 in all groups). Data presented as mean ± 95% CI.

4.3.4 Generation of mice with $G\alpha_O$ deletion in the RVLM of the brainstem and controls for *in vivo* experiments

To generate mice with specific deletion of $G\alpha_O$ in the RVLM of the brainstem (hereon referred to as $G\alpha_O$ floxed brainstem Cre mice), Cre/GFP AVV was microinjected in 1:100 dilution to the brainstem of $G\alpha_O$ flx/flx mice as described previously. For controls, $G\alpha_O$ flx/flx mice were injected with GFP AVV in 1:100 dilution instead.

The mice were allowed to recover and then subsequently studied at 7 to 14 days (experimental details and results are described in Chapters 5 and 6).

Following the experiments (detailed in Chapters 5 and 6), the mice were then euthanized and brainstem fixed, sliced and immunostained to label TH positive cells as previously described.

Only mice with good co-localisation of GFP and TH expression (ie: transfection of catecholaminergic C1 neurones of the RVLM with adenoviral vectors) are included in data analysis in Chapters 5 and 6.

The distribution of transduced neurones in a representative brainstem is illustrated in Figure 4.3.4.

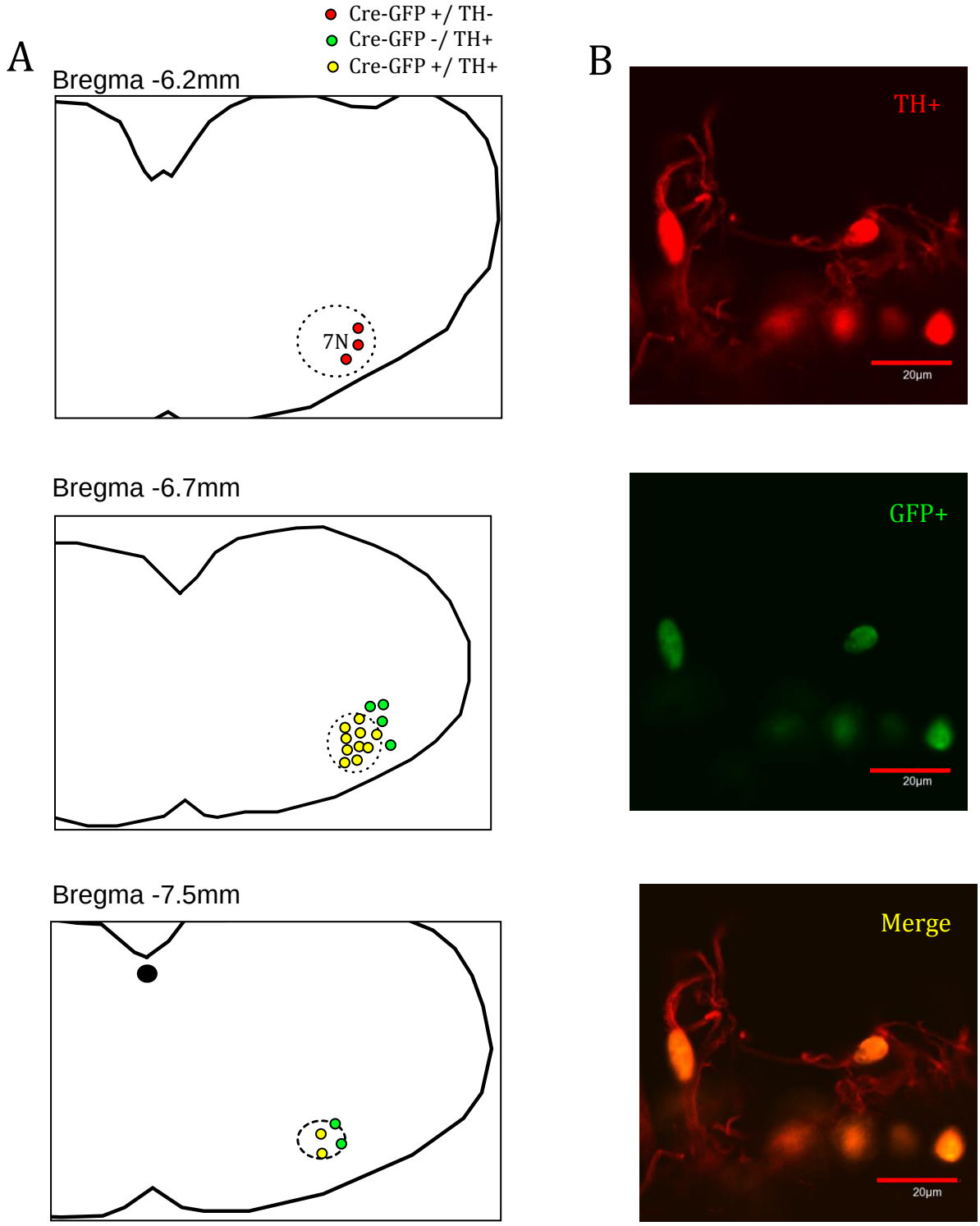

Figure 4.3.4 Distribution of RVLM C1 neurones expressing Cre/GFP

(A) Distribution of TH-immunoreactive neurones expressing Cre/GFP in one representative mouse brainstem 1 week after microinjection of Cre/GFP AVV into the RVLM. Each symbol represents 5 neurones. 7N, facial motor nucleus. **(B)** High magnification images showing co-localisation of GFP expression in the nuclei of TH-positive neurones. Scale bar 20μm.

4.4 Discussion

In this chapter I discussed the results of two methods used to generate mice with conditional knockout of $G\alpha_O$ in the central nervous system of $G\alpha_O$ flx/flx mice. The pan-neuronal Cre approach driven by a nestin promoter was found to be a non-viable strategy and associated with poor tissue specificity. Targeting the RVLM directly using a Cre/GFP expressing AVV driven by a CMV promoter was found to result in good knockdown of $G\alpha_O$ expression at the RVLM with appropriate controls generated by using GFP AVV.

4.4.1 Choice of adenoviral vector to target Cre expression

Recombinant adenoviruses have been shown to efficiently transduce genes into a wide spectrum of non-dividing cells in vivo (Yang et al. 1994). However, they are also known to induce an immunogenic response which may limit the duration of expression of the viral transgene and may also result in non-transgene specific effects secondary to inflammatory response (Naldini et al. 1996).

A 1:100 dilution of viral titres was chosen to minimise the non-specific inflammatory response. Furthermore, mice were studied at 1-2 weeks post injection and hence longevity of transgene expression is not an issue with our experimental models.

4.4.2 Limitations

Use of a CMV promoter to drive the expression of Cre/GFP and GFP is non-specific with regards to the cell type that ultimately expresses the construct.

There are two main implications. Firstly, cells surrounding the region of the RVLM including the A5 and A1 groups of cell in CVLM, the nucleus ambiguous and the surrounding central respiratory neurones may also be transfected by the viral construct, resulting in expression of Cre and unintended deletion of $G\alpha_O$ protein.

Secondly, there are different cell types located within the RVLM. Other than the C1 neurones, astrocytes are emerging as important in cardio-respiratory regulation within the RVLM via its role in neurovascular coupling. G protein mediating signalling specifically via $G\alpha_q$ by neuropeptides such as neuropeptide Y (NPY) and also by purines such as adenosine and ATP/ADP are implicated in gliotransmission within the RVLM (Gourine et al. 2009). Hence, the precise mechanisms underlying any observed phenotype may not be simply due to loss of $G\alpha_O$ mediated signalling in the C1 neurones of the RVLM as discussed in Chapter 1.

The first problem highlighted can be overcome to some degree by using small volumes for microinjection and histologically verifying the sites of injection as I have done. However, a better solution that would address both issues would be use of a promoter which is specifically expressed only by the cell population of interest.

In the case of targeting the C1 neurones of the RVLM, an example would be to use the PRSx8 promoter which is specific for cells expressing Phox 2a and 2b (Marina et al. 2011).

4.4.3 Summary

Despite the limitations outlined above, I have developed a technique to direct deletion of $G\alpha_O$ proteins in the region of the RVLM. Further experiments using this model are described in the following two Chapters.

Chapter 5

Results III

Cardiorespiratory phenotype of mice with conditional $G\alpha_O$ deletion in the RVLM

5.1 Introduction

As described in Chapter 3, mice with conditional deletion of $G\alpha_O$ in cardiac conduction tissue did not exhibit any HR and HRV phenotype (in contrast to $G\alpha_O$ global knock out mice) suggesting that it has an extra-cardiac role in autonomic regulation of the heart. Given the abundance of $G\alpha_O$ expression in the brain and the key role played by the vasomotor centre in the brainstem, especially the RVLM, in generating sympathetic tone, we postulated that loss of the inhibitory influence of $G\alpha_O$ to the RVLM may result in changes in autonomic tone and account for the phenotype seen in mice with global deletion of the protein. In Chapter 4, we described the methods used to generate mice with conditional deletion of $G\alpha_O$ in the RVLM of the brainstem. Specifically, $G\alpha_O$ flx/flx mice were injected with Cre/GFP expressing adenovirus (Cre AVV) in the RVLM ($G\alpha_O$ floxed brainstem Cre) and in the control group $G\alpha_O$ flx/flx mice were injected with GFP expressing adenovirus (GFP AVV) in the RVLM (control).

In this chapter, I present data obtained in experiments using conscious $G\alpha_O$ floxed brainstem Cre and control mice under baseline physiological conditions and exposed to hypoxic and hypercapnic conditions to characterise alterations in the central nervous mechanisms of autonomic cardio-respiratory control.

5.2 Recordings of BP in conscious freely moving $G\alpha_O$ floxed brainstem Cre and control mice

To determine the effect of $G\alpha_O$ deletion in the RVLM in conscious freely moving mice, BP radiotelemetry probes were implanted in $G\alpha_O$ floxed brainstem Cre and control mice and allowed to recover for at least 10 days as previously described. All mice were then studied before and 7 to 14 days after viral injections.

5.2.1 Normal diurnal heart rate and blood pressure profile in mice with conditional deletion of $G\alpha_O$ in the brainstem

The mice were first studied under normal conditions to evaluate diurnal HR and BP changes as described in Chapter 2. Figure 5.2.1 shows a representative BP trace and derived HR tachogram obtained over a 24-hour recording period in a control mouse.

The HR profile of $G\alpha_O$ floxed brainstem Cre mice was similar to that recorded in control mice and was not affected following injections of the viral vectors (before the injections: 520±18 bpm day, 610±12 bpm night; vs 540±20 bpm day, 620±15 bpm night, p=0.921, n=6 in both groups; and after the injections: 538±10 bpm day, 622±8 bpm night; vs 540±8 bpm day, 605±12 bpm night, p=0.784, n=6 in both groups).

Arterial BP measurements revealed a similar diurnal profile of systolic BP changes when comparing $G\alpha_O$ floxed brainstem cre mice to control animals (before the injections: 108±14 mmHg day, 128±16 mmHg night; vs 110±14 mmHg day, 130±16 mmHg night, p=0.887, n=6 in both groups; and after the injections: 116±6 mmHg day, 140±5 mmHg night; vs 108±4 mmHg day, 142±16 mmHg night, p=0.727, n=6 in both groups). The data are summarised in Figure 5.2.2.

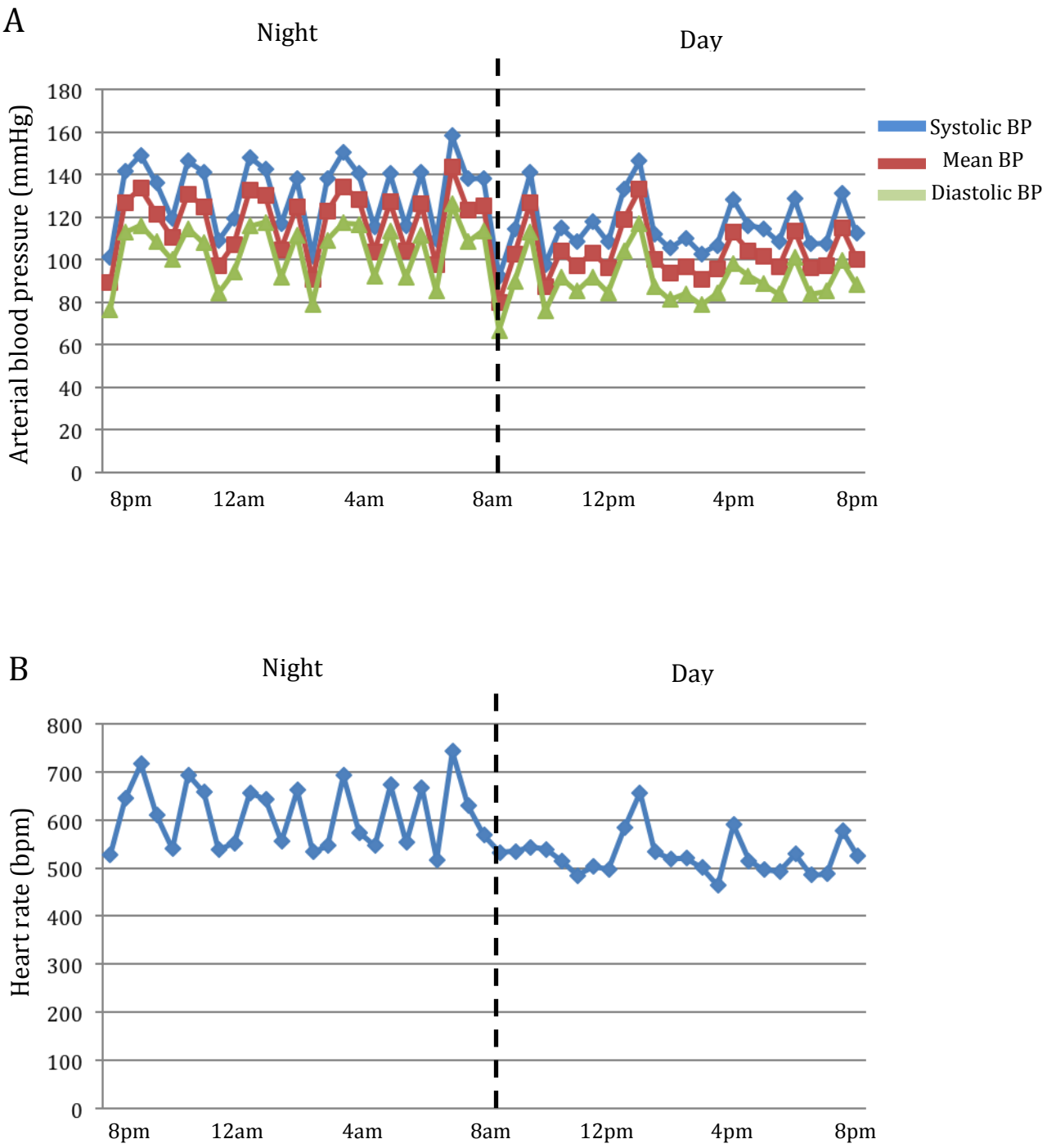

Figure 5.2.1. Diurnal haemodynamic profile of a control mouse

Representative BP trace (panel A) and derived HR tachogram (panel B) obtained from 24 hour recordings in a conscious freely moving control mouse.

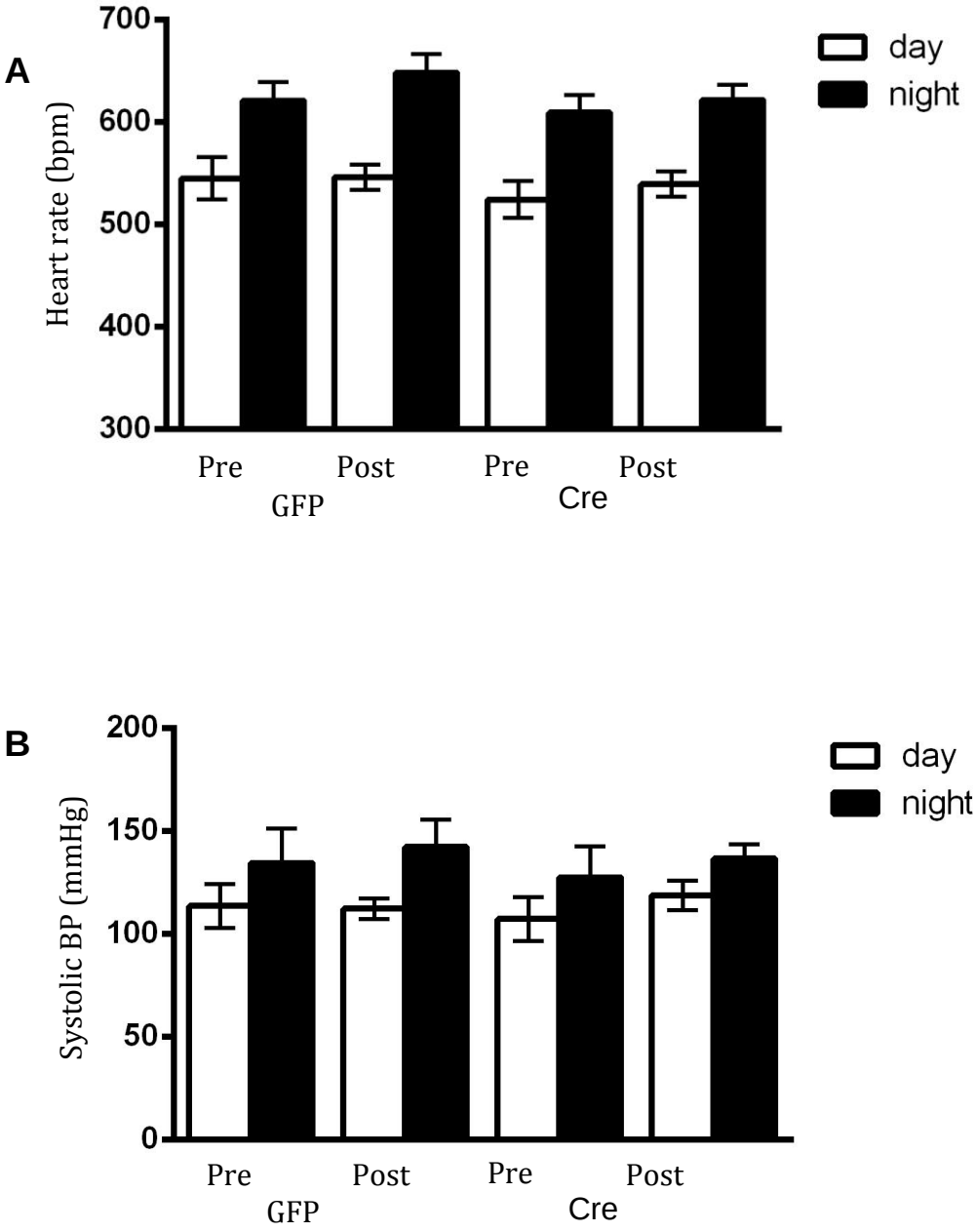

Figure 5.2.2. Summary data of averaged HR and systolic BP values during the day and during the night in mice with conditional deletion of $G\alpha_O$ in the brainstem and control animals.

Day and night measurements of (A) HR and (B) systolic arterial BP recorded using biotelemetry in $G\alpha_O$ flx/flx mice pre and post GFP AVV (control mice) and Cre AVV (Gαo floxed brainstem Cre mice) injections into the RVLM. Data expressed as mean ± SEM, n=6 in all groups.

5.3 Haemodynamic and respiratory responses to hypoxia

Hypoxia is known to induce a robust sympathetic response and this is in part mediated by increased activity of the C1 neurones of the RVLM (Guyenet et al. 2013). We hence tested the cardio-respiratory response to hypoxic conditions of the same cohort of $G\alpha_O$ floxed brainstem Cre mice (all 6 of 6) and control animals (4 of 6) implanted with BP biotelemetry using whole-body plethysmography as described previously.

Figure 5.3.1 shows a representative trace of the haemodynamic and respiratory responses to hypoxic challenge in a control mouse. Mice responded to hypoxia (10% O_2) with an increase in the HR but no significant change in arterial BP, and an increased respiratory rate and tidal volume. During recovery from hypoxia, heart rate decreased close to baseline. There was a post-hypoxic depression of respiratory activity with reduced respiratory rate below baseline and normalisation of tidal volume. Table 5.1 reports summary data of HR, systolic BP, respiratory rate (RR), tidal volume (V_T) and minute volume (V_E) changes recorded in our cohort of $G\alpha_O$ flx/flx mice.

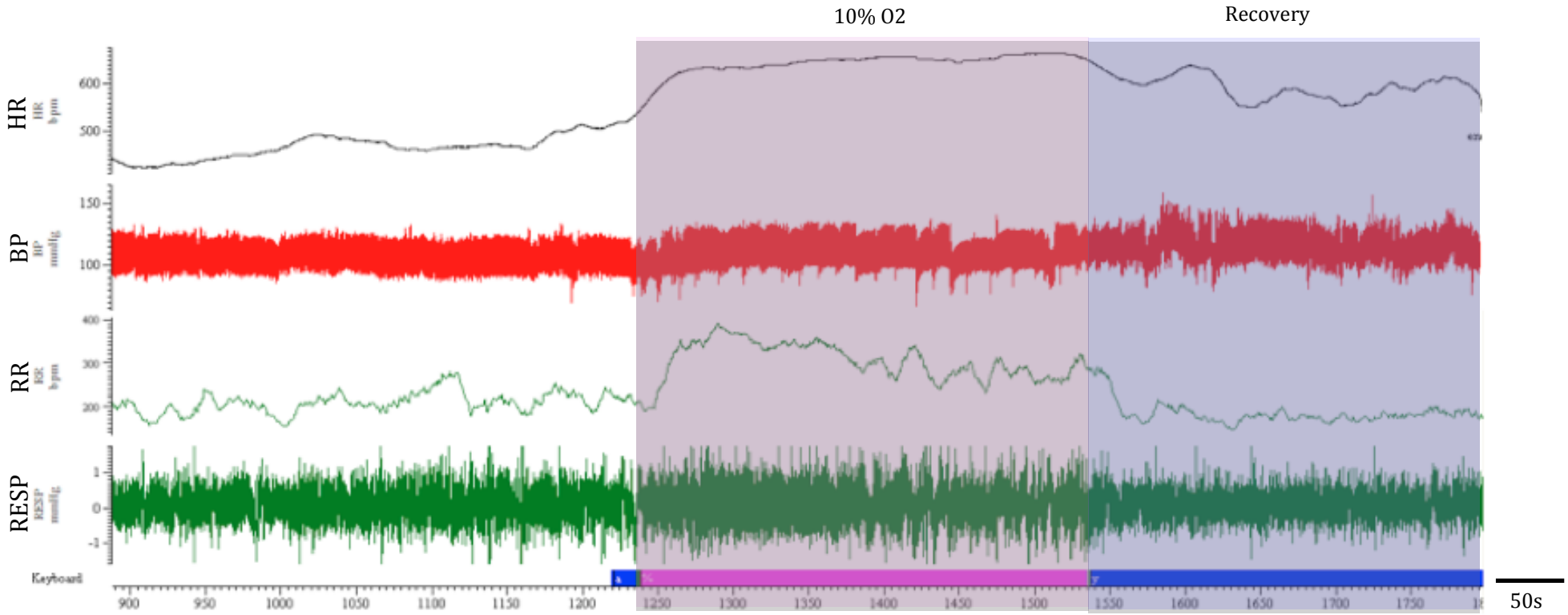

Figure 5.3.1 Representative recording of haemodynamic and respiratory responses of a $G\alpha_O$ flx/flx mouse injected with control GFP AVV to hypoxic challenge (10% of O_2 in the inspired air)

From top to bottom, heart rate (HR), arterial BP (BP), respiratory rate (RR), and raw respiratory tracings (RESP). Time is represented on the X-axis in seconds with the hypoxic period highlighted in pink and recovery period in blue.

5.3.1 Haemodynamic and respiratory responses to hypoxic challenge in mice with conditional deletion of $G\alpha_O$ in the brainstem

There were no significant differences in the hypoxia-induced haemodynamic and respiratory responses mounted by control mice before and after injections of GFP AVV. Post Cre AVV injections, $G\alpha_O$ floxed brainstem Cre mice were more tachycardic at baseline after acclimatisation to the chamber environment (579±10 vs 504±26 bpm, p=0.023) and this difference in heart rate is maintained in response to hypoxic challenge with a similar magnitude of HR change (721±7 vs 656±10 bpm, p<0.001) and during recovery of heart rate in the re-oxygenation period (633±14 vs 560±26 bpm, p=0.049). $G\alpha_O$ floxed brainstem Cre mice were also more hypertensive at baseline (152±7 vs 128±5 mmHg, p=0.025) but this difference is not maintained and systolic BP during (132±3 vs 129±5 mmHg, p=0.671) and after hypoxia (124±6 vs 126±6 mmHg, p= 0.796) were similar pre and post Cre AVV injections. There were also no significant differences in the respiratory rate or tidal volume in $G\alpha_O$ floxed brainstem Cre mice before and after the injections of Cre AVV during baseline, hypoxia or recovery. This resulted in a similar profile of minute ventilation changes (Table 5.1, Figures 5.3.2 and 5.3.3).

		Baseline		10% O_2		Recovery	
		GFP (n=4)	Cre (n=6)	GFP (n=4)	Cre (n=6)	GFP (n=4)	Cre (n=6)
Heart rate (BPM)	Pre	527±13	504±26	665±11	656±10	559±20	560±26
	Post	495±28	* **579±10**	665±16	*** **721±7**	524±30	* **633±14**
Blood pressure (mmHg)	Pre	129±6	128±5	124±3	132±3	129±4	124±6
	Post	135±5	* **152±7**	126±6	129±5	128±7	126±6
Respiratory rate (min^{-1})	Pre	185±5	199±7	280±6	263±7	145±11	167±10
	Post	191±3	199±8	271±3	266±6	153±9	155±9
Tidal volume ($ml\ kg^{-1}$)	Pre	5.3±0.3	4.5±0.5	12.0±0.4	12.6±0.6	7.4±0.4	7.2±0.8
	Post	5.2±0.4	5.6±0.5	12.0±0.7	13.2±0.6	7.0±0.5	8.9±0.5
Minute volume ($L\ min^{-1}\ kg^{1}$)	Pre	1.0±0.1	1.0±0.1	3.4±0.1	3.3±0.2	1.1±0.1	1.2±0.1
	Post	1.0±0.1	1.1±0.1	3.2±0.2	3.5±0.2	1.1±0.1	1.4±0.1

Table 5.1 Summary data of hypoxia-induced changes in haemodynamic and respiratory variables recorded in Control (n=4) and $G\alpha_O$ floxed brainstem Cre mice (n=6) pre- and post- viral injections.

Data are expressed as means ± SEM. Values highlighted in bold are significantly different when compared to pre-injection values.

** p<0.05, *** P<0.001*

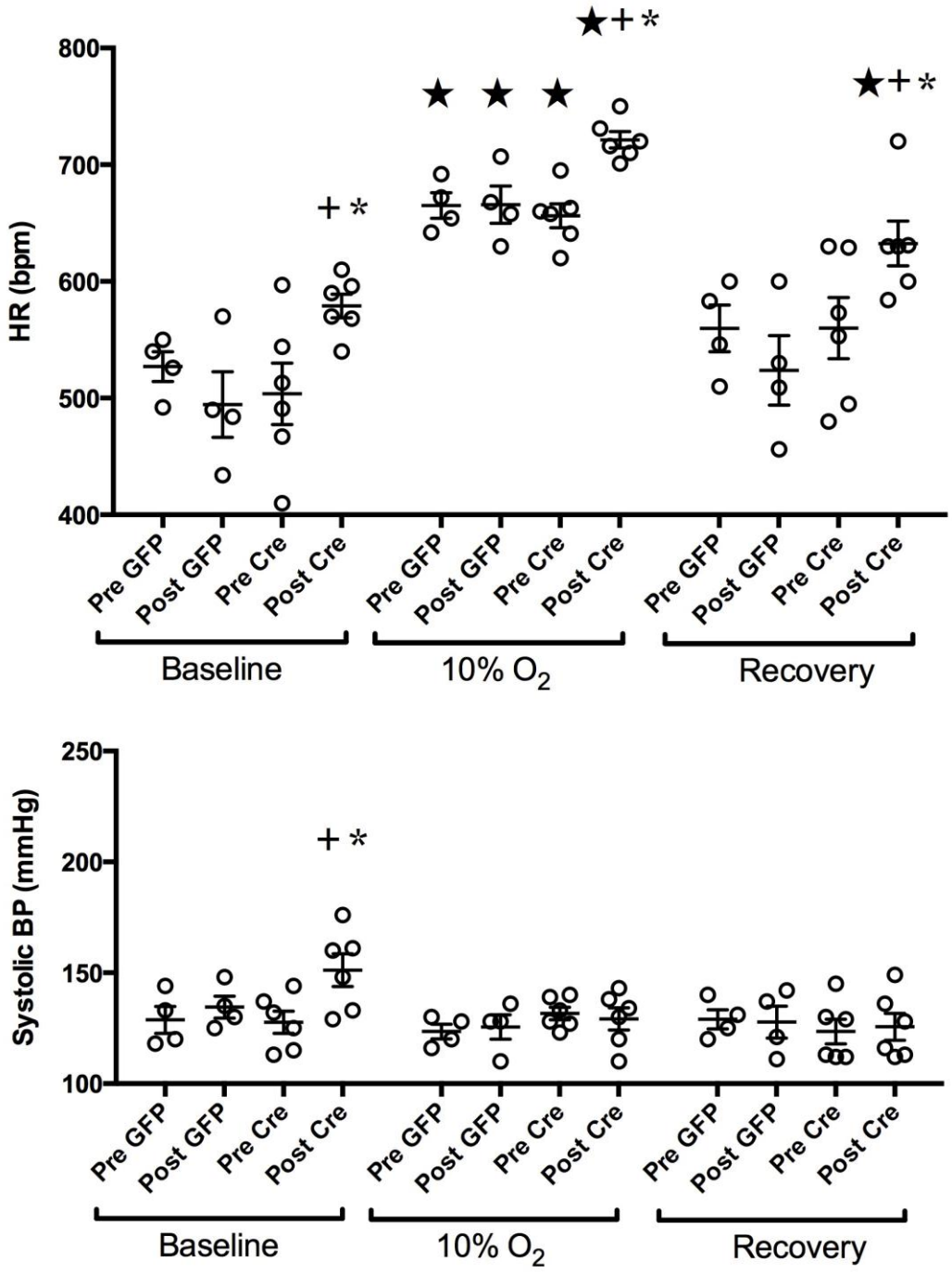

Figure 5.3.2 Haemodynamic response to hypoxic challenge (10% inspired O2) in $G\alpha_O$ floxed brainstem Cre mice and controls

Heart rate (HR) and systolic blood pressure (BP) pre and post Cre AVV and GFP AVV injections. Individual data and means ± SEM are shown. indicates significant difference from normoxia; + indicates significant difference from post GFP; * indicates significant difference from pre Cre.

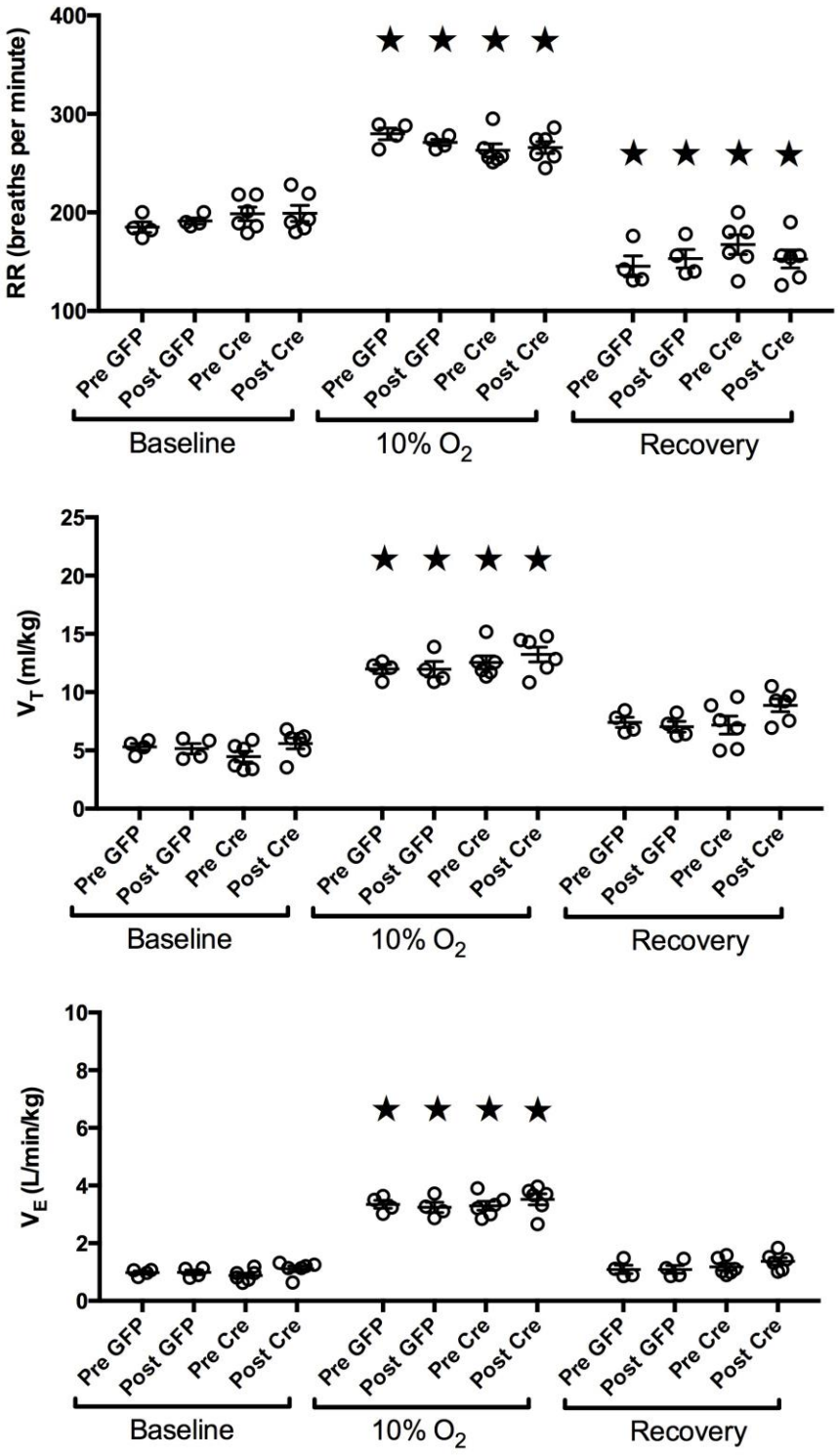

Figure 5.3.3 Respiratory response to hypoxic challenge (10% inspired) in Gα_O floxed brainstem Cre mice and control.

Respiratory rate (RR), tidal volume (V_T) and minute volume (V_E) pre and post Cre AVV and GFP AVV injections. indicates significant difference from normoxia.

5.4 Haemodynamic and respiratory responses to hypercapnia

Respiratory and cardiovascular responses to hypercapnia were determined in the same cohort of 6 $G\alpha_O$ floxed brainstem Cre mice and 4 controls as before. Figure 5.4.1 shows a representative trace of the haemodynamic and respiratory responses evoked by an increase in the level of inspired CO_2 in a control mouse. The control mice responded to 3% and 6% CO_2 with a decrease in heart rate, accompanied by an increase in arterial BP. Hypercapnia also evoked stereotypic increases in respiratory rate and tidal volume. Table 5.2 summarises the HR, systolic BP, respiratory rate (RR), tidal volume (V_T) and minute volume (V_E) data recorded in our cohort of $G\alpha_O$ flx/flx mice during CO_2 exposure.

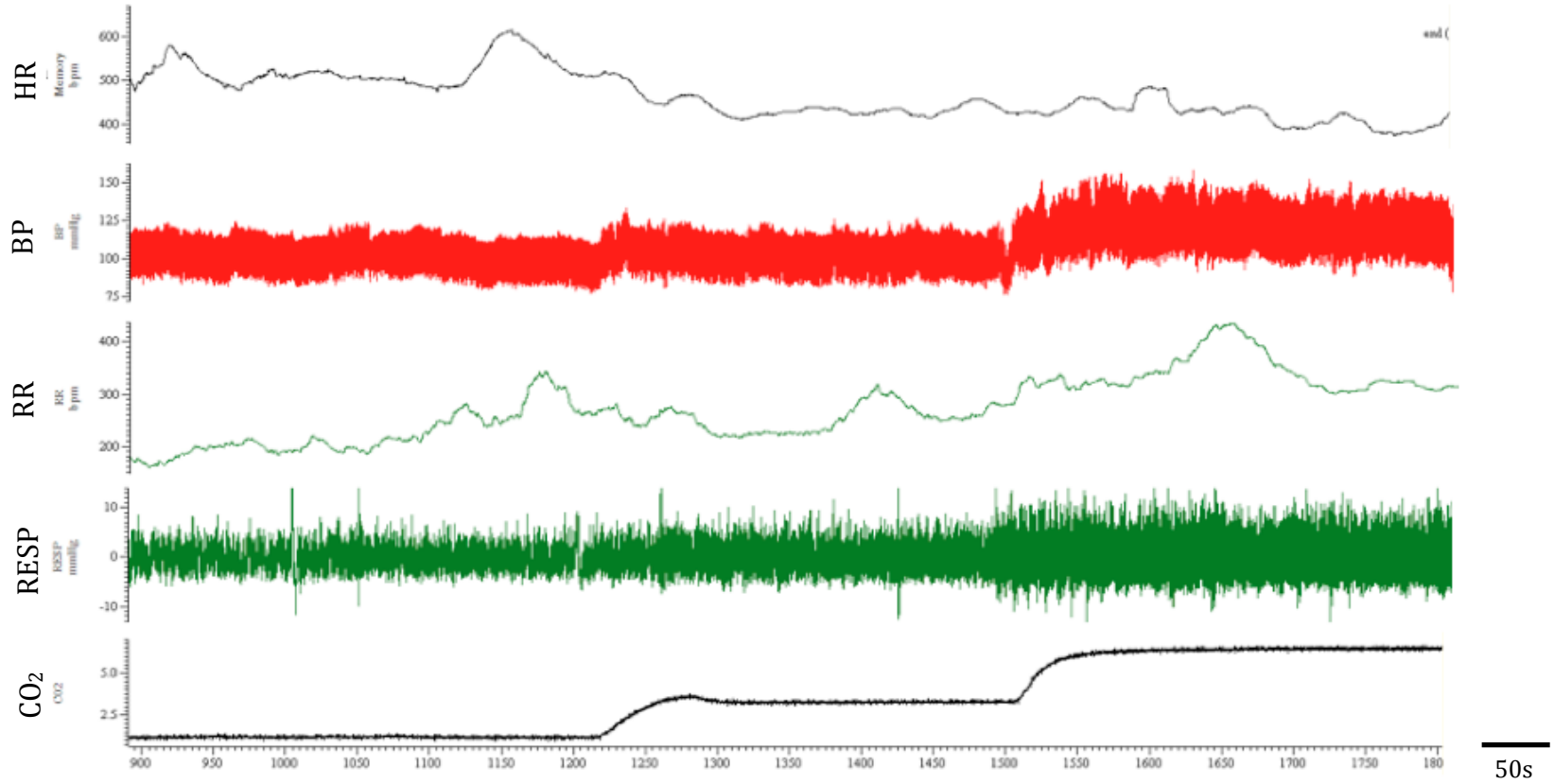

Figure 5.4.1. Representative recording of haemodynamic and respiratory responses of a control mouse to hypercapnic challenge (3% and 6% CO_2 in the inspired air).

From top to bottom, heart rate (HR), arterial BP (BP), respiratory rate (RR), and raw respiratory tracings (RESP) and $FiCO_2$ (CO_2). Time is represented on the X-axis in seconds.

5.4.1 Haemodynamic and respiratory responses to hypercapnic challenge in mice with conditional deletion of $G\alpha_O$ in the brainstem

No significant differences in CO_2-evoked responses (haemodynamic and respiratory) of the control mice before and after GFP AVV injections were observed. $G\alpha_O$ floxed brainstem Cre mice displayed higher heart rate at baseline after acclimatisation to the chamber environment (654±16 vs 587±23 bpm, p=0.012) post Cre AVV injections. HR depression during 3% and 6% CO_2 was attenuated in $G\alpha_O$ floxed brainstem Cre mice after Cre AVV injections (3% CO2: 616±23 vs 539±28 bpm, p=0.049; 6% CO2: 633±19 vs 499±27 bpm, p=0.003). Systolic BP was significantly higher in $G\alpha_O$ floxed brainstem Cre mice at baseline (159±4 vs 136±6 mmHg, p=0.012). Control mice responded to 6% CO_2 with significantly elevated systolic BP (164±9 vs 136±6 mmHg, p=0.005) but this response was attenuated in $G\alpha_O$ floxed brainstem Cre mice (170±10 vs 159±4 mmHg, p=0.669). Respiratory responses to 6% CO2 in GαO floxed brainstem Cre mice were higher (V_E 4.7±0.9 vs 3.0±0.4 L min^{-1} kg^{-1}, p=0.114) when challenged with 6% CO2 post Cre Adv injections but did not reach statistical significance (Table 5.3, Figure 5.4.2 and Figure 5.4.3).

		Baseline		3% CO_2		6% CO_2	
		GFP (n=4)	Cre (n=6)	GFP (n=4)	Cre (n=6)	GFP (n=4)	Cre (n=6)
Heart rate (BPM)	Pre	521±41	587±23	518±22	539±28	518±22	499±27
	Post	507±24	* **654±16**	474±26	* **616±23**	474±26	** **633±19**
Blood pressure (mmHg)	Pre	135±9	136±6	155±14	152±9	169±8	164±9
	Post	137±8	* **159±4**	160±9	163±9	173±10	170±10
Respiratory rate (min^{-1})	Pre	198±4	196±6	218±4	223±8	260±12	269±14
	Post	202±7	201±5	229±12	221±11	265±10	307±23
Tidal volume ($ml\ kg^{-1}$)	Pre	5.1±0.6	4.7±0.7	8.7±0.9	7.4±0.5	11.2±0.6	11.3±1.6
	Post	4.2±.8	5.2±0.5	7.6±0.9	8.5±0.9	11.0±0.8	15.2±2.1
Minute volume ($L\ min^{-1}\ kg^{-1}$)	Pre	1.0±0.1	0.9±0.1	1.9±0.2	1.7±0.1	2.9±0.1	3.0±0.4
	Post	0.8±0.2	1.0±0.1	1.7±0.3	1.9±0.3	2.9±0.3	4.7±0.9

Table 5.2 Summary data of hypercapnia-induced changes in haemodynamic and respiratory variables recorded in control (n=4) and $G\alpha_o$ floxed brainstem Cre mice (n=6) pre- and post- viral injections.

Data are expressed as means ± SEM. Values highlighted in bold are significantly different when compared to pre-injection values.

** p<0.05, ** P<0.01*

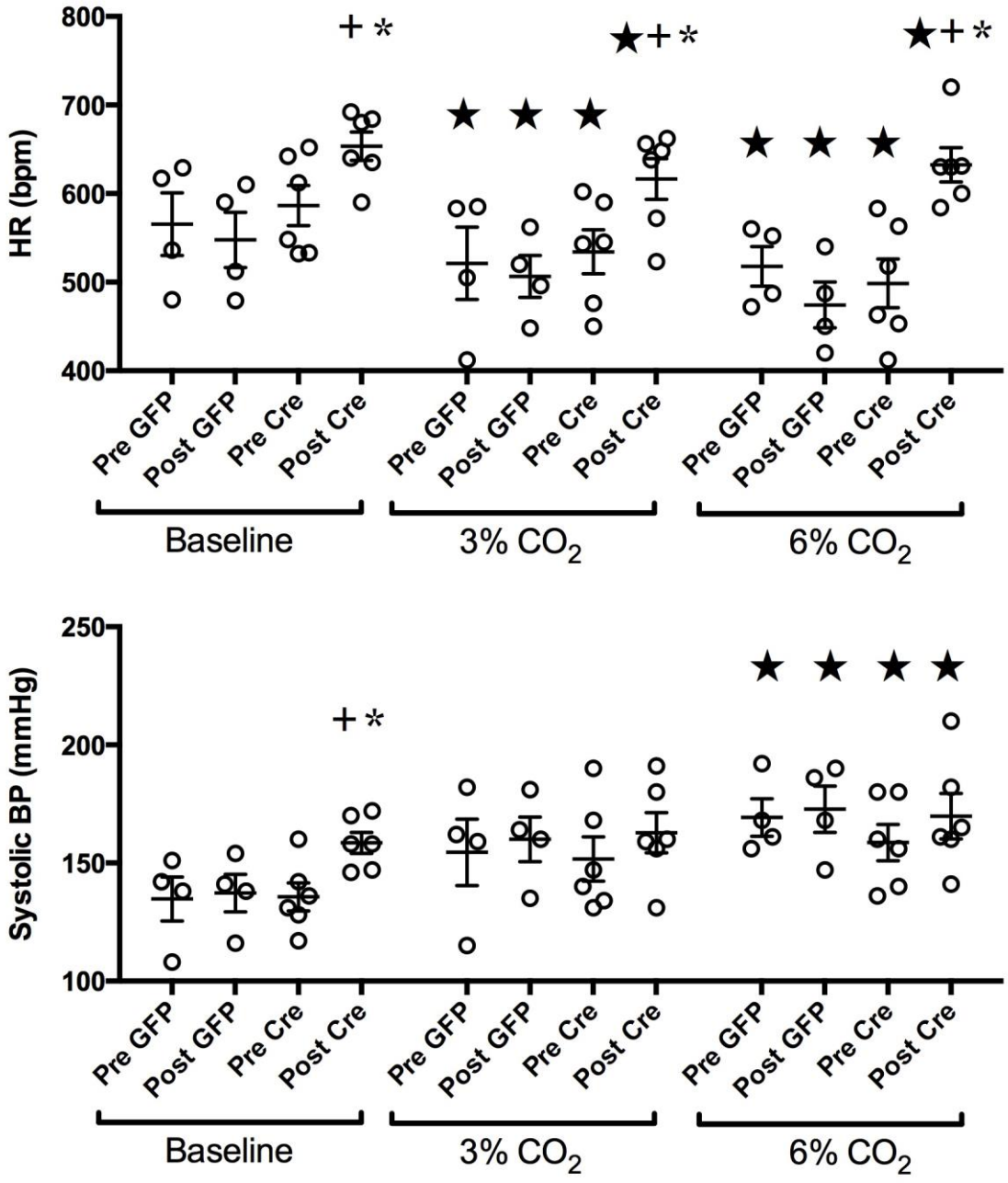

Figure 5.4.2 Haemodynamic response to hypercapnic challenge in $G\alpha_o$ floxed brainstem Cre mice and control.

Heart rate (HR) and systolic blood pressure (BP) pre and post Cre/GFP AVV and GFP AVV injections. Individual data and means ± SEM are shown. indicates significant difference from normoxia; + indicates significant difference from post GFP; * indicates significant difference from pre Cre.

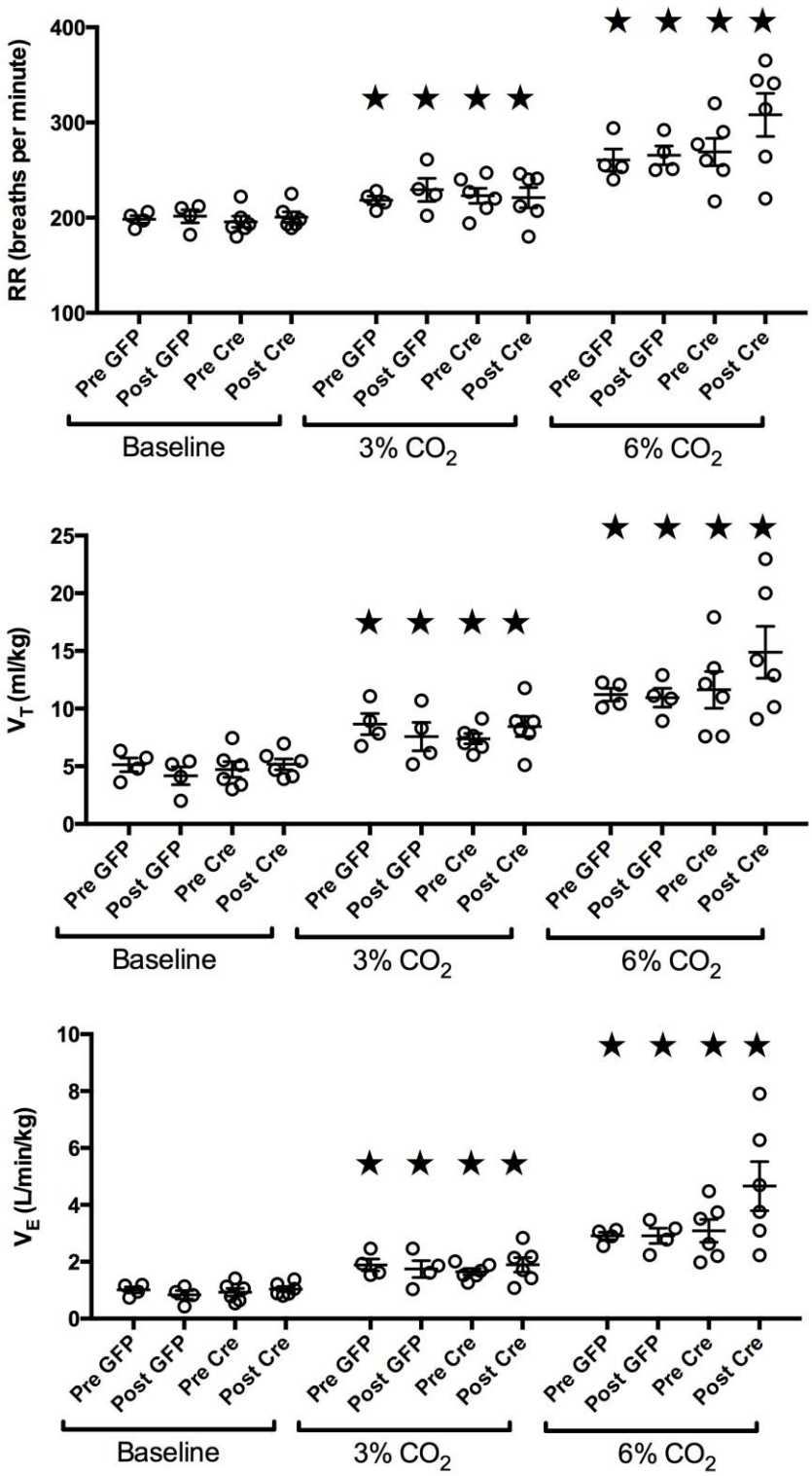

Figure 5.4.3 Respiratory response to hypercapnic challenge in $G\alpha_O$ floxed brainstem Cre mice and control.

Respiratory rate (RR), tidal volume (V_T) and minute volume (V_E) pre and post Cre/GFP AVV and GFP AVV injections. Individual data and means ± SEM are shown. indicates significant difference from normoxia

5.5 Discussion

In this chapter, I described the results of experiments aimed to investigate the effect of $G\alpha_O$ deletion in the presympathetic circuits of the brainstem on central cardiovascular control in the conscious mice. $G\alpha_O$ flx/flx mice were studied in a conscious state before and after Cre AVV and control GFP AVV injections into the RVLM, which contains a principal group of sympathoexcitatory neurones which generate sympathetic tone. There were no differences in 24-hour HR and BP profile in mice when compared before and after Cre AVV injections when the animals were studied in the freely ambulatory state. However, when the animals were placed in the plethysmography chamber, $G\alpha_O$ floxed brainstem Cre mice displayed higher resting HR and systolic BP, and abnormal HR response to hypoxia and hypercapnia. There were no significant changes in respiratory parameters. Thus, the exposure to novel environment and stressors in a plethysmography chamber reveals the role of $G\alpha_O$ in the central nervous mechanisms of HR and BP control.

5.5.1 No effect of $G\alpha_O$ deletion in the RVLM on HR and BP profile in conscious freely moving mice housed in standard conditions

There were no significant differences in HR and BP profile after $G\alpha_O$ deletion in the presympathetic area of the brainstem in conscious freely moving mice housed in standard conditions. This observation is in agreement with findings obtained in rats demonstrating that chronic C1 lesions in the conscious state is associated with only a modest reduction in BP and no changes in HR (Madden et al. 2003, Schreihofer et al. 2000). These data suggested that the role of RVLM in HR and BP control under normal resting conditions is at most moderate.

As discussed above, the prevailing autonomic tone in mice is dependent on ambient temperature, housing conditions and recovery time post surgery. When the conditions are optimum, mice exhibit a significant resting vagal tone as mentioned in Chapter 3 (Swoap et al. 2008; Just et al. 2000; Zuberi

et al. 2008). In this context, another possible explanation for the observations made is that the inhibitory influences on the RVLM mediated via $G\alpha_O$ do not make a significant contribution to the overall autonomic tone to the cardiovascular system when vagal tone predominates.

5.5.2 Mice with $G\alpha_O$ deletion in the RVLM display elevated HR and BP in a novel environment (plethysmography chamber)

When placed in the plethysmography chamber, $G\alpha_O$ floxed brainstem Cre mice had significantly elevated HR and BP whilst these parameters have normalised in control mice towards the end of 20 minutes of acclimatisation. There was no difference in the respiratory parameters.

Activation of the RVLM by supramedullary structures including the hypothalamic PVN, lateral parabrachial nuclei and midbrain central gray via a cholinergic pathway has been shown to occur in response to a variety of stress paradigms including emotional or psychological stressors (Li et al. 1995; Kubo et al. 2000). In a stress-induced model of hypertension, microinjection of μ and σ opiod receptor agonists, which are known to signal via inhibitory G proteins, have been shown to attenuate the hypertensive response (Li et al. 1995). The observed phenotype in our mice with $G\alpha_O$ deletion may hence be due to loss of inhibitory influence to the RVLM in this context.

5.5.3 Haemodynamic and respiratory responses to hypoxia and hypercapnia in control mice

Campen et al (Campen et al. 2005) studied the haemodynamic responses to hypoxia in different strains of mice and found heterogenous BP and HR responses. BP response can range from maintenance of normotension to a hypotensive response and an equally variable HR response. In contrast, the responses to hypercapnia are more homogenous with a generally hypertensive response and corresponding baroreflex-mediated reduction in HR.

Mice used in this study responded to hypoxia with elevations in HR and no significant change in BP. In accord with observations of Campen et al, the mice responded to hypercapnia with a reduction in HR associated with an increase in BP.

Mammals respond to hypoxia and hypercapnia with increases in minute ventilation. However, the respiratory rate and tidal volume components can differ significantly between different mouse strains (Teppema & Dahan 2010). In mice used in this study, there was a vigorous increase in minute ventilation to both hypoxia and hypercapnia, with a larger relative increase in respiratory rate compared to tidal volume.

5.5.4 Altered haemodynamic responses to hypoxia in mice with conditional deletion of $G\alpha_O$ in the brainstem

Mice with conditional deletion of $G\alpha_O$ in the RVLM respond to hypoxia with enhanced HR response to 10% O_2 and HR remained elevated during recovery with no significant changes to arterial BP.

Hypoxia induces both local and centrally mediated changes to HR and arterial BP. Hypoxia stimulates the carotid body peripherally and also central chemoreceptors and results in vigorous activation of presympathetic barosensitive RVLM neurones resulting in sympathetic activation and this response can be modified by the baroreflex (Koshiya et al. 1993) and central respiratory generator drive (Mandel et al. 2006). Changes to arterial BP during hypoxia are due to a combination of decrease in arteriolar resistance due to locally mediated vasodilation and baroreceptor-mediated constriction of larger vessels as well changes to HR and contractility due to the altered autonomic output (Campen et al. 2004; Ray et al. 2002).

Richter et al. (Richter et al. 1999) studied the release of neurotransmitters and neuromodulators in the ventral medullary region of anaesthetised cats subjected to 5 minutes of hypoxia (7% O_2 in the inspired air) using a

microdialysis technique. There was a rapid but transient rise in glutamate and GABA concentrations initially, reaching a peak level by 1 minute of exposure to hypoxia. This correlated with a period of augmented respiratory activity. Subsequently, a delayed rise in 5-HT levels was detected towards the end of the hypoxic period followed by a rise in adenosine levels, which were thought to contribute to post hypoxic respiratory depression. By using the more sensitive amperometric probes in rats, Gourine et al. found that acute hypoxia induced a significant increase in adenosine level in the NTS and a much smaller increase in adenosine level in the ventral medullary region (only about 10 % of that in the NTS) (Gourine et al. 2002). Adenosine levels peaked during the reoxygenation period after termination of the hypoxic challenge, in agreement with the findings of Richter et al.

GABA, 5-HT and adenosine can all mediate inhibitory influences via $G\alpha_{i/O}$ coupled receptors. Loss of inhibitory signalling via $G\alpha_{O}$ could hence potentially explain the augmented HR response during both hypoxia and the post hypoxic recovery period.

The co-release of GABA with glutamate with similar temporal kinetics (Richter et al. 1999) suggests a role for GABA as a restraining influence to the excitatory effects of glutamate during hypoxia. Indeed, there is evidence that GABA-ergic inhibitory mechanisms are important in modulating RVLM activity during hypoxia in rat neonatal brainstem preparations (Boychuk et al. 2012).

Inhibitory influences of 5-HT and adenosine have also been shown to regulate sympathetic responses in the brainstem region. Activation of 5-HT 1A receptors in the brain stem which signal via $G\alpha_{i/O}$ causes a potent and selective suppression of the hypertensive and sympathoexcitatory response evoked by stimulation of the dorsomedial hypothalamic nucleus (Horiuchi et al. 2005). Adenosine has been shown to evoke an increase in arterial pressure when injected into rostral areas of the RVLM and also to augment increases in BP in response to stimulation of the hypothalamic defense area via its action on the RVLM (Thomas & Spyer 1996).

Extracellular adenosine can arise during systemic hypoxia either from the action of nucleoside transporters or from the breakdown of ATP released from neural structures which are then broken down by ectonucleotidases into adenosine (Spyer & Thomas 2000). Peripherally, adenosine has been shown to have vasodilatory effect on peripheral vasculature (Ray et al. 2002), which may counteract the effect on arterial BP resulting from increased sympathetic tone and explain the lack of difference seen.

5.5.5 Altered haemodynamic responses to hypercapnia in mice with conditional deletion of $G\alpha_O$ in the brainstem

Increase in arterial pCO_2 elicits a sympathetic response in rodents (Campen et al. 2005). The cardiovascular effect is manifested by a predominantly pressor response with concomitant baroreflex mediated drop in HR. There is hence also co-stimulation of the vagal preganglionic neurones as part of the baroreflex arc resulting in increased vagal tone to the pacemaking cells of the heart (Paton & Butcher 1998; Spyer & Gilbey 1988).

The RVLM has been implicated with evidence of increased activity during hypercapnia *in vivo* (Seller et al. 1990) and permanent depletion of catecholaminergic C1 neurones abolished sympathoexcitation induced by activation of peripheral chemoreceptors (Schreihofer et al. 2005) but not from central actions of CO_2 (Marina et al. 2011). Purinergic signalling involving P2 receptors have also been implicated as an important mediator in chemosensory transduction in the brainstem (Gourine et al. 2005).

$G\alpha_O$ deletion in the RVLM attenuated the drop in HR with no significant effect on the increase in arterial BP during hypercapnia when compared to control mice. Given that there is co-stimulation of both pre-sympathetic and vagal preganglionic neurones activated via baroreflex input, it would appear that loss of $G\alpha_O$ results in either increase in sympathoexcitation and/or decrease in activation of vagal preganglionic neurones, or an increase in both sympathetic and vagal outputs with the sympathetic output dominating.

Given that there was no significant difference in arterial BP concomitant to an increase in HR, this would suggest a change in the baroreflex sensitivity associated with loss of $G\alpha_O$ proteins in the RVLM.

5.5.6 Summary

This chapter described the results of experiments aimed to determine the role of $G\alpha_O$ in the brainstem mechanisms of cardiovascular control in the conscious mice. It was found that mice with conditional deletion of $G\alpha_O$ in the brainstem displayed similar HR and arterial BP profile to control mice under normal physiological resting conditions (conscious, freely-moving in normal housing). However, when exposed to novel environment or environmental stressors like hypoxia or hypercapnia the same mice demonstrated a phenotype consistent with increased sympathetic activity. Taken together, loss of inhibitory signaling in the RVLM and the resulting dis-inhibition of pre-sympathetic circuits under conditions of stress is the likely explanation of the cardiovascular phenotype seen in mice with conditional $G\alpha_O$ deletion in the brainstem.

To investigate this cardiovascular phenotype further and examine the effect of increased sympathetic tone on *in vivo* cardiac electrophysiology and predisposition to cardiac arrhythmia, we studied cardiac baroreceptor reflexes and performed programmed electrical stimulation on these mice using an *in vivo* anaesthetised preparation.

Chapter 6

Results IV

Baroreflex sensitivity and electrophysiological properties of the heart in mice with $G\alpha_O$ deletion in the RVLM

6.1 Introduction

As described above (Chapter 5), mice with conditional deletion of $G\alpha_O$ in the brainstem appear to have higher sympathetic tone when exposed to novel environment or environmental stressors like hypoxia and hypercapnia. This Chapter describes the results of experiments aimed to further dissect the mechanisms underlying this phenotype by assessing the baroreflex sensitivity of these mice using an *in vivo* anaesthetised preparation. The mice were also subjected to pharmacological blockade of vagal and sympathetic influences using atropine and atenolol, respectively, to investigate the relative contribution of each autonomic arm to the observed phenotype. The significance of $G\alpha_O$ deletion in the brainstem on *in vivo* cardiac electrophysiology was then studied using the programmed electrical stimulation paradigm.

6.1.1 Baroreflex sensitivity and alterations in sympathovagal tone

As discussed previously, arterial BP-HR baroreflex studies can provide an indirect assessment of the neural control of the cardiovascular system. Alteration in autonomic tone is associated with changes in baroreflex sensitivity. In particular, increase in sympathetic tone with resulting sympathovagal imbalance is shown in humans and animal models to correlate with depressed baroreflex sensitivity and associated with poorer prognosis (Nolan et al. 1998).

6.1.2 *In vivo* cardiac electrophysiology assessed by programmed electrical stimulation

By applying methodologies of programmed electrophysiological stimulation used in humans to the *in vivo* mouse model, the effect of alteration in autonomic tone on the electrical properties of the ventricular myocardium can be studied. In particular, increase in sympathetic tone to the heart is known to reduce the ventricular effective refractory period (VERP) with an opposite effect mediated by vagal tone (Zipes and Douglas 2013).

Burst pacing to induce VT provides a quantifiable and robust measure of arrhythmia susceptibility, allowing the examination of how changes in autonomic tone to the heart can affect electrical stability (Yoon et al. 1977; Kent et al. 1973).

6.2 Resting cardiovascular parameters in $G\alpha_O$ floxed brainstem Cre mice and controls under urethane anaesthesia

A separate cohort of $G\alpha_O$ floxed brainstem Cre mice (n=14) and controls (n=12) were studied under urethane anaesthesia as described in detail in Chapter 2. Baroreflex sensitivity was assessed in five mice from each group following cannulation of both jugular veins for administration of test compounds, the left internal carotid artery for arterial BP measurement and implantation of needle electrodes for surface ECG recordings as described in Chapter 2. The remaining animals underwent *in vivo* cardiac electrophysiological study with the EPR-800 catheter inserted to the right ventricle via the right internal jugular vein and surface ECG recorded from needle electrodes (see section 6.5).

Baseline measurements were obtained 30 minutes after mice were anaesthetised and instrumented. Table 6.1 summarises the baseline HR, BP and ECG parameters obtained for $G\alpha_O$ floxed brainstem Cre mice and controls under urethane anaesthesia. Figures 6.2.1 and 6.2.2 summarises the HR and systolic BP data for $G\alpha_O$ floxed brainstem Cre mice and controls when studied under the two different conscious states described in Chapter 5 and the urethane anaesthetised state.

Under urethane anaesthesia, $G\alpha_O$ floxed brainstem Cre mice had significantly higher HR compared to controls (614±5 v 587±5 bpm, $p<0.001$) with no difference in systolic BP between $G\alpha_O$ floxed brainstem Cre mice and controls (86±5 vs 81±5 mmHg, $p=0.125$).

	Control	$G\alpha_O$ floxed brainstem Cre	*p* value
HR (bpm) (n= 12 v 14)	**587±5**	**614±5 *****	**<0.001**
SBP ($mmHg^{-1}$) (n= 5 v 5)	81±5	86±5	0.125
PR (ms) (n= 7 v 9)	33±2	33±2	0.837
QRS (ms) (n= 7 v 9)	14±1	15±2	0.519
QT_C (ms) (n= 7 v 9)	84±5	95±5	0.150

Table 6.1 Summary data of HR, systolic BP (SBP) and ECG parameters of control and $G\alpha_O$ floxed brainstem Cre mice studied under urethane anaesthesia .

Data are expressed as means ± SEM. Values highlighted in bold are significantly different when compared to controls. *** *P<0.001*

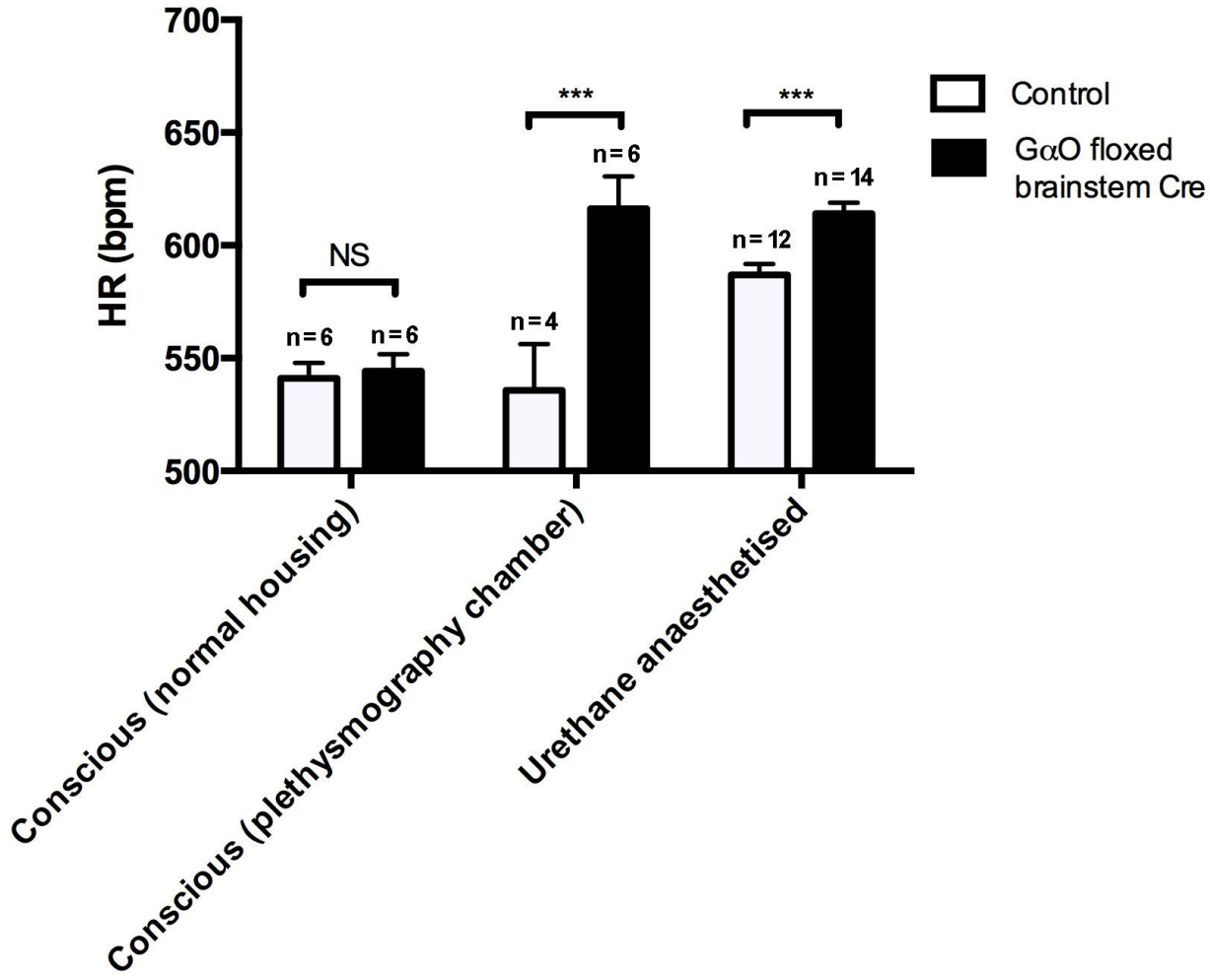

Figure 6.2.1 HR of mice with conditional deletion of $G\alpha_O$ in the RVLM compared to controls during conscious and anaesthetised experiments.

Summary data comparing HR of $G\alpha_O$ floxed brainstem Cre mice and controls (all after AVV injections) during conscious and anaesthetised experiments. Data expressed as mean ± SEM. NS $p \geq 0.05$, *** $p < 0.001$.

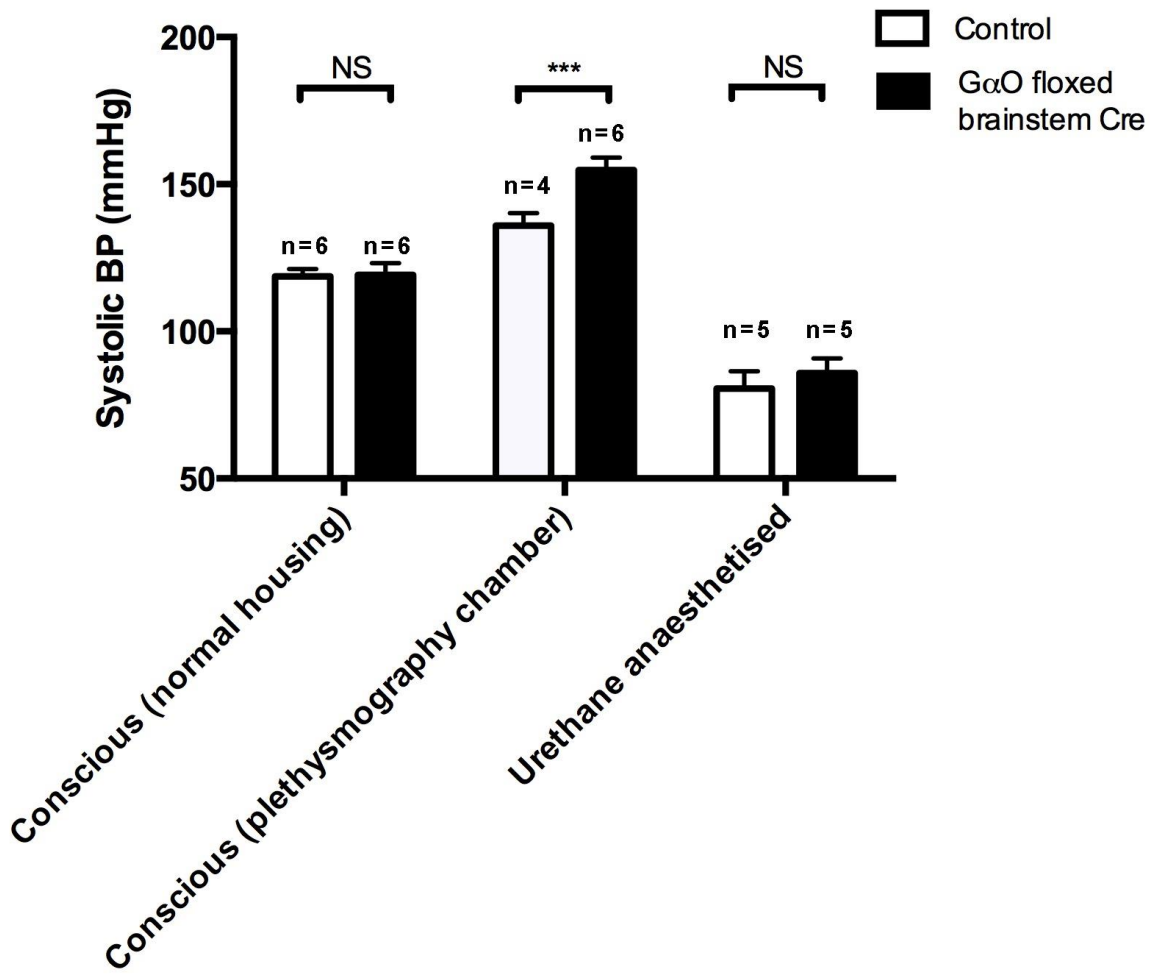

Figure 6.2.2 Systolic BP of mice with conditional deletion of $G\alpha_O$ in the RVLM compared to controls during conscious and anaesthetised experiments.

Summary data comparing systolic BP of $G\alpha_O$ floxed brainstem Cre mice and controls (all after AVV injections) during conscious and anaesthetized experiments. Data expressed as mean ± SEM. NS *p≥0.05*, *** *p<0.001.*

6.3 HR changes in urethane anaesthetised mice following autonomic blockade

To further study the contribution of the sympathetic and parasympathetic limbs of the autonomic nervous system to the HR of urethane anaesthetised mice, atenolol (1 mg/kg) followed 30 minutes later by atropine (1 mg/kg) was given intraperitoneally to nine $G\alpha_O$ floxed brainstem Cre mice and seven control mice undergoing *in vivo* cardiac electrophysiological studies. The HR measurements were obtained after a 10 minute period following each drug administration and are shown in Figure 6.3.1.

The HR difference between the group was abolished after administration of atenolol (450±10 v 440±12, p=0.893) with a small increase in heart rate after administration of atropine (460±10 v 455±8, p=0.824) which was not significantly different between the groups.

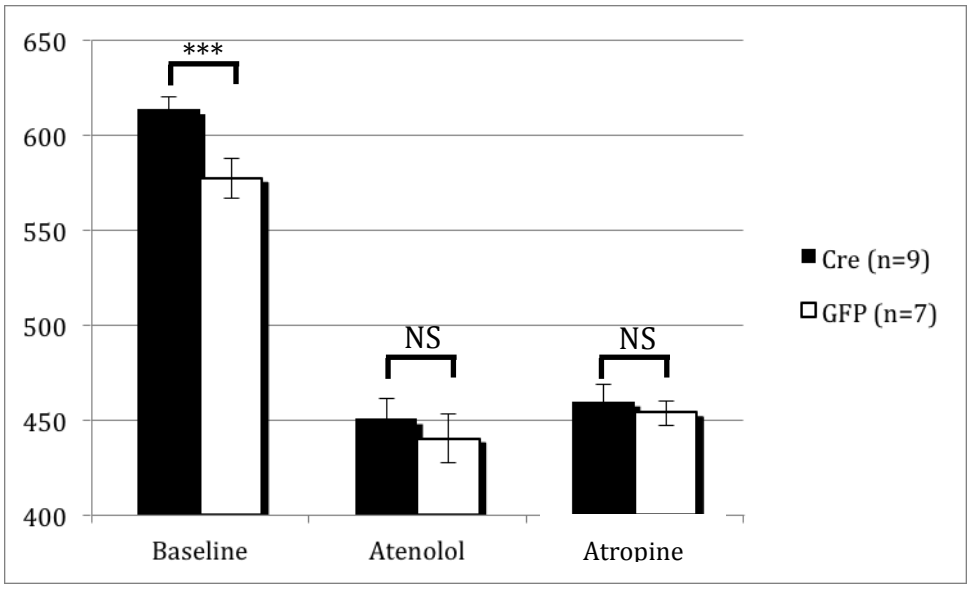

Figure 6.3.1 HR of mice with deletion of $G\alpha_O$ in the RVLM compared to controls following autonomic blockade.

Comparison of HR between $G\alpha_O$ floxed brainstem Cre mice and controls at baseline and after administration of atenolol 1mg/kg ip followed by atropine 1mg/kg ip. Data expressed as mean ± SEM. NS $p \geq 0.05$, *** $p < 0.001$.

6.4 Baroreflex sensitivity in $G\alpha_O$ floxed brainstem Cre mice and controls

$G\alpha_O$ floxed brainstem Cre mice had elevated HR compared to controls with increased minimum HR (604±2 v 575±9 bpm, p=0.028), maximum HR (654±6 v 620±4 bpm, p=0.017) and HR at half BP range (629±3 v 598±5 bpm, p=0.017). This is associated with a greater baroreflex gain compared to controls (0.65±0.07 v 0.35±0.01 p=0.012). There were no significant differences in the BP parameters.

Figure 6.4.1 summarises the HR-systolic BP baroreflex plots constructed from the HR and BP data obtained when $G\alpha_O$ floxed brainstem Cre and control mice were given iv boluses of phenylephrine (0.5-2.5 mg kg^{-1} iv in 2-10 µL boluses) and sodium nitroprusside (0.1-1 mg kg^{-1} iv in 1-10µL boluses) as described in Chapter 2.

Table 6.2 summarises the data derived from the baroreflex curves.

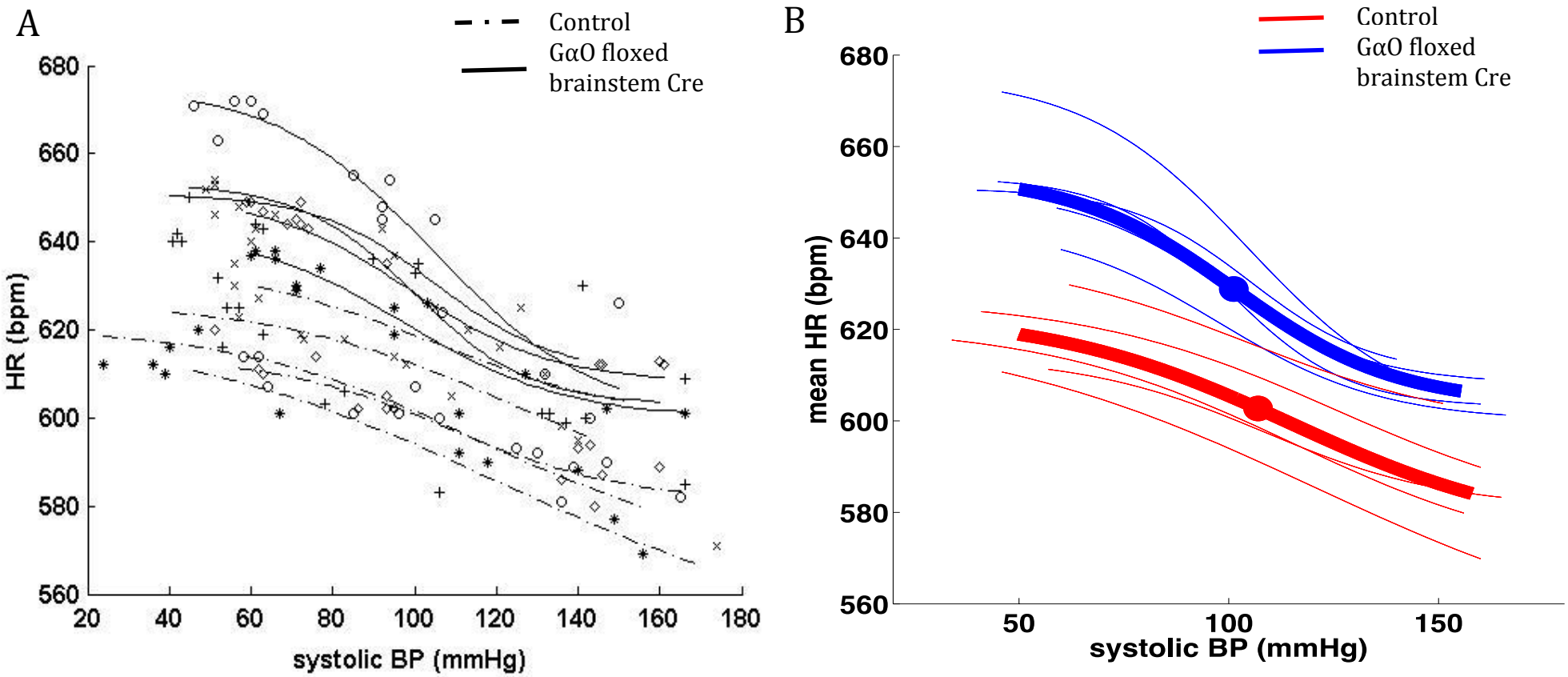

Figure 6.4.1 HR and systolic BP baroreflex response curves of mice with conditional deletion of $G\alpha_O$ in the RVLM compared to controls

(A) Individual plots of HR and systolic BP for $G\alpha_O$ floxed brainstem Cre mice and controls (n=5 for each group) following pharmacological challenges with iv phenylephrine and sodium nitroprusside as described. A best fit sigmoidal baroreflex response curve is then plotted for each subject. (B) Mean baroreflex curves (bold lines) for $G\alpha_O$ floxed brainstem Cre mice and controls. Bold points represent mean HR 50 and SBP 50 for each group.

	Cre (n=5)	GFP control (n=5)	P value
HR min (bpm)	**604±2**	**575±9 ***	**0.028**
HR 50 (bpm)	**629±3**	**598±5****	**0.002**
HR max (bpm)	**654±6**	**620±4 ***	**0.017**
HR range (bpm)	50±6	48±7	0.451
SBP min (mmHg)	50±4	43±6	0.399
SBP 50 (mmHg)	115±4	111±2	0.074
SBP max (mmHg)	155±5	153±5	0.850
BP range (mmHg)	114±6	117±2	0.325
BR gain (ms/mmHg)	**0.65±0.07**	**0.35±0.01***	**0.012**

Table 6.2 Summary data of parameters derived from mean baroreflex curves for mice with conditional deletion of $G\alpha_o$ in the RVLM compared to controls

Data are expressed as means ± SEM. Values highlighted in bold are significantly different when compared to controls. * *P<0.05*, ** *P<0.01*

6.5 Programmed electrical stimulation in $G\alpha_O$ floxed brainstem Cre mice and controls

In a separate experiment, cardiac electrophysiological properties of 9 Cre AVV and 7 GFP AVV injected mice were studied using the octapolar EPR-800 catheter placed in the right ventricle. S1/S2 and burst pacing protocols were applied to obtain VERP and to induce VT (Figure 6.5.1)

$G\alpha_O$ floxed brainstem Cre mice had a significantly reduced $VERP_{750}$ compared to controls ($VERP_{750}$ 48±3 vs 65±4 ms, $p<0.001$). When $VERP_{750}$ measurements were repeated 30 minutes after administration of atenolol (1mg/kg ip), the difference in VERP was no longer observed (63±3 vs 61±2, $p=0.72$) (Figure 6.4.2).

The mice were then subjected to burst pacing stimulation protocol. V_T was induced in 3 out of 9 mice expressing Cre in the RVLM compared to 0 out of 7 control mice.

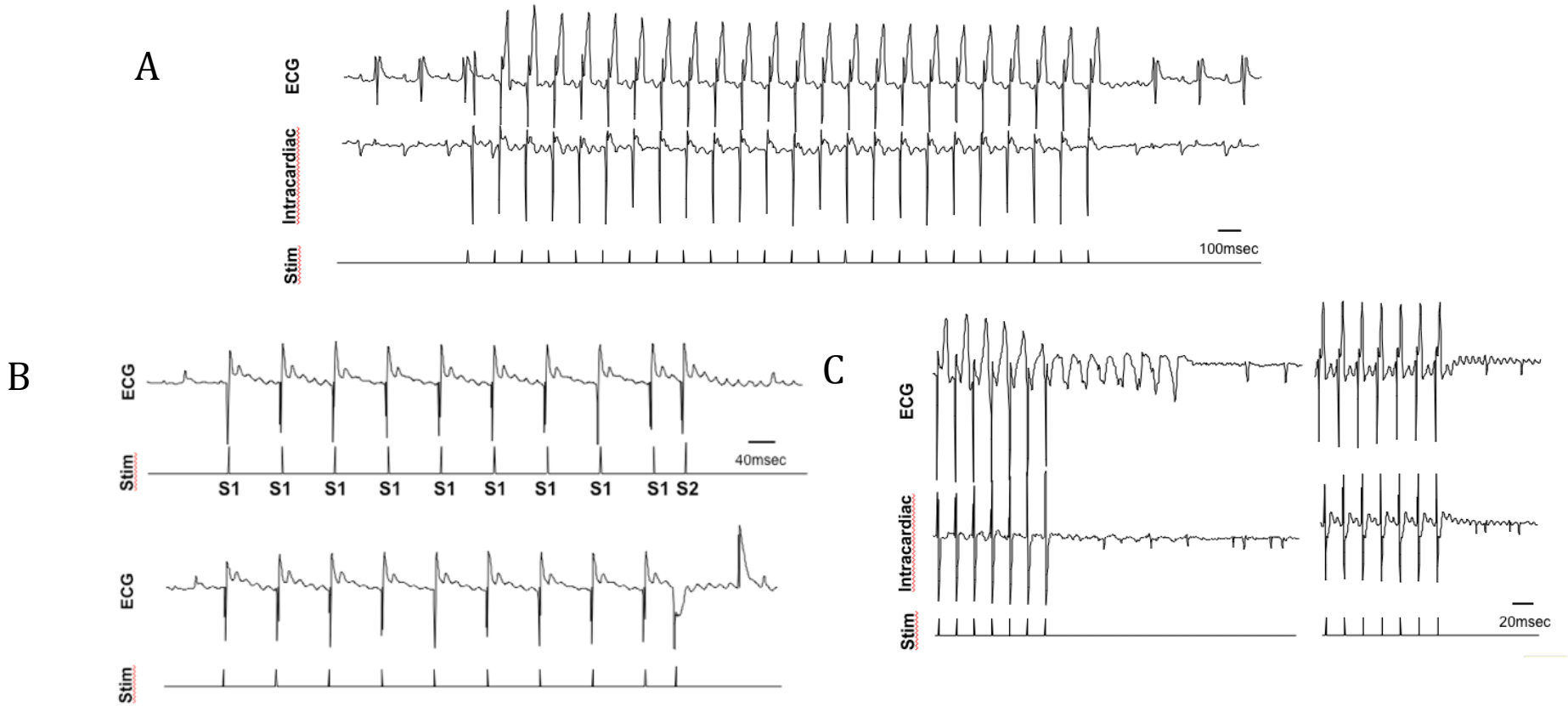

Figure 6.5.1 Programmed electrical stimulation in mice with conditional deletion of $G\alpha_o$ in the RVLM and controls.

(A) Pacing the right ventricle with ventricular capture at a cycle length of 80msec (resulting in ventricular rate of 750bpm). (B) S1-S2 pacing protocol by pacing the ventricle at a cycle length of 80msec initially for 9 beats and bringing in an S2 beat at a shorter coupling interval of 40msec with capture of ventricle at top panel but by reducing S2 coupling interval to 38msec resulted in loss of capture at bottom panel. VERP is hence 38msec. (C) Burst pacing at 50Hz induced VT in left panel but not in right panel. ECG: surface ECG; Intracardiac: intracardiac electrograms; Stim: pacing stimulus.

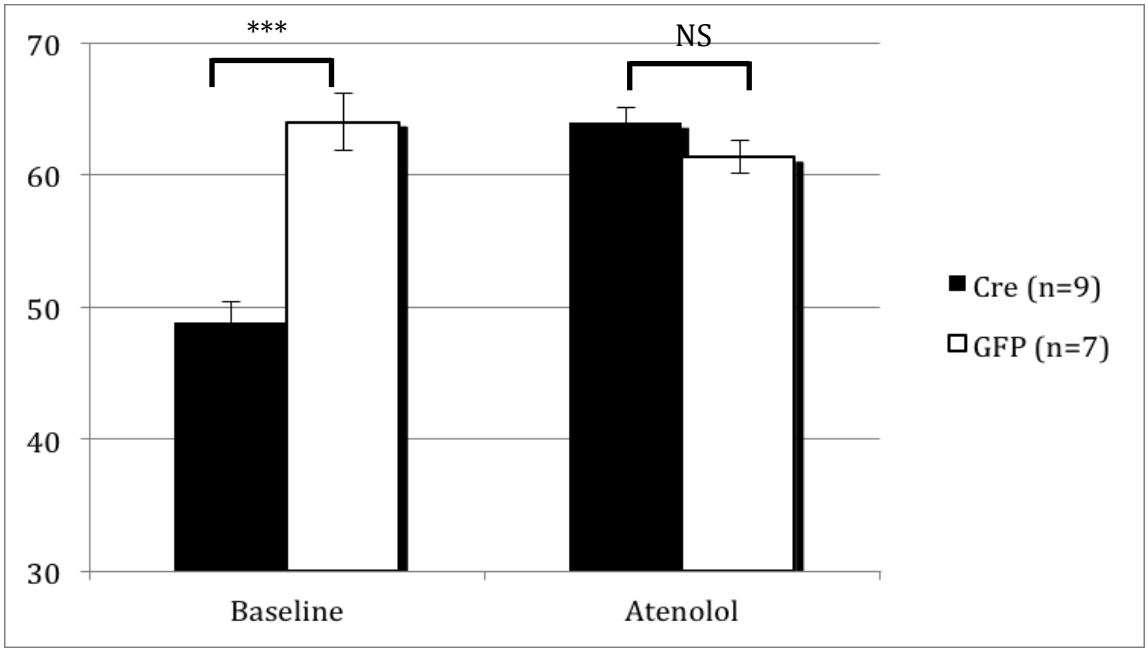

Figure 6.5.2 $VERP_{750}$ in mice with conditional deletion of $G\alpha_O$ in the RVLM compared to controls pre and post atenolol

Comparison of $VERP_{750}$ between $G\alpha_O$ floxed brainstem Cre mice and controls at baseline and after administration of atenolol 1mg/kg ip.
Data expressed as mean ± SEM. NS *p≥0.05*, *** *p<0.001.*

6.6 Discussion

Experiments described in this chapter studied $G\alpha_O$ floxed brainstem Cre mice in the urethane anaesthetised state and compared them to controls injected with GFP AVV. It was found that mice under urethane anaesthesia displayed higher HR and lower arterial BP compared to the conscious state. Mice with $G\alpha_O$ deletions in the RVLM were more tachycardic and had increased baroreflex sensitivity compared to controls. They also displayed pro-arrhythmic phenotype in the cardiac ventricle as evident from a decreased VERP and susceptibility to VT during programmed electrical stimulation. The differences in HR and VERP between experimental and control animals were abolished following administration of atenolol, suggesting that the differences observed are due to higher sympathetic activity resulting from G□$_O$ deletion in the RVLM.

6.6.1 Autonomic tone during urethane anaesthesia

Mice studied under urethane anaesthesia have previously been shown to have little vagal tone and have reduced arterial pressure and increased HR compared to the conscious state (Paton & Butcher 1998; Desai et al. 1997). Similar findings were obtained here with urethane anaesthetised mice being significantly more hypotensive and generally more tachycardic. Sequential challenges with atenolol and atropine revealed low vagal tone and demonstrated that sympathetic activity indeed dominates heart rate control in mice under urethane anaesthesia.

6.6.2 Increased HR and baroreflex sensitivity in mice with conditional deletion of $G\alpha_O$ in the brainstem

$G\alpha_O$ floxed brainstem Cre mice display increased heart rate and enhanced baroreflex sensitivity compared to controls. Taken together with the fact that our mice display a sympathetic predominance under urethane anaesthesia, this suggests that in mice with conditional deletion of $G\alpha_O$ in the brainstem increased sympathetic outflow (rather than vagal withdrawal) is largely

responsible for sympathovagal imbalance and autonomic phenotype observed.

The finding that there is little vagal tone in our urethane aneasthetised preparation may also explain why there is increased and not decreased baroreflex sensitivity associated with increased sympathetic outflow as normally seen. When sympathetic and vagal influences are both present, increased sympathetic outflow is normally associated with reduction in vagal tone and as the vagal component usually makes a larger contribution to baroreflex sensitivity there is normally a resulting depression of baroreflex sensitivity. However, in the absence of a prevailing vagal tone, the sympathetic limb is largely responsible for the baroreflex response and hence may account for the increase in baroreflex sensitivity seen in mice with $G\alpha_O$ deletion in the brainstem.

6.6.3 Reduced VERP and increased susceptibility to VT in mice with conditional deletion of $G\alpha_O$ in the brainstem

On programmed electrical stimulation, $G\alpha_O$ floxed brainstem Cre mice had significantly reduced VERP and this was associated with an increase in susceptibility to VT during burst pacing. A reduction in VERP is pro-arrhythmic in situations of both re-entry and triggered activity (Zipes and Jalife 2009). It is worth noting that the 129/Sv strain is relatively resistant to ventricular arrhythmia (Maguire et al. 2003) and we were able to induce VT in one third of mice with conditional deletion of $G\alpha_O$ in the brainstem but none in the controls. The difference in VERP was abolished after administration of atenolol. Taken together with previous observations, the change in ventricular refractoriness and susceptibility to VT observed in $G\alpha_O$ floxed brainstem Cre mice appears to be due to increased sympathetic outflow to the heart.

It is well known that the autonomic nervous system modulates cardiac electrophysiology. Increase in sympathetic tone to the heart has been shown to reduce action potential duration with a corresponding increase in

conduction velocity, resulting in a change in the restitution properties of action potential duration and dispersion of ventricular repolarisation and increased susceptibility to ventricular arrhythmia (Zipes and Jalife 2009).

6.6.4 Limitations

Pharmacological measurements of arterial baroreflex sensitivity takes into account the entire arterial baroreflex arc, from the input into the system to the ensuing end-organ response. Thus the derived baroreflex sensitivity takes into account all 3 components of the reflex arc: the arterial baroreflex afferent input, central processing, and efferent output. As a result, alterations in one limb of the baroreflex network may be compensated for by other areas and therefore it may be necessary to investigate the individual pieces of the reflex pathway independently to conclude any changes seen is due to alterations in central processing. Examples of ways to dissect out the different mechanisms would include direct stimulation of the aortic depressor nerve to bypass the afferent pathway and directly evaluate central and efferent components or recording the efferent sympathetic nerve to directly measure the efferent output. These approaches are of course technically very challenging.

6.6.5 Summary

In this chapter I have shown that urethane anaesthetised mice are tachycardic and hypotensive compared to the conscious state. Deletion of $G\alpha_O$ in the RVLM leads to increased HR and baroreflex gain. Given that sympathetic tone appears to predominate with little vagal input upon dual autonomic blockade, it is likely that the changes seen are due to increased sympathetic tone due to loss of inhibitory influences to the RVLM. Lastly, this increase in sympathetic tone to the heart is associated with shortened VERP and an increased predisposition to ventricular arrhythmia on programmed electrical stimulation of the heart.

Chapter 7

General Discussion

7.1 Summary of findings

In this thesis, I sought to study the role of inhibitory G protein $G\alpha_O$ in the autonomic regulation of the heart.

I found that $G\alpha_{i2}$ and not $G\alpha_O$ is important in modulating vagal effects at the level of the cardiac conduction tissue. Loss of $G\alpha_{i2}$ in the cardiac conduction tissue resulted in increased daytime HR association with loss of HF power on HRV analysis. This is in contrast to mice with similar loss of $G\alpha_O$ in the cardiac conduction tissue which had normal HR profile and HRV.

Mice with deletion of $G\alpha_O$ in the presympathetic circuits of the brainstem (RVLM) had normal HR and arterial BP under normal resting conditions. However, when stressed in a novel environment or under urethane anaesthesia, these mice developed a pronounced elevation in HR with abnormal HR responses during hypoxic and hypercapnic conditions and is associated with altered baroreflex sensitivity. Dual autonomic blockade with atenolol and atropine suggests that this phenotype is largely due to an increase in sympathetic tone. Finally, this increase in sympathetic tone to the heart is associated with alterations in ventricular electrophysiology as evidenced by reduction in VERP and increased susceptibility to VT during burst pacing.

I conclude that $G\alpha_O$ plays an important role in mediating inhibitory influences in the presympathetic circuits of the brainstem under conditions of ‘stress’. Loss of $G\alpha_O$ results in increased sympathetic tone to the heart with resulting abnormal cardiovascular reflexes and alterations in cardiac electrophysiology.

7.2 Findings in the context of what is currently known

The findings of this study build on and add on to current understanding in a number of areas. Firstly, our data contributes to the increasing body of evidence demonstrating G protein subtype specificity in mediating biological processes *in vivo.* Work in our group has previously shown that two subtypes of inhibitory G proteins, $G\alpha_{i2}$ and $G\alpha_{O}$ appear to be important for the autonomic modulation of HR *in vivo* in global KO mice (Zuberi et al. 2008). I have now shown in conditional knockout models that $G\alpha_{i2}$ is important in modulating vagal tone at the level of the cardiac conduction tissue, probably by coupling to M2 receptors, whilst $G\alpha_{O}$ appears to play a role in mediating inhibitory influences to the brainstem presympathetic circuits.

Using HCN4 to target the deletion of $G\alpha_{i2}$ in the cardiac conduction tissue has also lead to several insights. HCN4 and HCN1 were found to be the predominant isoforms expressed in murine cardiac SA nodal (SAN) cells (Herrmann et al. 2011). Mice with conditional deletion of HCN4 in the SAN had frequent sinus pauses but otherwise normal mean heart rate when sinus pauses are excluded and preserved circadian rhythm (Herrmann et al. 2007, Hoesl et al. 2008). I have now shown that loss of $G\alpha_{i2}$ signalling in HCN4 expressing cells does lead to abnormality of HR phenotype with increased daytime HR and loss of circadian rhythm. This suggests that HCN4 expressing SAN cells are indeed important in cardiac pacemaking. Similar to the findings in HCN4 KO mice, I found no differences in the conduction and repolarisation intervals on the ECG in mice with conditional KO of $G\alpha_{i2}$ in HCN4 expressing cells. This could either mean that signalling via $G\alpha_{i2}$ is not important in determining the conduction and repolarisation properties of other tissues in the cardiac conduction system, or that other HCN subtypes such as HCN1 can compensate for loss of $G\alpha_{i2}$ signalling in these HCN4 expressing cells.

An increasing body of evidence is accumulating on the importance of the presympathetic network, and more specifically the RVLM, in mediating responses to a variety of physiological and pathological stressors (Guyenet

et al. 2013). Our data adds to the body of evidence of the key role played by the RVLM under conditions of stress including hypoxia and hypercapnia.

In addition, it would appear that inhibitory signaling in the brainstem is an important mechanism by which sympathetic activity is regulated centrally. For example, the RVLM is activated by increased dorsomedial hypothalamus activity in response to psychological stressors (Madden & Morrison 2004, Nalivaiko & Blessing 2001). This increased sympathetic activity is reversibly inhibited by intracisternal and direct administration of selective serotonin-1A (5-HT1A) receptor agonist 8-hydroxy-2-(di-n-propylamino)tetralin (8-OH-DPAT) into the medullary raphe region (Ngampramuan et al. 2008, Nalivaiko et al. 2005). 5-HT1A receptors are one of many GPCRs in the brainstem that signal via inhibitory $G\alpha_{i/o}$, with other inhibitory neurotransmitters and neuromodulators implicated in a variety of homeostatic and physiological responses as discussed previously. I have found in this study that loss of inhibitory G protein signaling in the RVLM resulted in a cardiovascular phenotype that was apparent only under conditions of stress. This adds to the body of literature as it suggests that co-activation of inhibitory inputs to the RVLM occurs during sympathoexcitation in response to physiological stressors.

Furthermore, this study has contributed to our understanding of the identity of inhibitory G protein subtype that is important in mediating inhibitory influences in the RVLM. Parker et al (Parker et al. 2012) has previously shown that $G\alpha_{i2}$ and $G\alpha_{O}$ are the most ubiquitous inhibitory G proteins in the rostral C1 cells of the RVLM. In keeping with this, our data suggests an important role for $G\alpha_{O.}$ Although we cannot exclude a role for $G\alpha_{i2}$ as this was not studied directly with a conditional knockout of $G\alpha_{i2}$ in the brainstem, it would appear that loss of $G\alpha_{O}$ signaling cannot be adequately compensated for by other inhibitory G protein subtypes.

Finally, alterations in autonomic tone is well known to contribute to changes in cardiac electrophysiology and contribute to arrhythmogenesis (Verrier & Antzelevitch 2004, Shen & Zipes 2014). I have shown that increased

sympathetic tone due to loss of $G\alpha_O$ proteins in the RVLM leads to alterations in cardiac ventricular electrophysiology, resulting in a pro-arrhythmic state. This adds to the body of evidence that alteration in autonomic tone has a direct effect on cardiac electrophysiology.

7.3 Insights into cardiovascular regulation in man

It is well recognised in humans that autonomic regulation of cardiac function is important in health and disease states. Many of the drugs used in the treatment of common cardiovascular diseases target the autonomic nervous system. Beta blockers is a good example of a class of drug that has reduced mortality in cardiovascular diseases (Al-Gobari et al. 2013).

With the development of techniques and devices that are able to directly modulate autonomic afferents and efferents such are renal nerve denervation (Myat et al. 2013), baroreceptor (Heusser et al. 2010) and vagal nerve stimulation devices (De Ferrari at al. 2011), there is a pressing need to understand better the autonomic pathways that regulate cardiovascular function in disease and health.

My work has shown that perturbations of inhibitory signalling in the presympathetic area of the brainstem results in sympathetic overactivity under conditions of stress but not during normal resting conditions. This has implications to cardiovascular disease where sympathetic overactivity is known to drive disease progression. Indeed, there is good preclinical (Geraldes et al. 2014, Marina et al. 2013) and clinical data (Smith et al. 2004, Malpas 2010) that attenuation of sympathetic activity can help arrest the development of hypertension and heart failure. The inhibitory circuits in the brainstem are hence potential druggable targets to attenuate sympathetic overactivity.

In addition, our mouse model can also be used to study the contributory effect of increased sympathetic activity of central origin on the development of cardiac pathologies. One example would be to study the incidence of

ventricular arrhythmias post coronary ligation to induce myocardial infarction in mice with $G\alpha_O$ deletion in the brainstem compared to controls to study the effect of increased sympathetic activity on arrhythmogenesis post myocardial infarction.

7.4 Limitations

I sought to study whether targeted deletion of different inhibitory G protein subtypes along the neuro-cardiac autonomic axis would lead to changes in cardiovascular reflexes and cardiac electrophysiology in an intact whole animal in both the conscious and anaesthetised state. The techniques used are inherently challenging and there are a number of limitations associated with the approaches used.

Firstly, conditional gene deletion strategy was achieved using an inducible HCN4 promoter at the level of the pacemaking tissue of the heart and by targeted delivery of an adenoviral vector to the medullary brainstem region of interest. The use of inducible HCN4 promoter has been previously validated in other experimental models to study cardiac pacemaking function. However, as HCN4 is also expressed in other areas of the heart (Herrmann et al. 2011) and also in extracardiac tissues (Brewster et al. 2007, Cho et al. 2009) including the spinal cord interneurons (Hughes et al. 2013), this may potentially confound our interpretation of results. The use of a non-specific CMV promoter to drive Cre expression in the CNS is potentially more problematic. The A1 and A5 cell groups and the vagal preganglionic neurones lie in close proximity in the medullary brainstem region (Strack et al. 1989, Dampney 1994). Great care was taken to target delivery to the RVLM area but it is likely that some of the neurones in the neighbouring regions would have undergone Cre mediated deletion of $G\alpha_O$. In any case, we have shown that inhibitory signalling via $G\alpha_O$ in the medullary brainstem region is important. Given that the subsequent histological studies of mice included in the study has shown that expression of GFP is mainly concentrated in Th-ir cells in the RVLM region, the observed phenotype is likely to be due mainly to loss of $G\alpha_O$ in the RVLM.

I studied the cardiovascular phenotype of mice by measuring HR and BP profile under different conditions, and computation of baroreflex sensitivity from baroreflex HR-BP responses. The relative contributions of the sympathetic and parasympathetic influences were assessed by pharmacological blockade. These are indirect measures of autonomic function. A more direct approach would involve direct recordings of efferent nerve activity such as of the renal sympathetic nerve (Ma et al. 2002) or other experimental paradigms such as in the working heart brainstem preparations (Paton 1996). These are technically very challenging and although I did explore these approaches, I was unable to get them to work consistently. On the other hand, although the approaches I used are indirect measures, they are methods which are clinically applicable and have been shown to be prognostic (Nolan 1998). The complexity of the experimental paradigm used meant that there was a limit to the number of interventions that could be performed. As a result, some of the obvious control experiments such as autonomic blockade during hypoxic and hypercapnic challenges were not performed.

The precise mechanism by which loss of $G\alpha_O$ at the RVLM results in alterations in autonomic tone remains unknown. We attempted to study this *in vitro* by patch-clamping brainstem slices transfected with Cre AVV but this proved technically challenging. We suggest that $G\alpha_O$ is important in mediating inhibitory influences on the RVLM with loss of this resulting in disinhibition and increased sympathetic outflow. $G\alpha_O$ coupled receptors can cause pre- or post-synaptic inhibition either via GIRK channels or by inhibiting calcium channels. The precise neurotransmitter or neuromodulator involved is unknown.

7.5 Future directions

Future studies should aim to investigate the mechanisms underlying the cardiovascular phenotype observed. Use of more specific promoters to drive Cre expression would help to identify the precise cellular population for which $G\alpha_O$ signalling is important in the brainstem. Refinement of *in vivo* experimental preparation may also allow more direct assessment of autonomic function and direct stimulation and recording from pre-ganglionic neurones of interest in the brainstem. The use of indirect measures of neuronal activity such as calcium imaging in brainstem slices may also allow for *in vitro* study to elucidate the mechanism of inhibitory G protein signalling responsible for the phenotype seen.

It would also be interesting to study mice with conditional deletion of $G\alpha_O$ in the RVLM in other models of disease or pathology for example the myocardial infarction model of heart failure to study the role played by increased sympathetic tone in progression of this disease. This may lead to further insight in central mechanisms of autonomic regulation of the heart that may lead to translatable therapies in the future.

7.5 Conclusion

The data obtained in this study suggest that $G\alpha_O$-mediated signalling within the presympathetic circuits of the RVLM contributes to the autonomic control of the heart. $G\alpha_O$–mediated signalling plays no significant role at the level of cardiac conduction system. $G\alpha_O$ deficiency in the RVLM is associated with exaggerated cardiovascular responses to stress, altered cardiovascular reflexes and electrical properties of the heart.

Bibliography

Ang, R., Opel, A. & Tinker, A., 2012. The Role of Inhibitory G Proteins and Regulators of G Protein Signaling in the in vivo Control of Heart Rate and Predisposition to Cardiac Arrhythmias. *Frontiers in physiology*, 3, p.96.

Albarran-Juarez, J. et al., 2009. Modulation of 2-Adrenoceptor Functions by Heterotrimeric G i Protein Isoforms. *Journal of Pharmacology and Experimental Therapeutics*, 331(1), pp.35–44.

Al-Gobari, M. et al., 2013. Beta-blockers for the prevention of sudden cardiac death in heart failure patients: a meta-analysis of randomized controlled trials. *BMC Cardiovascular Disorders*, 13(1), pp.1–1.

Amano, M. & Kubo, T., 1993. Involvement of both GABAA and GABAB receptors in tonic inhibitory control of blood pressure at the rostral ventrolateral medulla of the rat. *Naunyn-Schmiedeberg's archives of pharmacology*, 348(2), pp.146–153.

Amendt, K. et al., 1979. Bulbospinal projections to the intermediolateral cell column: a neuroanatomical study. *Journal of the autonomic nervous system*, 1(1), pp.103–107.

Avanzino, G.L. et al., 1994. GABAB receptor-mediated mechanisms in the RVLM studied by microinjections of two GABAB receptor antagonists. *American journal of physiology Heart and circulatory physiology*, 35(5), p.H1722.

Bacon, S.J., Zagon, A. & Smith, A.D., 1990. Electron microscopic evidence of a monosynaptic pathway between cells in the caudal raphe nuclei and sympathetic preganglionic neurons in the rat spinal cord. *Experimental Brain Research*, 79(3).

Barman, S.M. & Gebber, G.L., 1985. Axonal projection patterns of ventrolateral medullospinal sympathoexcitatory neurons. *Journal of Neurophysiology*, 53(6), pp.1551–1566.

Baudrie, V., Laude, D. & Elghozi, J.-L., 2007. Optimal frequency ranges for extracting information on cardiovascular autonomic control from the blood pressure and pulse interval spectrograms in mice. *American journal of physiology Regulatory, integrative and comparative physiology*, 292(2), pp.R904–12.

Benians, A. et al., 2003. The dynamics of formation and action of the ternary complex revealed in living cells using a G-protein-gated K+ channel as a biosensor. *The Journal of biological chemistry*, 278(12), pp.10851–10858.

Berntson, G.G., Cacioppo, J.T. & Quigley, K.S., 1991. Autonomic determinism: the modes of autonomic control, the doctrine of autonomic space, and the laws of autonomic constraint. *Psychological review*, 98(4), pp.459–487.

Bettoni, M. & Zimmermann, M., 2002. Autonomic tone variations before the onset of paroxysmal atrial fibrillation. *Circulation*, 105(23), pp.2753–2759.

Bhatt, D.L. et al., 2014. A controlled trial of renal denervation for resistant hypertension. *The New England journal of medicine*, 370(15), pp.1393–1401.

Birnbaumer, L., 2007(a). The discovery of signal transduction by G proteins: a personal account and an overview of the initial findings and contributions that

led to our present understanding. *Biochimica et biophysica acta*, 1768(4), pp.756–771.

Birnbaumer, L., 2007(b). Expansion of signal transduction by G proteins. The second 15 years or so: from 3 to 16 alpha subunits plus betagamma dimers. *Biochimica et biophysica acta*, 1768(4), pp.772–793.

Boknik, P. et al., 2009. Genetic disruption of G proteins, G(i2)alpha or G(o)alpha, does not abolish inotropic and chronotropic effects of stimulating muscarinic cholinoceptors in atrium. *British journal of pharmacology*, 158(6), pp.1557–1564.

Boychuk, C.R., Woerman, A.L. & Mendelowitz, D., 2012. Modulation of bulbospinal rostral ventral lateral medulla neurons by hypoxia/hypercapnia but not medullary respiratory activity. *Hypertension*, 60, pp. 1491-1497.

Brack, K.E. et al., 2007. Nitric oxide mediates the vagal protective effect on ventricular fibrillation via effects on action potential duration restitution in the rabbit heart. *The Journal of Physiology*, 583(Pt 2), pp.695–704.

Brack, K.E., Coote, J.H. & Ng, G.A., 2011. Vagus nerve stimulation protects against ventricular fibrillation independent of muscarinic receptor activation. *Cardiovascular research*, 91(3), pp.437–446.

Brewster, A.L. et al., 2007. Quantitative analysis and subcellular distribution of mRNA and protein expression of the hyperpolarization-activated cyclic nucleotide-gated channels throughout development in rat hippocampus. *Cerebral cortex (New York, N.Y. : 1991)*, 17(3), pp.702–712.

Brown, D.L. & Guyenet, P.G., 1985. Electrophysiological study of cardiovascular neurons in the rostral ventrolateral medulla in rats. *Circulation research*, 56(3), pp.359–369.

Bruinstroop, E. et al., 2012. Spinal projections of the A5, A6 (locus coeruleus), and A7 noradrenergic cell groups in rats. *The Journal of comparative neurology*, 520(9), pp.1985–2001.

Byrum, C.E. & Guyenet, P.G., 1987. Afferent and efferent connections of the A5 noradrenergic cell group in the rat. *The Journal of comparative neurology*, 261(4), pp.529–542.

Campen, M.J. et al., 2005. Heart rate variability responses to hypoxic and hypercapnic exposures in different mouse strains. *Journal of applied physiology (Bethesda, Md. : 1985)*, 99(3), pp.807–813.

Campen, M.J. et al., 2004. Phenotypic variation in cardiovascular responses to acute hypoxic and hypercapnic exposure in mice. *Physiological genomics*, 20(1), pp.15–20.

Casadei, B., 2001. Physiological Society Symposium-Vagal Control: From Axolotl to Man. *Experimental Physiology*, 86(6), pp. 817-823.

Caulfield, M.P. et al., 1994. Muscarinic M-current inhibition via G alpha q/11 and alpha-adrenoceptor inhibition of Ca2+ current via G alpha o in rat sympathetic neurones. *The Journal of Physiology*, 477 (Pt 3), pp.415–422.

Charlton, C.G. & Helke, C.J., 1987. Substance P-containing medullary projections to the intermediolateral cell column: identification with retrogradely transported rhodamine-labeled latex microspheres and immunohistochemistry. *Brain research*, 418(2), pp.245–254.

Cheng, Z. et al., 2004. Differential control over postganglionic neurons in rat cardiac ganglia by NA and DmnX neurons: anatomical evidence. *American journal of physiology Regulatory, integrative and comparative physiology*, 286(4), pp.R625–33.

Cho, H.-J. et al., 2009. Hyperpolarization-activated cyclic-nucleotide gated 4 (HCN4) protein is expressed in a subset of rat dorsal root and trigeminal ganglion neurons. *Cell and tissue research*, 338(2), pp.171–177.

Clark, F.M. & Proudfit, H.K., 1993. The projections of noradrenergic neurons in the A5 catecholamine cell group to the spinal cord in the rat: anatomical evidence that A5 neurons modulate nociception. *Brain research*, 616(1-2), pp.200–210.

Cleland, J.G.F. et al., 2014. Long-term mortality with cardiac resynchronization therapy in the Cardiac Resynchronization-Heart Failure (CARE-HF) trial. *European Journal of Heart Failure*, 14(6), pp.628–634.

Coote, J.H., 2013. Myths and Realities of the Cardiac Vagus. *The Journal of Physiology*, 591(17), pp. 4073-4085.

Dampney, R.A. et al., 1982. Role of ventrolateral medulla in vasomotor regulation: a correlative anatomical and physiological study. *Brain research*, 249(2), pp.223–235.

De Ferrari, G.M. et al., 2011. Chronic vagus nerve stimulation: a new and promising therapeutic approach for chronic heart failure. *European heart journal*, 32(7), pp.847–855.

DeGeorge, B.R.J. et al., 2008. Targeted inhibition of cardiomyocyte Gi signaling enhances susceptibility to apoptotic cell death in response to ischemic stress. *Circulation*, 117(11), pp.1378–1387.

Deighton, N.M. et al., 1990. Muscarinic cholinoceptors in the human heart: demonstration, subclassification, and distribution. *Naunyn-Schmiedeberg's archives of pharmacology*, 341(1-2), pp.14–21.

Desai, K.H. et al., 1997. Cardiovascular indexes in the mouse at rest and with exercise: new tools to study models of cardiac disease. *The American journal of physiology*, 272(2 Pt 2), pp.H1053–61.

DiFrancesco, D., 2010. The role of the funny current in pacemaker activity. *Circulation research*, 106(3), pp.434–446.

Dolphin, A.C., 2003. G Protein Modulation of Voltage-Gated Calcium Channels. *Pharmacological Reviews*, 55(4), pp.607–627.

Duan, S.Z. et al., 2007. Go but not Gi2 or Gi3 is required for muscarinic regulation of

heart rate and heart rate variability in mice. *Biochemical and biophysical research communications*, 357(1), pp.139–143.

Dutar, P. & Nicoll, R.A., 1988. A physiological role for GABAB receptors in the central nervous system. *Nature*, 332(6160), pp.156–158.

Ecker, P.M. et al., 2006. Effect of targeted deletions of beta1- and beta2-adrenergic-receptor subtypes on heart rate variability. *American journal of physiology Heart and circulatory physiology*, 290(1), pp.H192–9.

Ewald, D.A. et al., 1989. Differential G protein-mediated coupling of neurotransmitter receptors to Ca2+ channels in rat dorsal root ganglion neurons in vitro. *Neuron*, 2(2), pp.1185–1193.

Farrell, T.G. et al., 1992. Prognostic value of baroreflex sensitivity testing after acute myocardial infarction. *British heart journal*, 67(2), pp.129–137.

Feldberg, W. & Guertzenstein, P.G., 1976. Vasodepressor effects obtained by drugs acting on the ventral surface of the brain stem. *The Journal of Physiology*, 258(2), pp.337–355.

Floras, J.S., 2009. Sympathetic nervous system activation in human heart failure: clinical implications of an updated model. *Journal of the American College of Cardiology*, 54(5), pp.375–385.

Fontes, M.A. et al., 2001. Descending pathways mediating cardiovascular response from dorsomedial hypothalamic nucleus. *American journal of physiology Heart and circulatory physiology*, 280(6), pp.H2891–901.

Franklin K.B.J. & Paxinos G. 2008. The mouse brain in stereotaxic coordinates (3rd edition). Academic Press Elsevier, PA, USA.

Frenneaux, M.P., 2004. Autonomic changes in patients with heart failure and in post-myocardial infarction patients. *Heart (British Cardiac Society)*, 90(11), pp.1248–1255.

Fu, Y. et al., 2006. Endogenous RGS proteins and Galpha subtypes differentially control muscarinic and adenosine-mediated chronotropic effects. *Circulation research*, 98(5), pp.659–666.

Fu, Y. et al., 2007. Endogenous RGS proteins modulate SA and AV nodal functions in isolated heart: implications for sick sinus syndrome and AV block. *American journal of physiology Heart and circulatory physiology*, 292(5), pp.H2532–9.

Garcia Perez, M. & Jordan, D., 2001. Effect of stimulating non-myelinated vagal axons on atrio-ventricular conduction and left ventricular function in anaesthetized rabbits. *Autonomic neuroscience : basic & clinical*, 86(3), pp.183–191.

Gehrmann, J. & Berul, C.I., 2000. Cardiac electrophysiology in genetically engineered mice. *J Cardiovasc Electrophysiol*, 11(3), pp.354–368.

Gehrmann, J. et al., 2000. Phenotypic screening for heart rate variability in the mouse. *American journal of physiology Heart and circulatory physiology*, 279(2), pp.H733–40.

Gellen, B. et al., 2008. Conditional FKBP12.6 overexpression in mouse cardiac myocytes prevents triggered ventricular tachycardia through specific alterations in excitation-contraction coupling. *Circulation*, 117(14), pp.1778–1786.

Geraldes, V. et al., 2014. Autonomic Neuroscience: Basic and Clinical. *Autonomic neuroscience : basic & clinical*, 186(C), pp.22–31.

Gourine, A.V., Llaudet, E. & Thomas, T., 2002. Adenosine release in nucleus tractus solitarii does not appear to mediate hypoxia-induced respiratory depression in rats. *The Journal of Physiology,* 544(1), pp. 161-170.

Gilyarov, A., 2008. Nestin in central nervous system cells. *Neuroscience and behavioral physiology*, 38(2), pp. 165-169

Go, A.S. et al., 2013. Executive summary: heart disease and stroke statistics--2013 update: a report from the American Heart Association. *Circulation*, 127(1), pp.143–152.

Gourine, A.V. et al., 2005. ATP is a mediator of chemosensory transduction in the central nervous system. *Nature*, 436(7047), pp.108–111.

Gourine, A.V., Wood, J.D. & Burnstock, G., 2009. Purinergic signalling in autonomic control. *Trends in neurosciences*, 32(5), pp.241–248.

Granata, A.R. et al., 1986. A1 noradrenergic neurons tonically inhibit sympathoexcitatory neurons of C1 area in rat brainstem. *Brain research*, 377(1), pp.127–146.

Grassi, G. et al., 1995. Sympathetic Activation and Loss of Reflex Sympathetic Control in Mild Congestive Heart Failure. *Circulation*, 92(11), pp.3206–3211.

Gross, V. et al., 2005. Autonomic nervous system and blood pressure regulation in RGS2-deficient mice. *American journal of physiology Regulatory, integrative and comparative physiology*, 288(5), pp.R1134–42.

Guertzenstein, P.G. & Silver, A., 1974. Fall in blood pressure produced from discrete regions of the ventral surface of the medulla by glycine and lesions. *The Journal of Physiology*, 242(2), pp.489–503.

Guyenet, P.G., 2006. The sympathetic control of blood pressure. *Nature reviews Neuroscience*, 7(5), pp.335–346.

Guyenet, P.G. et al., 2013. C1 neurons: the body's EMTs. *AJP: Regulatory, Integrative and Comparative Physiology*, 305(3), pp.R187–R204.

Haskell, R.E. et al., 2003. Viral-mediated delivery of the late-infantile neuronal ceroid lipofuscinosis gene, TPP-I to the mouse central nervous system. *Gene therapy*, 10(1), pp.34–42.

Head, G.A. & McCarty, R., 2002. Vagal and sympathetic components of the heart rate range and gain of the baroreceptor-heart rate reflex in conscious rats. *Journal of the autonomic nervous system*, 21(2-3), pp.203–213.

Helke, C.J., McDonald, C.H. & Phillips, E.T., 1993. Hypotensive effects of 5-HT1A receptor activation: ventral medullary sites and mechanisms of action in the rat. *Journal of the autonomic nervous system*, 42(2), pp.177–188.

Herrmann, S. et al., 2007. HCN4 provides a “depolarization reserve” and is not required for heart rate acceleration in mice. *The EMBO journal*, 26(21), pp.4423–4432.

Herrmann, S., Layh, B. & Ludwig, A., 2011. Novel insights into the distribution of cardiac HCN channels: an expression study in the mouse heart. *Journal of Molecular and Cellular Cardiology*, 51(6), pp.997–1006.

Heusser, K. et al., 2010. Carotid baroreceptor stimulation, sympathetic activity, baroreflex function, and blood pressure in hypertensive patients. *Hypertension*, 55(3), pp.619–626.

Hirsch, M.D. & Helke, C.J., 1988. Bulbospinal thyrotropin-releasing hormone projections to the intermediolateral cell column: a double fluorescence immunohistochemical-retrograde tracing study in the rat. *Neuroscience*, 25(2), pp.625–637.

Hoesl, E. et al., 2008. Tamoxifen-inducible gene deletion in the cardiac conduction system. *Journal of Molecular and Cellular Cardiology*, 45(1), pp.62–69.

Hood, S.G. & Woods, R.L., 2004. Vagal reflex actions of atrial natriuretic peptide survive physiological but not pathological cardiac hypertrophy in rat. *Experimental Physiology*, 89(4), pp.445–454.

Horiuchi, J. & Dampney, R., 1998. Dependence of sympathetic vasomotor tone on bilateral inputs from the rostral ventrolateral medulla in the rabbit: role of baroreceptor reflexes. *Neuroscience letters*, 248(2), pp.113–116.

Huang, X. et al., 2006. Pleiotropic phenotype of a genomic knock-in of an RGS-insensitive G184S Gnai2 allele. *Molecular and cellular biology*, 26(18), pp.6870–6879.

Hughes, D.I. et al., 2013. HCN4 subunit expression in fast-spiking interneurons of spinal cord and hippocampus. *Neuroscience*, 237(C), pp.7–18.

Janssen, B.J.A. & Smits, J.F.M., 2002. Autonomic control of blood pressure in mice: basic physiology and effects of genetic modification. *American journal of physiology Regulatory, integrative and comparative physiology*, 282(6), pp.R1545–64.

Jiang, M., Gold, M. & Boulay, G., 1998. Multiple neurological abnormalities in mice deficient in the G protein Go. *Proceedings of the National Academy of Sciences of the United States of America*, 95, pp. 3269-3274.

Jones, J., 2001. Physiological Society Symposium–Vagal Control: From Axolotl to Man. *Experimental Physiology*, 86, pp. 797-801.

Jones, J.F., Wang, Y. & Jordan, D., 1995. Heart rate responses to selective stimulation of cardiac vagal C fibres in anaesthetized cats, rats and rabbits. *The Journal of Physiology*, 489 (Pt 1), pp.203–214.

Just, A., Faulhaber, J. & Ehmke, H., 2000. Autonomic cardiovascular control in conscious mice. *American journal of physiology Regulatory, integrative and comparative physiology*, 279(6), pp.R2214–21.

Kaese, S. & Verheule, S., 2012. Cardiac electrophysiology in mice: a matter of size. *Frontiers in physiology*, 3, p.345.

Kent, K.M. et al., 1973. Electrical stability of acutely ischemic myocardium. Influences of heart rate and vagal stimulation. *Circulation*, 47(2), pp.291–298.

Koizumi, K. & Kollai, M., 1981. Control of reciprocal and non-reciprocal action of vagal and sympathetic efferents: study of centrally induced reactions. *Journal of the autonomic nervous system*, 3(2-4), pp.483–501.

Koizumi, K. et al., 1982. Functional significance of coactivation of vagal and sympathetic cardiac nerves. *Proceedings of the National Academy of Sciences of the United States of America*, 79(6), pp.2116–2120.

Koshiya, N., Huangfu, D. & Guyenet, P.G., 1993. Ventrolateral medulla and sympathetic chemoreflex in the rat. *Brain research*, 609(1-2), pp.174–184.

Kovoor, P. et al., 2001. Evaluation of the role of I(KACh) in atrial fibrillation using a mouse knockout model. *Journal of the American College of Cardiology*, 37(8), pp.2136–2143.

Kramer, K. et al., 1993. Use of telemetry to record electrocardiogram and heart rate in freely moving mice. *Journal of pharmacological and toxicological methods*, 30(4), pp.209–215.

Kubo, T. et al., 2000. Cholinergic inputs to rostral ventrolateral medulla pressor neurons from hypothalamus. *Brain research bulletin*, 53(3), pp.275–282.

Lakatta, E.G. & DiFrancesco, D., 2009. What keeps us ticking: a funny current, a calcium clock, or both? *Journal of Molecular and Cellular Cardiology*, 47(2), pp.157–170.

La Rovere, M.T. et al., 1998. Baroreflex sensitivity and heart-rate variability in prediction of total cardiac mortality after myocardial infarction. ATRAMI (Autonomic Tone and Reflexes After Myocardial Infarction) Investigators. *The Lancet*, 351(9101), pp.478–484.

LaVallie, E.R. et al., 2006. Protein kinase Czeta is up-regulated in osteoarthritic cartilage and is required for activation of NF-kappaB by tumor necrosis factor and interleukin-1 in articular chondrocytes. *The Journal of biological chemistry*, 281(34), pp.24124–24137.

Leaney, J.L. et al., 2004. Rapid desensitization of G protein-gated inwardly rectifying K(+) currents is determined by G protein cycle. *American journal of physiology Cell physiology*, 287(1), pp.C182–91.

Leaney, J.L., Milligan, G. & Tinker, A., 2000. The G protein alpha subunit has a key role in determining the specificity of coupling to, but not the activation of, G protein-gated inwardly rectifying K(+) channels. *The Journal of biological chemistry*, 275(2), pp.921–929.

Li, A.-J. et al., 2009. Simultaneous silencing of Npy and Dbh expression in hindbrain A1/C1 catecholamine cells suppresses glucoprivic feeding. *The Journal of neuroscience : the official journal of the Society for Neuroscience*, 29(1), pp.280–287.

Li, P. et al., 1995. Role of acetylcholine, corticoids and opioids in the rostral ventrolateral medulla in stress-induced hypertensive rats. *Biological signals*, 4(3), pp.124–132.

Li, Y.W. & Guyenet, P.G., 1995. Neuronal inhibition by a GABAB receptor agonist in the rostral ventrolateral medulla of the rat. *American journal of physiology Regulatory, integrative and comparative physiology*, 268(2), pp.R428–R437.

Liu, J. et al., 2007. Organisation of the mouse sinoatrial node: structure and expression of HCN channels. *Cardiovascular research*, 73(4), pp.729–738.

Link, R.E. et al., 1996. Cardiovascular Regulation in Mice Lacking α2-Adrenergic Receptor Subtypes b and c. *Science (New York, NY)*, 273(5276), pp.803–805.

López-González, M.V. et al., 2013. Neurons of the A5 region are required for the tachycardia evoked by electrical stimulation of the hypothalamic defence area in anaesthetized rats. *Experimental Physiology*, 98(8), pp.1279–1294.

López, M. et al., 2008. Hypothalamic fatty acid metabolism mediates the orexigenic action of ghrelin. *Cell metabolism*, 7(5), pp.389–399.

Logothetis, D.E. et al., 1987. The beta gamma subunits of GTP-binding proteins activate the muscarinic K+ channel in heart. *Nature*, 325(6102), pp.321–326.

Lüscher, C. & Slesinger, P.A., 2010. Emerging roles for G protein-gated inwardly rectifying potassium (GIRK) channels in health and disease. *Nature reviews Neuroscience*, 11(5), pp.301–315.

Lüscher, C. et al., 1997. G protein-coupled inwardly rectifying K+ channels (GIRKs) mediate postsynaptic but not presynaptic transmitter actions in hippocampal neurons. *Neuron*, 19(3), pp.687–695.

Ma, X., Abboud, F.M. & Chapleau, M.W., 2002. Analysis of afferent, central, and efferent components of the baroreceptor reflex in mice. *American journal of physiology Regulatory, integrative and comparative physiology*, 283(5), pp.R1033–40.

MacMillan, L.B. et al., 1996. Central Hypotensive Effects of the α2a-Adrenergic Receptor Subtype. *Science (New York, NY)*, 273(5276), pp.801–803.

Madden, C.J. & Morrison, S.F., 2004. Excitatory amino acid receptors in the dorsomedial hypothalamus mediate prostaglandin-evoked thermogenesis in brown adipose tissue. *American journal of physiology Regulatory, integrative and comparative physiology*, 286(2), pp.R320–5.

Madden, C.J. & Sved, A.F., 2003. Cardiovascular regulation after destruction of the C1 cell group of the rostral ventrolateral medulla in rats. *American journal of physiology Heart and circulatory physiology*, 285(6), pp.H2734–48.

Madden, C.J., Stocker, S.D. & Sved, A.F., 2006. Attenuation of homeostatic responses to hypotension and glucoprivation after destruction of catecholaminergic rostral ventrolateral medulla neurons. *American journal of physiology Regulatory, integrative and comparative physiology*, 291(3), pp.R751–9.

Maguire, C.T. et al., 2003. Implications of ventricular arrhythmia vulnerability during murine electrophysiology studies. *Physiological genomics*, 15(1), pp.84–91.

Malik, M. et al., 1996. Heart rate variability standards of measurement, physiological interpretation, and clinical use. *European heart journal*, 17(3), pp.354–381.

Malliani, A. et al., 1991. Cardiovascular neural regulation explored in the frequency domain. *Circulation*, 84(2), pp.482–492.

Malpas, S.C., 2010. Sympathetic Nervous System Overactivity and Its Role in the Development of Cardiovascular Disease. *Physiological reviews*, 90(2), pp.513–557.

Maltsev, V.A. & Lakatta, E.G., 2008. Dynamic interactions of an intracellular Ca2+ clock and membrane ion channel clock underlie robust initiation and regulation of cardiac pacemaker function. *Cardiovascular research*, 77(2), pp.274–284.

Mandel, D.A. & Schreihofer, A.M., 2006. Central respiratory modulation of barosensitive neurones in rat caudal ventrolateral medulla. *The Journal of Physiology*, 572(3), pp.881–896.

Marina, N. et al., 2011. Control of sympathetic vasomotor tone by catecholaminergic C1 neurones of the rostral ventrolateral medulla oblongata. *Cardiovascular research*, 91(4), pp.703–710.

Marina, N. et al., 2013. Purinergic signalling in the rostral ventro-lateral medulla controls sympathetic drive and contributes to the progression of heart failure following myocardial infarction in rats. *Basic research in cardiology*, 108(1), p.317.

Milner, T.A. et al., 1999. Alpha2A-adrenergic receptors are primarily presynaptic heteroreceptors in the C1 area of the rat rostral ventrolateral medulla. *Brain research*, 821(1), pp.200–211.

Milner, T.A., Drake, C.T. & Aicher, S.A., 2002. C1 adrenergic neurons are contacted by presynaptic profiles containing DELTA-opioid receptor immunoreactivity. *Neuroscience*, 110(4), pp.691–701.

Misgeld, U., Bijak, M. & Jarolimek, W., 1995. A physiological role for GABA B receptors and the effects of baclofen in the mammalian central nervous system. *Progress in neurobiology*, 46(4), pp.423–462.

Miyawaki, T., Goodchild, A.K. & Pilowsky, P.M., 2002. Evidence for a tonic GABA-ergic inhibition of excitatory respiratory-related afferents to presympathetic neurons in the rostral ventrolateral medulla. *Brain research*, 924(1), pp.56–62.

Monfredi, O. et al., 2010. The Anatomy and Physiology of the Sinoatrial Node-A Contemporary Review. *Pacing and Clinical Electrophysiology*, 33(11), pp.1392–1406.

Myat, A. et al., 2013. Renal sympathetic denervation therapy for resistant hypertension: a contemporary synopsis and future implications. *Circulation. Cardiovascular interventions*, 6(2), pp.184–197.

Nagata, K. et al., 2000. Galpha(i2) but not Galpha(i3) is required for muscarinic inhibition of contractility and calcium currents in adult cardiomyocytes. *Circulation research*, 87(10), pp.903–909.

Nakamura, K. et al., 2005. Sympathetic premotor neurons mediating thermoregulatory functions. *Neuroscience research*, 51(1), pp.1–8.

Naldini, L. et al., 1996. Efficient transfer, integration, and sustained long-term expression of the transgene in adult rat brains injected with a lentiviral vector. *Proceedings of the National Academy of Sciences of the United States of America*, 93(21), pp.11382–11388.

Nalivaiko, E. & Blessing, W.W., 2001. Raphe region mediates changes in cutaneous vascular tone elicited by stimulation of amygdala and hypothalamus in rabbits. *Brain research*, 891(1-2), pp.130–137.

Nalivaiko, E., Ootsuka, Y. & Blessing, W.W., 2005. Activation of 5-HT1A receptors in the medullary raphe reduces cardiovascular changes elicited by acute psychological and inflammatory stresses in rabbits. *American journal of physiology Regulatory, integrative and comparative physiology*, 289(2), pp.R596–R604.

Ngampramuan, S. et al., 2007. Activation of 5-HT1A receptors attenuates tachycardia induced by restraint stress in rats. *AJP: Regulatory, Integrative and Comparative Physiology*, 294(1), pp.R132–R141.

Nolan, J. et al., 1998. Prospective study of heart rate variability and mortality in chronic heart failure: results of the United Kingdom heart failure evaluation and assessment of risk trial (UK-heart). *Circulation*, 98(15), pp.1510–1516.

Onodera, M. et al., 1997. Determination of ventilatory volume in mice by whole body plethysmography. *The Japanese journal of physiology*, 47(4), pp.317–326.

Pagani, M. et al., 1986. Power spectral analysis of heart rate and arterial pressure variabilities as a marker of sympatho-vagal interaction in man and conscious dog. *Circulation research*, 59(2), pp.178–193.

Parker, L.M. et al., 2012. Distribution and localisation of Gα proteins in the rostral ventrolateral medulla of normotensive and hypertensive rats: focus on catecholaminergic neurons. *Neuroscience*, 218, pp.20–34.

Paton, J.F., 1996. A working heart-brainstem preparation of the mouse. *Journal of neuroscience methods*, 65(1), pp.63–68.

Paton, J.F. & Butcher, J.W., 1998. Cardiorespiratory reflexes in mice. *Journal of the autonomic nervous system*, 68(1-2), pp.115–124.

Paton, J.F.R. et al., 2005. The yin and yang of cardiac autonomic control: Vago-sympathetic interactions revisited. *Brain Research Reviews*, 49(3), pp.555–565.

Pilowsky, P. et al., 1996. Respiratory Inputs to Central Cardiovascular Neuronsa. *Annals of the New York Academy of Sciences*, 783(1), pp.64–70.

Pilowsky, P.M. & Goodchild, A.K., 2002. Baroreceptor reflex pathways and neurotransmitters: 10 years on. *Journal of hypertension*, 20(9), pp.1675–1688.

Ray, C.J. et al., 2002. Interactions of adenosine, prostaglandins and nitric oxide in hypoxia-induced vasodilatation: in vivo and in vitro studies. *The Journal of Physiology*, 544(Pt 1), pp.195–209.

Richter, D.W. et al., 1999. Neurotransmitters and neuromodulators controlling the hypoxic respiratory response in anaesthetized cats. *The Journal of Physiology*, 514 (Pt 2), pp.567–578.

Robinson, R.B. & Siegelbaum, S.A., 2003. Hyperpolarization-activated cation currents: from molecules to physiological function. *Annual review of physiology*, 65, pp.453–480.

Rong, W. et al., 2003. Pivotal role of nucleotide P2X2 receptor subunit of the ATP-gated ion channel mediating ventilatory responses to hypoxia. *The Journal of neuroscience*, 23(36), pp.11315–11321.

Ross, C.A. et al., 1981. Adrenaline neurons in the rostral ventrolateral medulla innervate thoracic spinal cord: a combined immunocytochemical and retrograde transport demonstration. *Neuroscience letters*, 25(3), pp.257–262.

Ross, C.A. et al., 1983. Adrenaline synthesizing neurons in the rostral ventrolateral medulla: a possible role in tonic vasomotor control. *Brain research*, 273(2), pp.356–361.

Sauer, B., 1998. Inducible gene targeting in mice using the Cre/lox system. *Methods (San Diego, Calif)*, 14(4), pp.381–392.

Sartor, D.M. & Verberne, A.J.M., 2003. Phenotypic identification of rat rostroventrolateral medullary presympathetic vasomotor neurons inhibited by exogenous cholecystokinin. *The Journal of comparative neurology*, 465(4), pp.467–479.

Sasek, C.A. & Helke, C.J., 1989. Enkephalin-immunoreactive neuronal projections from the medulla oblongata to the intermediolateral cell column: relationship to substance P-immunoreactive neurons. *The Journal of comparative neurology*, 287(4), pp.484–494.

Schmittgen, T.D. & Livak, K.J., 2008. Analyzing real-time PCR data by the comparative C(T) method. *Nature protocols*, 3(6), pp.1101–1108.

Schreihofer, A.M. & Guyenet, P.G., 1997. Identification of C1 presympathetic neurons in rat rostral ventrolateral medulla by juxtacellular labeling in vivo. *The Journal of comparative neurology*, 387(4), pp.524–536.

Schreihofer, A.M. & Guyenet, P.G., 2000. Sympathetic reflexes after depletion of bulbospinal catecholaminergic neurons with anti-DβH-saporin. *American journal of physiology Regulatory, integrative and comparative physiology*, 279(2), pp.R729–R742.

Schreihofer, A.M., Ito, S. & Sved, A.F., 2005. Brain stem control of arterial pressure in chronic arterial baroreceptor-denervated rats. *American journal of physiology Regulatory, integrative and comparative physiology*, 289(6), pp.R1746–55.

Sebastian, S. et al., 2013. The in-vivo regulation of heart rate in the murine sinoatrial node by stimulatory and inhibitory heterotrimeric G-proteins. *AJP: Regulatory, Integrative and Comparative Physiology*.

Seller, H., König, S. & Czachurski, J., 1990. Chemosensitivity of sympathoexcitatory neurones in the rostroventrolateral medulla of the cat. *Pflügers Archiv : European journal of physiology*, 416(6), pp.735–741.

Shen, M.J. & Zipes, D.P., 2014. Role of the autonomic nervous system in modulating cardiac arrhythmias. *Circulation research*, 114(6), pp.1004–1021.

Shibata, N. et al., 2001. Pacemaker shift in the rabbit sinoatrial node in response to vagal nerve stimulation. *Experimental Physiology*, 86(2), pp.177–184.

Smith, P.A. et al., 2004. Relationship between central sympathetic activity and stages of human hypertension*. *American Journal of Hypertension*, 17(3), pp.217–222.

Smyth, H.S., Sleight, P. & Pickering, G.W., 1969. Reflex regulation of arterial pressure during sleep in man. A quantitative method of assessing baroreflex sensitivity. *Circulation research*, 24(1), pp.109–121.

Spyer, K.M., 1994. Annual review prize lecture. Central nervous mechanisms contributing to cardiovascular control. *The Journal of Physiology*, 474(1), pp.1–19.

Spyer, K.M. & Gilbey, M.P., 1988. Cardiorespiratory Interactions in Heart-Rate Controla. *Annals of the New York Academy of Sciences*, 533(1), pp.350–357.

Spyer, K.M. & Thomas, T., 2000. A role for adenosine in modulating cardio-respiratory responses: a mini-review. *Brain research bulletin*, 53(1), pp.121–124.

Stauss, H.M., 2003. Heart rate variability. *American journal of physiology Regulatory, integrative and comparative physiology*, 285(5), pp.R927–31.

Stieber, J. et al., 2003. The hyperpolarization-activated channel HCN4 is required for the generation of pacemaker action potentials in the embryonic heart. *Proceedings of the National Academy of Sciences of the United States of America*, 100(25), pp.15235–15240.

Sternweis, P.C. & Robishaw, J.D., 1984. Isolation of two proteins with high affinity for guanine nucleotides from membranes of bovine brain. *The Journal of biological chemistry*, 259(22), pp.13806–13813.

Strack, A.M. et al., 1989. CNS cell groups regulating the sympathetic outflow to adrenal gland as revealed by transneuronal cell body labeling with pseudorabies virus. *Brain research*, 491(2), pp.274–296.

Strittmatter, S.M. et al., 1990. G0 is a major growth cone protein subject to regulation by GAP-43. *Nature*, 344(6269), pp.836–841.

Swoap, S.J. et al., 2008. Vagal tone dominates autonomic control of mouse heart rate at thermoneutrality. *American journal of physiology Heart and circulatory physiology*, 294(4), pp.H1581–8.

Syrota, A. et al., 1985. Muscarinic cholinergic receptor in the human heart evidenced under physiological conditions by positron emission tomography. *Proceedings of the National Academy of Sciences of the United States of America*, 82(2), pp.584–588.

Swoap, S.J. et al., 2008. Vagal tone dominates autonomic control of mouse heart rate at thermoneutrality. *American journal of physiology Heart and circulatory physiology*, 294(4), pp.H1581–8.

Tagawa, T. et al., 2000. The physiological role of AT1 receptors in the ventrolateral medulla. *Brazilian journal of medical and biological research*, 33(6), pp.643–652.

Tankersley, C.G., Elston, R.C. & Schnell, A.H., 2000. Genetic determinants of acute hypoxic ventilation: patterns of inheritance in mice. *Journal of applied physiology (Bethesda, Md. : 1985)*, 88(6), pp.2310–2318.

Teppema, L.J. & Dahan, A., 2010. The ventilatory response to hypoxia in mammals: mechanisms, measurement, and analysis. *Physiological reviews*, 90(2), pp.675–754.

Thireau, J. et al., 2007. Heart rate variability in mice: a theoretical and practical guide. *Experimental Physiology*, 93(1), pp.83–94.

Thomas, T. & Spyer, K.M., 1999. A novel influence of adenosine on ongoing activity in rat rostral ventrolateral medulla. *Neuroscience*, 88(4), pp.1213–1223.

Thomas, T. & Spyer, K.M., 1996. The role of adenosine receptors in the rostral ventrolateral medulla in the cardiovascular response to defence area stimulation in the rat. *Experimental Physiology*, 81(1), pp.67–77.

Tronche, F. et al., 1999. Disruption of the glucocorticoid receptor gene in the nervous system results in reduced anxiety. *Nature genetics*, 23(1), pp.99–103.

Uechi, M., Asai, K., Osaka, M., Smith, A., Sato, N., et al., 1998. Depressed heart rate variability and arterial baroreflex in conscious transgenic mice with overexpression of cardiac Gsalpha. *Circulation research*, 82(4), pp.416–423.

Ustyugova, I.V. et al., 2012. IEX-1 deficiency protects against colonic cancer. *Molecular cancer research : MCR*, 10(6), pp.760–767.

Valenzuela, D. et al., 1997. G alpha(o) is necessary for muscarinic regulation of Ca2+ channels in mouse heart. *Proceedings of the National Academy of Sciences of the United States of America*, 94(5), pp.1727–1732.

van den Pol, A.N., 2012. Neuropeptide transmission in brain circuits. *Neuron*, 76(1), pp.98–115.

Verrier, R.L. & Antzelevitch, C., 2004. Autonomic aspects of arrhythmogenesis: the enduring and the new. *Current opinion in cardiology*, 19(1), pp.2–11.

Waldeyer, C. et al., 2009. Regional, age-dependent, and genotype-dependent differences in ventricular action potential duration and activation time in 410 Langendorff-perfused mouse hearts. *Basic research in cardiology*, 104(5), pp.523–533.

Wehrens, X.H., Kirchhoff, S. & Doevendans, P.A., 2000. Mouse electrocardiography: an interval of thirty years. *Cardiovascular research*, 45(1), pp.231–237.

West, M.J., Blessing, W.W. & Chalmers, J., 1981. Arterial baroreceptor reflex function in the conscious rabbit after brainstem lesions coinciding with the A1 group of catecholamine neurons. *Circulation research*, 49(4), pp.959–970.

Wettschureck, N. & Offermanns, S., 2005. Mammalian G proteins and their cell type specific functions. *Physiological reviews*, 85(4), pp.1159–1204.

Wickman, K. et al., 1998. Abnormal heart rate regulation in GIRK4 knockout mice. *Neuron*, 20(1), pp.103–114.

Willette, R.N. et al., 1983. Medullary gamma-aminobutyric acid (GABA) receptors and the regulation of blood pressure in the rat. *Journal of Pharmacology and Experimental Therapeutics*, 226(3), pp.893–899.

Winter, S. et al., 2005. Galphao2 regulates vesicular glutamate transporter activity by changing its chloride dependence. *The Journal of neuroscience : the official journal of the Society for Neuroscience*, 25(18), pp.4672–4680.

Woulfe, J.M., Flumerfelt, B.A. & Hrycyshyn, A.W., 1990. Efferent connections of the A1 noradrenergic cell group: a DBH immunohistochemical and PHA-L anterograde tracing study. *Experimental neurology*, 109(3), pp.308–322.

Yang, Y. et al., 1994. Cellular immunity to viral antigens limits E1-deleted adenoviruses for gene therapy. *Proceedings of the National Academy of Sciences of the United States of America*, 91(10), pp.4407–4411.

Yoon, M.S. et al., 1977. Effects of vagal stimulation, atropine, and propranolol on fibrillation threshold of normal and ischemic ventricles. *American heart journal*, 93(1), pp.60–65.

Young, C.N. & Davisson, R.L., 2011. In vivo assessment of neurocardiovascular regulation in the mouse: principles, progress, and prospects. *American journal of physiology Heart and circulatory physiology*, 301(3), pp.H654–62.

Yutzey, K.E. & Robbins, J., 2007. Principles of genetic murine models for cardiac disease. *Circulation*, 115(6), pp.792–799.

Zannad, F. et al., 2014. Chronic vagal stimulation for the treatment of low ejection fraction heart failure: results of the neural cardiac therapy for heart failure (NECTAR-HF) randomized controlled trial. *European heart journal*.

Zipes D.P. & Jalife J. (eds) 2009. Cardiac Electrophysiology: From Cell to Bedside (5th edition). Saunders Elsevier, PA, USA.

Zuberi, Z. et al., 2010. Absence of the inhibitory G-protein Galphai2 predisposes to ventricular cardiac arrhythmia. *Circulation Arrhythmia and electrophysiology*, 3(4), pp.391–400.

Zuberi, Z., Birnbaumer, L. & Tinker, A., 2008. The role of inhibitory heterotrimeric G proteins in the control of in vivo heart rate dynamics. *American journal of physiology Regulatory, integrative and comparative physiology*, 295(6), pp.R1822–30.

Appendix

Appendix 1

MatLab script developed by Varuna De Silva used to obtain best fit sigmoidal baroreflex curve

```
function varargout = Logistic(varargin)
% LOGISTIC M-file for Logistic.fig
%
% Copyright 2011 Varuna De Silva
% I-Lab, CVSSP, University of Surrey
% Guildford
% GU2-7XH
% UK
%
% Email: varunax@gmail.com
%
%
% This work is based on the excellent tutorial by David Arnold
%
http://online.redwoods.cc.ca.us/instruct/darnold/diffeq/logistic/log
istic
% .pdf
gui_Singleton = 1;
gui_State = struct('gui_Name',       mfilename, ...
                   'gui_Singleton',  gui_Singleton, ...
                   'gui_OpeningFcn', @Logistic_OpeningFcn, ...
                   'gui_OutputFcn',  @Logistic_OutputFcn, ...
                   'gui_LayoutFcn',  [] , ...
                   'gui_Callback',   []);
if nargin && ischar(varargin{1})
    gui_State.gui_Callback = str2func(varargin{1});
end

if nargout
    [varargout{1:nargout}] = gui_mainfcn(gui_State, varargin{:});
else
    gui_mainfcn(gui_State, varargin{:});
end
% End initialization code - DO NOT EDIT


% --- Executes just before Logistic is made visible.
function Logistic_OpeningFcn(hObject, eventdata, handles, varargin)
% This function has no output args, see OutputFcn.
% hObject    handle to figure
% eventdata  reserved - to be defined in a future version of MATLAB
% handles    structure with handles and user data (see GUIDATA)
% varargin   command line arguments to Logistic (see VARARGIN)

% Choose default command line output for Logistic
handles.output = hObject;
handles.numFrames = 14;
% Update handles structure
guidata(hObject, handles);

% UIWAIT makes Logistic wait for user response (see UIRESUME)
% uiwait(handles.figure1);
```

```
% --- Outputs from this function are returned to the command line.
function varargout = Logistic_OutputFcn(hObject, eventdata, handles)
% varargout  cell array for returning output args (see VARARGOUT);
% hObject    handle to figure
% eventdata  reserved - to be defined in a future version of MATLAB
% handles    structure with handles and user data (see GUIDATA)

% Get default command line output from handles structure
varargout{1} = handles.output;



function C_INP1_Path_Callback(hObject, eventdata, handles)
% hObject    handle to C_INP1_Path (see GCBO)
% eventdata  reserved - to be defined in a future version of MATLAB
% handles    structure with handles and user data (see GUIDATA)

% Hints: get(hObject,'String') returns contents of C_INP1_Path as
text
%        str2double(get(hObject,'String')) returns contents of
C_INP1_Path as a double


% --- Executes during object creation, after setting all properties.
function C_INP1_Path_CreateFcn(hObject, eventdata, handles)
% hObject    handle to C_INP1_Path (see GCBO)
% eventdata  reserved - to be defined in a future version of MATLAB
% handles    empty - handles not created until after all CreateFcns
called

% Hint: edit controls usually have a white background on Windows.
%       See ISPC and COMPUTER.
if ispc
    set(hObject,'BackgroundColor','white');
else

set(hObject,'BackgroundColor',get(0,'defaultUicontrolBackgroundColor
'));
end



function C_INP2_Path_Callback(hObject, eventdata, handles)
% hObject    handle to C_INP2_Path (see GCBO)
% eventdata  reserved - to be defined in a future version of MATLAB
% handles    structure with handles and user data (see GUIDATA)

% Hints: get(hObject,'String') returns contents of C_INP2_Path as
text
%        str2double(get(hObject,'String')) returns contents of
C_INP2_Path as a double


% --- Executes during object creation, after setting all properties.
function C_INP2_Path_CreateFcn(hObject, eventdata, handles)
% hObject    handle to C_INP2_Path (see GCBO)
% eventdata  reserved - to be defined in a future version of MATLAB
```

```
% handles    empty - handles not created until after all CreateFcns
called

% Hint: edit controls usually have a white background on Windows.
%       See ISPC and COMPUTER.
if ispc
    set(hObject,'BackgroundColor','white');
else

set(hObject,'BackgroundColor',get(0,'defaultUicontrolBackgroundColor
'));
end


% --- Executes on button press in C_INP1_Browse.
function C_INP1_Browse_Callback(hObject, eventdata, handles)
% hObject    handle to C_INP1_Browse (see GCBO)
% eventdata  reserved - to be defined in a future version of MATLAB
% handles    structure with handles and user data (see GUIDATA)
[FileName,PathName] = uigetfile('*.txt','Select the MOS File');
handles.C_INP1 = fullfile(PathName,FileName);
set(handles.C_INP1_Path,'String',handles.C_INP1);
handles.MOS = dlmread(handles.C_INP1)
guidata(hObject, handles);


% --- Executes on button press in C_INP2_Browse.
function C_INP2_Browse_Callback(hObject, eventdata, handles)
% hObject    handle to C_INP2_Browse (see GCBO)
% eventdata  reserved - to be defined in a future version of MATLAB
% handles    structure with handles and user data (see GUIDATA)
[FileName,PathName] = uigetfile('*.txt','Select the METRIC File');
handles.C_INP2 = fullfile(PathName,FileName);
set(handles.C_INP2_Path,'String',handles.C_INP2);
handles.METRIC = dlmread(handles.C_INP2)
guidata(hObject, handles);



% --- Executes on button press in resetBut.
function resetBut_Callback(hObject, eventdata, handles)
% hObject    handle to resetBut (see GCBO)
% eventdata  reserved - to be defined in a future version of MATLAB
% handles    structure with handles and user data (see GUIDATA)
cla(handles.axes1,'reset');
set(handles.final_params,'String','');
set(handles.final_params2,'String','');
set(handles.min_r,'String','0');
set(handles.max_r,'String','0');
set(handles.est_r,'String','0');
set(handles.est_t0,'String','0');
guidata(hObject, handles); %updates the handles


% --- Executes on button press in plotBut.
function plotBut_Callback(hObject, eventdata, handles)
% hObject    handle to plotBut (see GCBO)
% eventdata  reserved - to be defined in a future version of MATLAB
% handles    structure with handles and user data (see GUIDATA)
```

```
axes(handles.axes1)

plot(handles.METRIC,handles.MOS,'o')
%adds a title, x-axis description, and y-axis description


est_t0 = median(handles.METRIC);
xx = handles.METRIC-est_t0;
title('MOS Vs. METRIC')
ylabel('MOS')
xlabel('METRIC')

[max_xx down_idx]= min(xx);
for idx = 1:size(xx)
    if(xx(idx)<0)
        if(xx(idx)>max_xx)
            max_xx=xx(idx); down_idx = idx;
        end
    end
end
[min_xx up_idx]= max(xx); for idx = 1:size(xx)
    if(xx(idx)>0)
        if(xx(idx)<min_xx)
            min_xx=xx(idx); up_idx = idx;
        end
    end
end

mt0 = (handles.MOS(up_idx)-
handles.MOS(down_idx))/(handles.METRIC(up_idx)-
handles.METRIC(down_idx));

est_r = 4*mt0;

min_r = est_r/10;
max_r = est_r*10;

set(handles.min_r,'String',num2str(min_r));
set(handles.max_r,'String',num2str(max_r));
set(handles.est_r,'String',num2str(est_r));
set(handles.est_t0,'String',num2str(est_t0));

%Calculate the estimates
guidata(hObject, handles); %updates the handles




function edit5_Callback(hObject, eventdata, handles)
% hObject    handle to edit5 (see GCBO)
% eventdata  reserved - to be defined in a future version of MATLAB
% handles    structure with handles and user data (see GUIDATA)

% Hints: get(hObject,'String') returns contents of edit5 as text
%        str2double(get(hObject,'String')) returns contents of edit5
as a double
```

```
% --- Executes during object creation, after setting all properties.
function edit5_CreateFcn(hObject, eventdata, handles)
% hObject    handle to edit5 (see GCBO)
% eventdata  reserved - to be defined in a future version of MATLAB
% handles    empty - handles not created until after all CreateFcns
called

% Hint: edit controls usually have a white background on Windows.
%       See ISPC and COMPUTER.
if ispc
    set(hObject,'BackgroundColor','white');
else

set(hObject,'BackgroundColor',get(0,'defaultUicontrolBackgroundColor
'));
end



function est_t0_Callback(hObject, eventdata, handles)
% hObject    handle to est_t0 (see GCBO)
% eventdata  reserved - to be defined in a future version of MATLAB
% handles    structure with handles and user data (see GUIDATA)

% Hints: get(hObject,'String') returns contents of est_t0 as text
%        str2double(get(hObject,'String')) returns contents of
est_t0 as a double


% --- Executes during object creation, after setting all properties.
function est_t0_CreateFcn(hObject, eventdata, handles)
% hObject    handle to est_t0 (see GCBO)
% eventdata  reserved - to be defined in a future version of MATLAB
% handles    empty - handles not created until after all CreateFcns
called

% Hint: edit controls usually have a white background on Windows.
%       See ISPC and COMPUTER.
if ispc
    set(hObject,'BackgroundColor','white');
else

set(hObject,'BackgroundColor',get(0,'defaultUicontrolBackgroundColor
'));
end



function est_r_Callback(hObject, eventdata, handles)
% hObject    handle to est_r (see GCBO)
% eventdata  reserved - to be defined in a future version of MATLAB
% handles    structure with handles and user data (see GUIDATA)

% Hints: get(hObject,'String') returns contents of est_r as text
%        str2double(get(hObject,'String')) returns contents of est_r
as a double


% --- Executes during object creation, after setting all properties.
```

```
function est_r_CreateFcn(hObject, eventdata, handles)
% hObject    handle to est_r (see GCBO)
% eventdata  reserved - to be defined in a future version of MATLAB
% handles    empty - handles not created until after all CreateFcns
called

% Hint: edit controls usually have a white background on Windows.
%       See ISPC and COMPUTER.
if ispc
    set(hObject,'BackgroundColor','white');
else

set(hObject,'BackgroundColor',get(0,'defaultUicontrolBackgroundColor
'));
end



function min_r_Callback(hObject, eventdata, handles)
% hObject    handle to min_r (see GCBO)
% eventdata  reserved - to be defined in a future version of MATLAB
% handles    structure with handles and user data (see GUIDATA)

% Hints: get(hObject,'String') returns contents of min_r as text
%        str2double(get(hObject,'String')) returns contents of min_r
as a double


% --- Executes during object creation, after setting all properties.
function min_r_CreateFcn(hObject, eventdata, handles)
% hObject    handle to min_r (see GCBO)
% eventdata  reserved - to be defined in a future version of MATLAB
% handles    empty - handles not created until after all CreateFcns
called

% Hint: edit controls usually have a white background on Windows.
%       See ISPC and COMPUTER.
if ispc
    set(hObject,'BackgroundColor','white');
else

set(hObject,'BackgroundColor',get(0,'defaultUicontrolBackgroundColor
'));
end



function max_r_Callback(hObject, eventdata, handles)
% hObject    handle to max_r (see GCBO)
% eventdata  reserved - to be defined in a future version of MATLAB
% handles    structure with handles and user data (see GUIDATA)

% Hints: get(hObject,'String') returns contents of max_r as text
%        str2double(get(hObject,'String')) returns contents of max_r
as a double


% --- Executes during object creation, after setting all properties.
function max_r_CreateFcn(hObject, eventdata, handles)
```

```
% hObject    handle to max_r (see GCBO)
% eventdata  reserved - to be defined in a future version of MATLAB
% handles    empty - handles not created until after all CreateFcns
called

% Hint: edit controls usually have a white background on Windows.
%       See ISPC and COMPUTER.
if ispc
    set(hObject,'BackgroundColor','white');
else

set(hObject,'BackgroundColor',get(0,'defaultUicontrolBackgroundColor
'));
end


% --- Executes on button press in FindFit.
function FindFit_Callback(hObject, eventdata, handles)
% hObject    handle to FindFit (see GCBO)
% eventdata  reserved - to be defined in a future version of MATLAB
% handles    structure with handles and user data (see GUIDATA)

est_r = str2num(get(handles.est_r,'String'));
est_t0 = str2num(get(handles.est_t0,'String'));

min_x = min(handles.METRIC);
max_x = max(handles.METRIC);

min_r = est_r/10;
max_r = est_r*10;

r=linspace(min_r,max_r,40);
t0=linspace(min_x,max_x,40);
[r,t0]=meshgrid(r,t0);

[m,n]=size(r);
e=zeros(size(r));

for i=1:m
for j=1:n
e(i,j)=myerror([r(i,j);t0(i,j)],handles.METRIC,handles.MOS);
end
end

[row col] = find(min(min(e)));


min2=fminsearch(@myerror,[r(col);t0(row)],[],handles.METRIC,handles.
MOS);

r=min2(1);
t0=min2(2);

H=1./(1+exp(-r*(handles.METRIC-t0)));

K=(H'*handles.MOS)/(H'*H)

t=linspace(min(handles.METRIC),max(handles.METRIC));
```

```
y=K./(1+exp(-r*(t-t0)));
plot(handles.METRIC,handles.MOS,'o',t,y)

s_sq_e = sum_sq_e([r; t0; K;],handles.METRIC,handles.MOS)
y1 = K./(1+exp(-r*(handles.METRIC-t0)));
R = corrcoef(handles.MOS,y1);
C_cof = R(1,2);
RMSE = sqrt(s_sq_e/size(handles.METRIC,1));
finalparams = ['K = ',num2str(K), '  G = ', num2str(r), '  Dm = ',
num2str(t0)];
set(handles.final_params,'String',finalparams);
finalparams = ['C = ',num2str(C_cof), '  SSE = ', num2str(s_sq_e), '
RMSE = ', num2str(RMSE)];
set(handles.final_params2,'String',finalparams);

title('Y Vs. X')
ylabel('Y - Values')
xlabel('X - Values')


guidata(hObject, handles); %updates the handles
```